Wired embedded communication networks monitoring : a transferometry-based approach

Abdel Karim Abdel Karim

▶ **To cite this version:**

Abdel Karim Abdel Karim. Wired embedded communication networks monitoring : a transferometry-based approach. Automatic. Université de Lille, 2022. English. NNT : 2022ULILB029 . tel-04041772

HAL Id: tel-04041772
https://theses.hal.science/tel-04041772

Submitted on 22 Mar 2023

HAL is a multi-disciplinary open access archive for the deposit and dissemination of scientific research documents, whether they are published or not. The documents may come from teaching and research institutions in France or abroad, or from public or private research centers.

L'archive ouverte pluridisciplinaire **HAL**, est destinée au dépôt et à la diffusion de documents scientifiques de niveau recherche, publiés ou non, émanant des établissements d'enseignement et de recherche français ou étrangers, des laboratoires publics ou privés.

Université de Lille

UNIVERSITY OF LILLE

DOCTORAL SCHOOL SPI-MADIS

DOCTORATE IN AUTOMATIC PRODUCTION SYSTEMS

Wired embedded communication networks monitoring: a transferometry-based approach

---

Abdel Karim ABDEL KARIM

A thesis submitted in fulfillment of the requirements
for the degree of Doctor of Philosophy

Centre de Recherche en Informatique, Signal et Automatique de Lille (CRIStAL)
Institut d'électronique de microélectronique et de nanotechnologie (IEMN)

5 December 2022

Jury:

Pr. Jean-Charles LE BUNETEL	GREMAN Tours University	Reviewer
MDC, HDR Houcine CHAFOUK	ESIGELEC Rouen	Reviewer
Pr. Didier MAQUIN	CRAN Lorraine University	President
Dr. Wafa BEN HASSEN	R&D CEA	Examiner
Pr. Vincent COCQUEMPOT	CRIStAL Lille University	Supervisor
Pr. Virginie DEGARDIN	IEMN Lille University	Co-supervisor

Université de Lille

UNIVERSITÉ DE LILLE

ÉCOLE DOCTORALE SPI-MADIS

DOCTEUR EN AUTOMATIQUE PRODUCTIQUE

Surveillance des réseaux de communication filaires embarqués : une approche par transférométrie

---

Abdel Karim ABDEL KARIM

Thèse présentée en vue de satisfaire aux exigences du diplôme de doctorat.

Centre de Recherche en Informatique, Signal et Automatique de Lille (CRIStAL)
Institut d'électronique de microélectronique et de nanotechnologie (IEMN)

5 December 2022

Jury:

Pr. Jean-Charles LE BUNETEL	GREMAN Université de Tours	Rapporteur
MCF, HDR Houcine CHAFOUK	ESIGELEC Rouen	Rapporteur
Pr. Didier MAQUIN	CRAN Université de Lorraine	Président
Dr. Wafa BEN HASSEN	R&D CEA	Examinatrice
Pr. Vincent COCQUEMPOT	CRIStAL Université de Lille	Directeur de thèse
Pr. Virginie DEGARDIN	IEMN Université de Lille	Co-directrice de thèse

Acknowledgements

This research work is done in the framework of the ELSAT2020 project which is co-financed by the European Union with the European Regional Development Fund, the French state and the Hauts-de-France Region Council. The work presented in this thesis was carried out within the Centre de Recherche en Informatique, Signal et Automatique de Lille (UMR 9189 - CRIStAL) and the Institute of Electronics, Microelectronics and Nanotechnology (UMR 8520 - IEMN).

First I would like to thank all the Jury members Pr. Jean-Charles LE BUNETEL, Pr. Houcine CHAFOUK, Pr. Didier MAQUIN and Dr. Wafa BEN HASSEN for being a part of the examination of my thesis defence. I would also like to sincerely thank Pr. Vincent COCQUEMPOT and Pr. Virginie DEGARDIN who directed this work. Thanks to their scientific advice and support I was able to carry out this study. The experience I gained under their supervision allowed me to develop my research skills and knowledge. Their support during these three years has been heartwarming.

A big thanks to all the doctoral students and office mates with whom I shared many pleasant moments.

Many thanks to my family-like friends for helping to ease the sting of alienation. Already, I find myself missing our shared mornings and nights. Mikel, Lina, Robine, Yara, and Haitham, our paths may cross one day; in the meantime, I have had the honor of meeting you; I faced many difficulties and you helped me overcome them; and I hope we will keep in touch. P.S. I can't lose you since you know too much about me, therefore it's either friendship or death.

Finally, I would want to thank my family for their unwavering support throughout the years and for being there for me at every turn. To my idol, my father, whom I admire and strive to live up to his high expectations of me. You were and still are the dream I aspire to reach. To my lovely mother, whose voice I must hear in the morning. I seek happiness in yours. To my siblings, who have shown me nothing but unwavering confidence and support throughout my life. To my life partner, eagerly waiting for our meeting. To the souls I lost on this journey, Grandpa, Grandma, may your souls rest in peace.

Abstract

Wired embedded communication networks monitoring: a transferometry-based approach

In wired networked control systems (NCS), components such as sensors, actuators and controllers communicate through cables, by means of Electronic Control Units (ECU). All these connected components are prone to faults which may degrade the NCS performance. Detecting efficiently these faults and locating the faulty component are the subjects of intensive research. The cables which are used for data transmission and energy supply are generally considered to be fault-free. However, as any physical material, they degrade over time and may also become faulty.

Faults in wired networks are divided into two categories, namely *soft faults* and *hard faults*, depending on their severity and their impact on the system behavior. Soft faults or degradations result of cable wear, mechanical stress, excessive temperatures, or humidity. They have no immediate effect because communication or energy transfer is maintained. However, these soft faults tend to develop over time to hard faults (i.e. open circuit or short circuit) which result in losing the communication or energy supply. It is thus very important, especially in embedded wired networks, to monitor the health state of the cables, which consists in detecting the soft faults, in locating the faulty branch, and estimating the severity of the fault.

The objective of this thesis is to develop a health monitoring system for soft fault detection, localization, and diagnosis, in wired embedded communication networks. We propose a transferometry-based approach which uses the computation and transmission capabilities of the connected ECU. Dedicated monitoring signals are sent over the network by some ECU, acting as sources. The received signals by the other ECU, acting as receivers, are processed to estimate the online transmission coefficients (TC) of the transmission lines. Health indicators are computed by the receivers by comparing the estimated TC with a reference TC estimated under no fault hypothesis. Furthermore, it is well-known that a transmission wired network can be modeled by a classical matrix chain model, which is derived from the RLCG-parameters of each cable. A soft fault is modeled by an adding impedance. Using the model with soft fault, we prove that the health indicators are sensitive to the faults and we show that a set of structured residuals may be generated to detect the fault and locate the faulty branch of the network. The monitoring method is developed for several network topologies: point-to-point, Y-shaped, star, bus and hybrid topologies.

The proposed method is validated using experimental measured TC of a Y-shaped network test bench. Simulations are performed to study complex networks as bus or hybrid networks. The sensitivity of the residuals to soft faults and the robustness to noise are also analyzed using simulated TC. It is shown that, due to noise, the residuals form a cluster in the residuals space, whose characteristics depend on the severity and the localization of the fault.

Résumé

Surveillance des réseaux de communication filaires embarqués : une approche par transférométrie

Dans les systèmes de commande en réseau (NCS) câblés, les composants tels que les capteurs, les actionneurs et les contrôleurs communiquent par des câbles, au moyen d'unités de commande électronique (ECU). Tous ces composants connectés sont sujets à des pannes qui peuvent dégrader les performances du système. La détection efficace de ces défauts et la localisation du composant défectueux font l'objet de recherches intensives. Les câbles utilisés pour la transmission de données et l'alimentation en énergie sont généralement considérés comme exempts de défauts. Cependant, comme tout matériau physique, ils se dégradent avec le temps et peuvent aussi devenir défectueux.

Les défauts dans les réseaux câblés sont divisés en deux catégories, à savoir les *défauts non-francs* et les *défauts francs*, en fonction de leur gravité et de leur impact sur le comportement du système. Les défauts non-francs ou dégradations résultent de l'usure des câbles, des contraintes mécaniques, des températures excessives ou de l'humidité. Ces défauts non-francs n'ont pas d'effet immédiat car la communication ou le transfert d'énergie est maintenu. Cependant, ces défauts non-francs ont tendance à évoluer avec le temps vers des défauts francs (c'est-à-dire un circuit ouvert ou un court-circuit) qui entraînent la perte de la communication ou de l'alimentation en énergie. Il est donc très important, surtout dans les réseaux câblés embarqués, de surveiller l'état de santé des câbles, ce qui consiste à détecter les défauts non-francs, à localiser la branche défectueuse et à estimer la gravité du défaut.

L'objectif de cette thèse est de développer un système de surveillance de l'état de santé pour la détection, la localisation et le diagnostic des défauts non-francs, dans les réseaux de communication filaires embarqués. Nous proposons une approche basée sur la transferométrie qui utilise les capacités de calcul et de transmission de l'ECU connecté. Des signaux de surveillance dédiés sont envoyés sur le réseau par certaines ECU, agissant comme des sources. Les signaux reçus par les autres ECU, agissant en tant que récepteurs, sont analysés pour estimer les coefficients de transmission (TC) des lignes de transmission. Les indicateurs de santé sont calculés par les récepteurs en comparant les TC estimés en ligne avec un TC de référence estimé dans l'hypothèse d'une absence de défaut. En outre, il est bien connu qu'un réseau câblé de transmission peut être modélisé par un modèle de matrice chaîne classique, qui est dérivé des paramètres RLCG de chaque câble. Un défaut non-franc est modélisé par une addition d'impédance. En utilisant le modèle avec défaut non-franc, nous prouvons que les indicateurs de santé sont sensibles aux défauts et nous montrons qu'un ensemble de résidus structurés peut être généré pour détecter le défaut et localiser la branche défectueuse du réseau. La méthode de surveillance est développée pour plusieurs topologies de réseau : topologies point à point, en Y, en étoile, en bus et hybride.

La méthode proposée est validée à l'aide de TC expérimentaux mesurés sur un banc d'essai de réseau en forme de Y. Des simulations sont réalisées pour étudier des réseaux complexes comme les réseaux en bus ou hybrides. La sensibilité des résidus aux défauts non-francs et la robustesse au bruit sont également analysées à l'aide de TC simulés. Il est montré que, en raison du bruit, les résidus forment un cluster dans l'espace des résidus, dont les caractéristiques dépendent de la gravité et de la localisation du défaut.

Contents

List of Figures

List of Tables

List of Abbreviations

NCS	**N**etworked **C**ontrol **S**ystem
ECU	**E**lectronic **C**ontrol **U**nit
TC	**T**ransmission **C**oefficient
PLC	**P**ower **L**ine **C**ommunication
OFDM	**O**rthogonal **F**requency **D**ivision **M**ultiplexing
CAN	**C**ontrol **A**rea **N**etwork
LIN	**L**ocal **I**nterconnect **N**etwork
MOST	**M**edia **O**riented **S**ystems **T**ransport
UTP	**U**nshielded **T**wisted **P**air
STP	**S**hielded **T**wisted **P**air
CSMA	**C**arrier **S**ense **M**ultiple **A**ccess
CSMA/CA	**C**arrier **S**ense **M**ultiple **A**ccess **C**ollision **A**voidance
FDTD	**F**inite-**D**ifference **T**ime-**D**omain
WT	**W**ater **T**reeing
FDTD	**F**inite **D**ifference **T**ime **D**omain
FFT	**F**ast **F**ourier **T**ransform
IFFT	**I**nverse **F**ast **F**ourier **T**ransform
SCN	**S**tar **C**ommunication **N**etwork
SEN	**S**tar **E**nergy **N**etwork
AWGN	**A**dditive **W**hite **G**aussian **N**oise
HPAV2	**H**ome**P**lug **AV2**
ADSL	**A**symmetric **D**igital **S**ubscriber **L**ine
MoCA	**M**ulti-media **O**ver **C**oas **A**lliance
QAM	**Q**uadrature **A**mplitude **M**odulation
QPSK	**Q**uadrature **P**hase **S**hift **K**eying

OSI	**O**pen **S**ystems **I**nterconnection
OPEN	**O**ne-**P**air **E**ther-**N**et
ISI	**I**nter-**S**ymbol **I**nterference
FRAC	**F**requency **R**esponse **A**ssurance **C**riterion
MFRAC	**M**odified **F**requency **R**esponse **A**ssurance **C**riterion
VNA	**V**ector **N**etwork **A**nalyzer
FRFRMS	**F**requency **R**esponse **F**unction **R**oot **M**ean **S**quare
BW	**B**and**W**idth
IEEE	**I**nstitute of **E**lectrical and **E**lectronics **E**ngineers
TDR	**T**ime **D**omain **R**eflectomery
FDR	**F**requency **D**omain **R**eflectomery
LS	**L**east **S**quare
LMMSE	**L**inear **M**inimum **M**ean **S**quare **E**rror
SIG	**S**pecial **I**nterest **G**roup
OABR	**O**PEN **A**lliance **B**roadR-**R**each

Dedicated to my parents Abdel Rahman ABDEL KARIM and Oumayma EL MANSOUR. . .

General Introduction

Transportation systems, spacecrafts, manufacturing plants, and many other technological systems are Network Control Systems (NCS). In such NCS, components such as sensors, actuators and controllers communicate through wired networks, by means of associated Electronic Control Units (ECU). Wired networks are mainly composed of cables that carry power and/or data from one component to another. These NCS are subject to faults that can degrade the global system performance. Faults can occur in the connected components or even in the interconnected cables. Generally, fault diagnosis methods are designed and used to detect, to localize and to identify faults in sensors, actuators and controllers. The cables are usually considered to be non faulty. However, these cables are subject to physical wear and tear, oxidation, moisture infiltration, insect and rodent infestation, which damage the cables and may lead to electrical circuit failures [1]. Technological advances and the need of more and more functionalities have increased the number of connected components in NCS and consequently have also increased the network complexity, which results in increasing the risks of cables' faults. Faults in cables are divided into two categories, namely ***soft faults*** and ***hard faults*** based on their severity and impact on the system behavior [2]. A soft fault is a degradation of the cable that does not affect the transmission of data and energy. It evolves over time to a hard fault (i.e. a short circuit or an open circuit) that leads to lose data or/and energy transmission which results in system failure. Hard faults may thus have critical consequences and must be avoided by implementing a monitoring system capable of detecting the soft faults and tracking their time evolution. Moreover, in order to guide the maintenance operations or to reconfigure the transmission system, the monitoring system should be able to identify the faulty branch of the network.

Different methods can be found in the literature to detect and localize faults in a wired network. The most frequently used methods are reflectometry-based methods which are derived from the principle of radar. These methods require to

measure and analyze the reflection coefficients of the network. The reflectometry-based methods have proven their efficiency to detect and locate hard faults. However researches are still in progress to extend these methods for soft fault detection and localization. The difficulties come from the weak reflections associated with this type of faults in a complex network with many nodes and branches. Recently, alternative methods, namely transferometry-based methods [3, 4], were proposed in the literature, where the transmission coefficients, instead of the reflection coefficients, are estimated and analyzed. One advantage is that the transmission coefficients (TC) are often estimated for communication purposes, as for instance in power line communication (PLC) technology [5, 6], and thus may be directly used with no need of additional measurements. Orthogonal frequency division multiplexing (OFDM) process is a well-known technique that is used for such TC estimation.

Very few research work have been reported in the literature on such transferometry-based fault detection and localization methods. The objective of this thesis is to contribute in this field by designing a monitoring system based on the transmission coefficients between the embedded electronic control units. The diagnosis performance is analyzed theoretically and using data obtained from a real test bench and from simulated networks.

The general principle of our approach is to compare the reference transmission coefficients of a fault-free network with the transmission coefficients estimated online when the NCS is operating. It should be noted that this approach only addresses single soft faults and does not address multiple faults. Health indicators are first defined. Using the well-known chain matrix model of the network, the fault sensitivity of these indicators is proven. Thus, based on the health indicators, structured residuals are proposed. Structural fault signatures of the residuals show that the fault may be detected and the faulty branch may be localized. The proposed fault detection and localization method is first validated on a Y-shaped network using real data extracted from a test bench. This experimental platform was developed within the framework of the DIACA project - Autonomous Predictive Maintenance of Wired Transport Systems, of the CPER ELSAT 2020 in the Nord Pas-de-Calais region (OS 4: Dimensioning and performance of the vehicle functions Intelligent mobility). Then, several tests are conducted using simulated data of different kinds of more complex networks as bus networks or hybrid

networks. The robustness and the sensitivity of the proposed residuals are studied using extensive simulations.

The main contributions of this thesis are the following.

- PLC-type transmission systems are used for online soft fault detection and faulty branch localization in simple and complex networks. Multiple faults are not covered by this work, only single soft faults are considered. The general principle of this fault detection and localization method is based on monitoring the consistency between the reference transmission coefficients with the actual transmission coefficients estimated between an ECU acting as a source, and the other ECU acting as receivers.
- Fault-sensitive health indicators and residuals are defined to compare reference transmission coefficients with actual transmission coefficients. The well-known transmission chain matrix model is used to express the sensitivity of the residuals to fault. Based on this sensitivity expression and the studied network topology, a fault signature matrix can be constructed. This signature matrix is used to detect the presence of a fault and to localize the faulty branch.
- A network decomposition method is proposed to handle complex networks with many branches and nodes. The principle is to decompose a hybrid network into familiar basic sub-networks (bus network, star network, Y-shaped network, point-to-point network, etc...). The fault detection and localization transmission-based method may be applied on each sub-network.
- Due to noise, the residuals are not exactly zero when expected which can affect the final decision. It is shown that weighting the residuals with a correlation index between the health indicators improves the sensitivity and robustness of the residuals.
- The sensitivity/robustness analysis of the residuals is studied with respect to the fault characteristics, i.e., fault severity and position, and the environmental characteristics, i.e., noise level. This analysis is performed using intensive simulations.
- The fault detection and localization method is validated on real measurements extracted from a Y-shaped test bench.

- The fault detection and localization method is validated on realistic simulated data using the transmission chain model on a complex network (bus). The decomposition procedure is also validated using these simulations.

This thesis is structured as follows:

- Chapter 1 : In this chapter, a general introduction to wired communication networks is presented. The transmission coefficients of these networks serve as a defining characteristic. Using the ABCD modeling approach, the expressions of the transmission coefficients of various network topologies in their no-fault and faulty situations are also given.
- Chapter 2: This chapter presents several methods for wired network fault detection and localization. The general approach of our transferometry-based fault detection and localization method is then described for a Y-shaped network. This method is validated using real measurements taken from a test bench and data generated via extensive simulation of the ABCD modeling method.
- Chapter 3 : In this chapter, the proposed transferometry-based fault detection and localisation is extended to more complicated networks, namely networks with a combination of different network topologies. Then, three different fault detection and localization approaches are proposed for a bus network, and their computational cost and communication burden are compared.
- Chapter 4 : Conclusions and future work end this thesis.

Chapter 1

Transmission coefficients of wired networks in presence of fault

This chapter provides an overview of communication and power networks, as well as information on network characteristics. Faults can occur in these networks; these faults are then introduced and their influences are addressed. These networks can be characterised by their transmission coefficients, i.e. the transfer function of the network. These transmission coefficients are expressed for different network topologies in both their no-fault and faulty situations using the ABCD-matrix model, a well-known network modeling method. The Power Line Communication (PLC) technology is then detailed and the estimation of the transmission coefficients required for communication purpose is highlighted.

1.1 Network fundamentals

Wired networks are still necessary in many industrial applications despite all of the advancements made in wireless communication [7]. This is because using a wired network provides better data rates, less electromagnetic interference, more secure communication, etc [8]. Networked control systems (NCS) are systems whose components, such as sensors, actuators and controllers, are connected to the network to share resources and information used to control the system. These networks are mainly composed of cables whose function is to transport power and data. According to Fortune Business Insights, the global wire and cable market size

was USD 181.28 billion in 2021 and it is expected to grow to USD 294.73 billion by 2029 [9]. They are used in a wide range of end-use industries such as aerospace and defense, building and construction, oil and gas, computer and telecommunications, transportation systems and others. Networks are characterized by the type of the used cables (coaxial, twisted cables, etc...), the network topology (detailed in 1.2.3), the communication protocol [10, 11] (scheduled-based medium access [12–14], contention-based medium access [15, 16] and controlled access protocols [17, 18]) and the communication method (not advanced or advanced). The network characteristics are shown in Fig. 1.1.

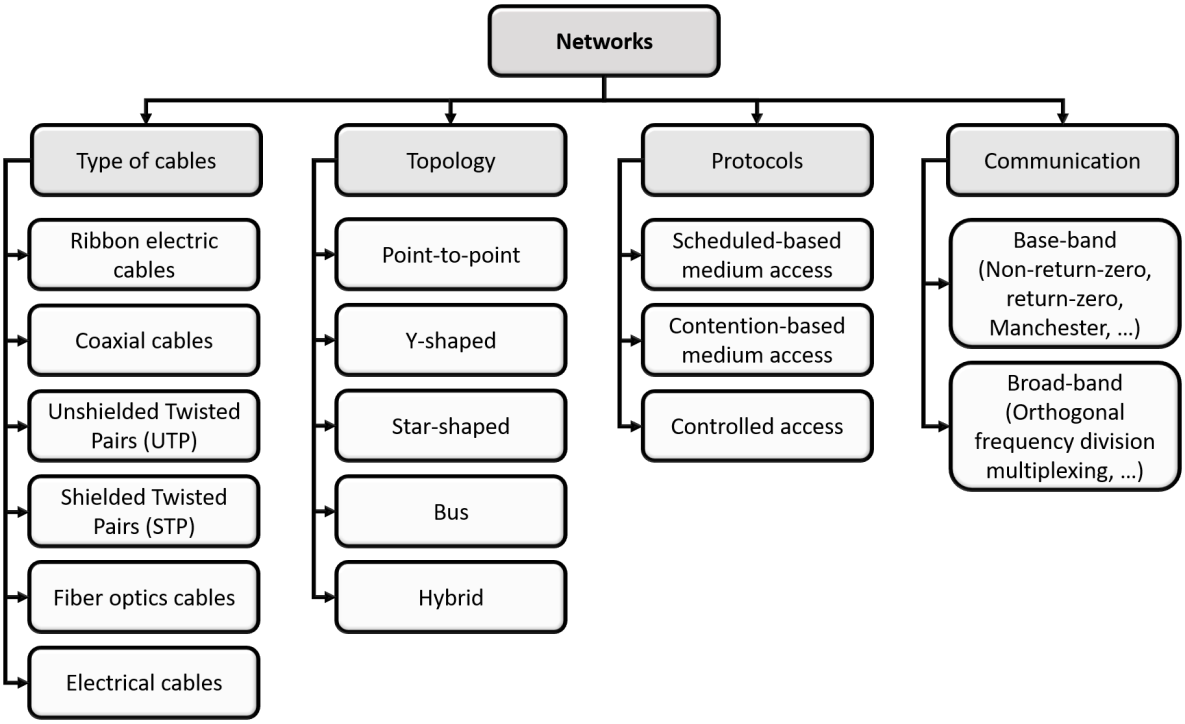

FIGURE 1.1: Network characteristics.

Depending on the characteristics of the network and the field of application, various types of communication networks can be found, such as Profibus for electrical networks in an industrial environment [19]. In transportation systems such as road vehicles, the traditional used wired networks are Control Area Network (CAN) [20], Local Area Network (LIN) [21], Media Oriented Systems Transport (MOST) [22] and FlexRay [23]. However, vehicular network may converge to an Ethernet-based network that could replace CAN, LIN and FlexRay networks with suitable Ethernet standards [24–26]. In smart grids applications [27, 28] and home automation applications [5, 29], G3-PLC technology operates in a powerline channel [30]. A summary of the characteristics of these networks is presented in the Table 1.1.

TABLE 1.1: Standard networks and their characteristics

	Type of cable	Topology	Protocol	Communication
Profibus	UTP/STP or fiber	Bus	Controlled (Token)	Base-band
CAN	UTP/STP	Bus	Contention-based (CSMA)	Base-band
LIN	Single cable	Bus	Controlled (Master-slave)	Base-band
Automotive Ethernet	UTP/STP	Point-to-point or Bus	Contention-based (CSMA)/CD)	Base-band
G3-PLC	Electrical	Hybrid	Contention-based (CSMA)	Broad-band (OFDM)

1.2 Network characterization

This section deals with the representation of transmission lines as a succession of RLCG elementary circuits, with a focus on unshielded twisted pair cables. Next, various network topologies are shown. Later, multiple networks will be modeled using the RLCG representation along with the network topologies.

1.2.1 RLCG circuit representation

The transmission lines are usually represented as small successive sections and each section can be represented as an elementary RLCG circuit like the one presented in Figure 1.2. The RLCG parameters are known as the primary parameters of a transmission line. They depend on the type and the geometry of the cable. They are also frequency dependent due to the tendency of the current to flow more on the outer than the inner strands of the conductor (skin effect) and the alternating magnetic flux produced by the current in one conductor caused by the current in a neighboring conductor (proximity effect) at high frequencies. The evolution of voltage v and current i on an electrical transmission line as a function of distance x and time t is described by a system of two partial differential equations known as the telegraphers' equations [31].

$$\begin{cases} \frac{\partial v(x,t)}{\partial x} = -L\frac{\partial i(x,t)}{\partial t} - Ri(x,t) \\ \frac{\partial i(x,t)}{\partial x} = -C\frac{\partial v(x,t)}{\partial t} - Gv(x,t) \end{cases} \tag{1.1}$$

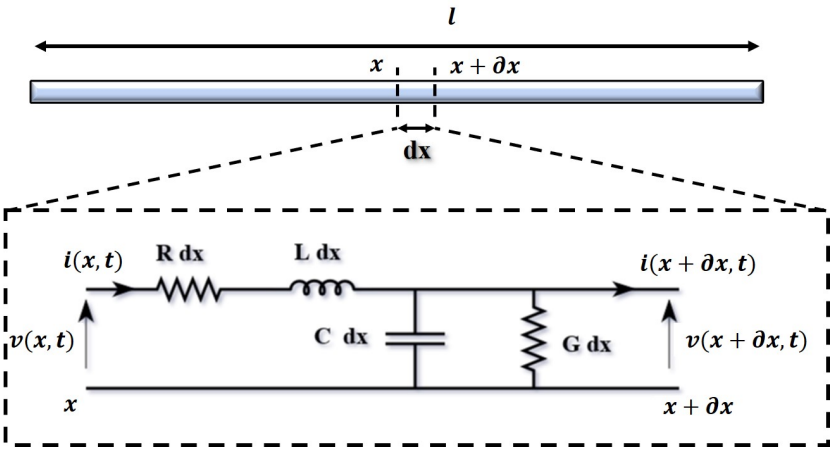

FIGURE 1.2: Representation of a transmission line section of unit length as an RLCG circuit for two conductor lines.

where R, L, C and G are the primary parameters that can be expressed in Table 1.2. The Finite Difference Time Domain (FDTD) method is a numerical method to find the solution of the telegraphers' equations [32]. The numerical implementation of this equation is detailed in [32]. The length of a line l, is divided into $ncells$ sections, each of length ∂x, similarly, the time of simulations $simtime$ is divided into nt segments of length ∂t. Each portion of length ∂x is represented by an RLCG circuit as seen in Fig. 1.2. To ensure the numerical stability of the solution, ∂x and ∂t must satisfy the Courant-Friedrichs-Lewy condition (CFL) which states that the time step must not be greater than the propagation time on each cell.

$$\partial t < \frac{\partial x}{v_p} \longrightarrow \partial t = cfln \cdot \frac{\partial x}{v_p} \tag{1.2}$$

where $cfln$ is a positive coefficient strictly smaller than 1. The ∂x is chosen small enough so that each ∂x section is electrically small (An electrically small section is a section much shorter than the wavelength of the signal it is intended to transmit or receive).

1.2.2 Primary parameters

The studied cable is an Unshielded Twisted Pair (UTP) cable. Twisted pair cables are classified by category. Each category is measured by the number of twists per inch, for example CAT 5 has three twists per inch [33]. It is well known that higher twist ratio reduces electromagnetic radiation and resists to external interference. However, it increases high-frequency attenuation due to the increased capacitance per meter. For a more accurate modeling of such a line, several important factors

must be taken into account such as : the material and composition of the structure, the twisting pitch, the skin effect and the proximity effect. Expressions of parameters R, L, C and G for an unshielded twisted pair cable are given in [34] for an unshielded twisted pair cable. These expressions are detailed in the table 1.2 for UTP cables:

R	L	C	G
$\frac{2\eta}{d}\sqrt{\frac{f\mu_0}{\pi\sigma}}$	$\frac{\mu_0}{\pi}acosh(\frac{D}{d}) + \frac{\sqrt{\pi f\frac{\mu_0}{\sigma}}}{2f\pi^3 d}\cdot\frac{1}{\sqrt{1-(\frac{f^2}{D})}}$	$\frac{\pi\epsilon}{acosh(\frac{D}{d})}$	$2\pi f\cdot tan(\delta)\cdot C$

TABLE 1.2: Analytical expression of primary parameters for UTP cables.

All the parameters and constants in table 1.2 are defined and their values are given in the table 1.3 [35]. The primary parameter values are computed using the expressions presented in table 1.2 and the values presented in table 1.3. The variation of the primary parameters as a function of the frequency are presented in Fig. 1.3. The values obtained are of the same order as the values obtained in [36] for an UTP. The values of the primary parameters are not provided and are challenging to get in real life application. Considering that we don't actually know these parameters' values, we will only use them for simulations in this thesis.

Frequency (f)	$[0.1 : 1e^{-3} : 100]\ MHz$
Conductor diameter (d)	$1.12e^{-3}\ m$
Distance between conductors (D)	$2.11e^{-3}\ m$
Copper conductivity (σ)	$5,8e^{7}\ S/m$
Vacuum permeability (μ_0)	$4\pi 10^{-7}\ H/m$
Dielectric loss tangent $\tan(\delta)$	$2,83e^{-2}$
Dielectric permittivity (ϵ)	$1.3773e-11$
Corrective term : (η)	$1 \leq \eta \leq 1.3\ (\eta = 1)$

TABLE 1.3: Definition and values of constants and parameters [35]

The different network topologies are then described in detail so that our proposed approach can be used to any network's topology.

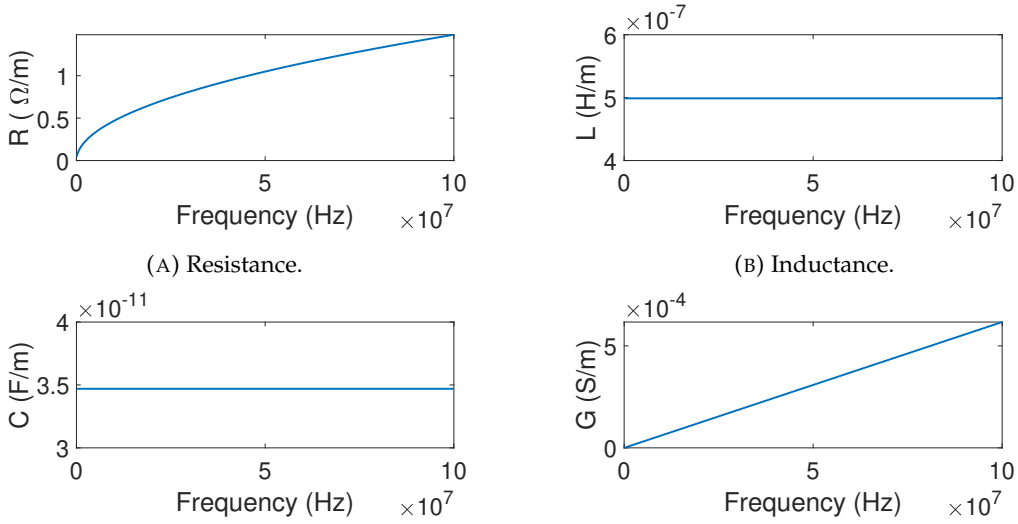

(A) Resistance.

(B) Inductance.

(C) Capacitance.

(D) Conductance.

FIGURE 1.3: Variation of computed RLCG parameters of an unshielded twisted pair as a function of the frequency.

1.2.3 Network topology

The network topology is the arrangement of the various geometric electronic devices (i.e., ECU, sensors, actuators, etc.) in the network, as well as their location and cable installation. It can be classified into two types namely: "physical topology" and "logical topology". The former represents the physical interconnections of the electronic devices in the network, while the latter represents the flow of data through the network. These two types are defined by the two lower layers of the Open Systems Interconnection (OSI) reference model [37].

Logical topologies may be of two types:

- Logical bus where data flow from the source device to all receiving devices. Only the device for which the data is intended will process it, the other devices will ignore it.
- A logical ring where data flow from the source device to the recipient device. Since the receiver is not the intended recipient of the data, the receiver transfer the data to another device until the intended recipient of the data receives it.

The most well-known physical topology types, shown in Fig. 1.4 [38], [39], [40], are :

- Point-to-point topology: two devices are connected directly together with a common cable forming a point-to-point link.
- Bus topology: this network is made up of a main line, called the backbone, to which all the devices are connected by short connecting cables at different connection points.
- Star topology: all the devices are connected by their own cable with a point-to-point connection to a central device (hub - switch - router) which plays the role of master. The master coordinates the communication between the other devices called slaves. The latter cannot communicate directly with each other.
- Ring topology: each device is connected to two other devices on each side of it (point-to-point link) forming a single ring-shaped data path.
- Mesh topology: each device is directly connected to all other devices on the network with a point-to-point connection.
- Tree topology: the connected devices are arranged like branches of a tree, with a point-to-point connection.
- Hybrid topology: a combination of two or more topologies.

In smart grid applications, the most used topologies for Home Area Networks are bus topology, tree topology and mesh topology [41]. In industrial and instrumentation applications [42], a bus network is one of the most widely used topology for data transmission. In transportation systems applications, the massive deployment of electronic components has led to the migration from a point-to-point connection between devices to multiplexing, i.e. bus and hybrid topologies [43].

The wiring harness in an electrical vehicle distributes power and signals. The complexity of such a harness is shown in Table 1.4, where, for an average class vehicle, the number of wires is around 750. Compared to conventional wiring, bus

TABLE 1.4: Cable bundle complexity (typical values) [44]

	Small vehicle	medium-class vehicle	luxury-class vehicle
Number of connectors	70	120	250
Number of cables	350	750	1500
Total length of cabling	700 m	1500 m	3200 m

networks offer significant advantages, among them

- Lower material costs for the cables.

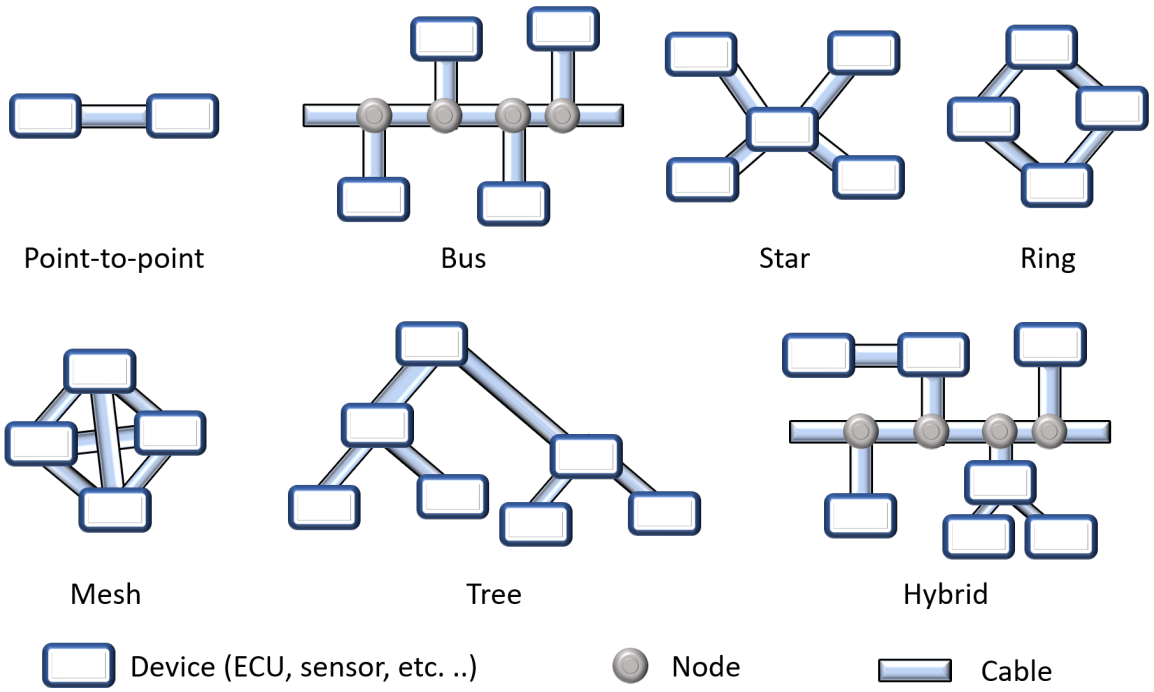

FIGURE 1.4: Network topologies.

- Less space is required and the weight of the cabling is reduced.
- Fewer connectors are likely to fail.
- Data can be distributed to various receivers.

Cables are generally installed in harsh environments, making them prone to degradation or faults. These faults are addressed in the next section.

1.3 Faults in cables

1.3.1 Introduction to soft and hard faults

Cables are prone to faults due to their environment: moisture can cause water-tree degradation [45], mechanical stresses and strains can crack the cable insulation (Fig. 1.5a, 1.5b), heat can cause thermal degradation (Fig. 1.5c) and chemicals can contaminate the wire.
A number of potential faults can occur in cables such as bad connections or insulation failure and possibly conductor cuts. These faults are divided into two categories, namely *soft* faults (Fig. 1.5) and *hard* faults (Fig. 1.6), based on their

severity and impact on data and energy transmission [2]. Degradation, faults, soft faults and hard faults have several different meaning in the literature. In this thesis, the following definitions are used:

Definition 1 *A degradation or a soft fault is defined as an irreversible localized alteration of at least one characteristic of a system component [46]. A system with a degraded component can still perform its functions. In the context of wired networks, the cable can still be used to carry data and/or power in presence of a degradation (or soft fault) [47]. In this manuscript, the words degradation and soft fault will be used indifferently.*

Definition 2 *A hard fault or a fault is defined as a deviation of at least one characteristic property of the system which leads to an inability to perform the required task [46, 48, 49]. In the context of wired networks, the cable is not able to carry data and/or power in presence of a hard fault (i.e. short-circuit or open-circuit) [47].*

Improper cable installation conditions (e.g., irregular twist, sharp bend, etc ...) do not immediately affect the performance of the unshielded twisted pair (UTP) transmission line. However, they are degraded by such conditions [50]. Over time, the degradation tends to develop to hard faults where cable degradation can result in a short circuit (Fig. 1.6a) or an open circuit (Fig. 1.6b) interrupting data and energy transmission and resulting in total system breakdown.
Specimens of soft faults are shown in Fig.1.5: rubbing of the wires against each other for long periods of time can cause an insulation cut, as shown in Fig. 1.5a and in Fig. 1.5b. If this rubbing persists, the exposed conductor can also be cut, resulting in an open circuit. In Fig. 1.5c, the physical characteristics of the insulation changes with excess heat, if overheated the insulation may be damaged by fusion and can cause a hard fault.
Hard faults can lead to dramatic events such as the explosion and crash of the TWA 800 Boeing 747 (1996) and Swissair MD-11 (1998) [51], or vehicle fires[1], and therefore they must be avoided.
Analytical and empirical representations of the different types of soft faults are developed in the following.

1.3.2 Characterization of the influence of soft faults

The influence of a soft fault (or degradation) on the model results in a local alteration of one or more of the primary parameters R, L, C, G, which inevitably leads to a small

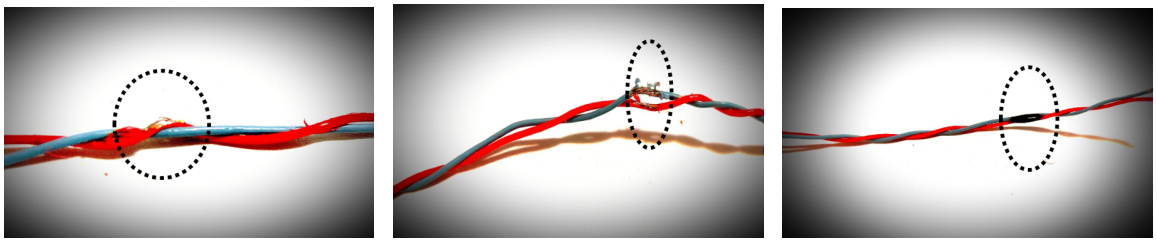

(A) Insulation cut. (B) Double insulation cut. (C) Thermal degradation.

FIGURE 1.5: Soft faults specimens.

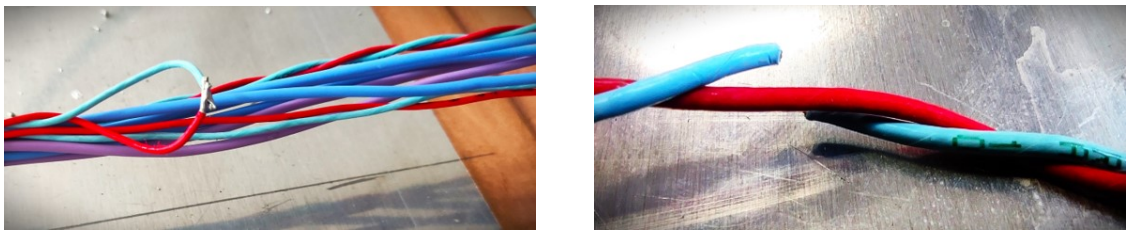

(A) Short-circuit. (B) Open circuit.

FIGURE 1.6: Hard faults specimens.

change in the local impedance, thus a change in the propagation velocity. Different characterizations of the influence of soft faults are presented in Table 1.5. A brief description of these characterizations is given below:

- The finite-integral technique is a numerical method that solves electromagnetic field problems in the spatial and frequency domain. It is used in [52] to calculate the value of the impedance of a cut insulation.
- The impact of Water-Treeing (WT) on the affected area of the cable is a change in its dielectric parameters according to [53, 54]. The total permittivity of the degraded area of the cable is a function of the dielectric permittivity of water and the dielectric permittivity of the insulation.
- A local or homogeneous cable degradation that is due to thermal effect (excess heat) can be represented by a variation in the linear capacitance C of the cable [34, 55].
- A pullout of the jacket and shield of a twisted pair cable (AWG24) or a coaxial cable (RG58CU) is represented by an insertion of an impedance $Z_f = [25 - 125]\Omega$ in series or in parallel [55].
- The faulty section represented by a shielding cut of a coaxial cable can be replaced by an equivalent circuit which results in localized changes in the linear capacitance C and the linear inductance L of the cable [56].

Ref	Cable	Soft fault	Impact	Characterization
[52]	Coaxial	Insulation cut	Small change in the wire impedance	Finite-integral technique to compute Z_f
[53, 59]	Multi-core N2XSEY	Homogeneous or local Water-treeing	Change in the dielectric permittivity	Variation of ϵ
[34, 55]	Coaxial	Degradation (Thermal)	Growth of relative permittivity and dielectric loss	Variation of C $[0.2 : 0.2 : 1.2] \cdot C$
[55]	STP, Coaxial	Sheath and shielding torn off	Local Alteration of the characteristic impedance Z_c	Insertion of a parallel or serial impedance [25-125 Ω]
[56]	Coaxial	Shielding cut	Modifications of the radiation and induction effect ($\Delta L \geq 0$), modification of the radius of the outer conductor ($\Delta C \leq 0$)	Equivalent circuit : Z_d in series and Y_d in parallel
[57]	Coaxial	Partial degradation of the shielding	Change in relative permittivity	Variation of ϵ : $\epsilon_0 \leq \epsilon \leq \epsilon_{insulator}$
[58]	Triple-core	Water-treeing	low-impedance short circuit	Insertion of an impedance R_f

TABLE 1.5: Characterization of the influence of the fault.

- The degraded section of a cable is represented by a change in the relative permittivity of the cable insulation in [57] in such a way that the modified relative permittivity must be between the value of the permittivity of the air and that of the cable insulation.
- Soft faults caused by an excess of humidity are represented in [58] as an insertion of an impedance R_f where the value of this impedance can change to emulate different set of cables' faults.

The local variation of the primary parameters due to the influence of the soft fault may be represented by an adding impedance Z_f. The effect of moisture inside a connector or a series arc can be represented by the insertion of an impedance Z_f in series and an insulation fault or a large local heating (hot spot) or a parallel arc can be represented by the insertion of an impedance Z_f in parallel [60]. The nature of a fault, represented by Z_f, is related to information about the predominant linear parameter R, L, C or G. If the linear resistance R is predominant, the fault is called a resistive fault. It causes a faster degradation than a fault of a different nature [61]. This is due to the fact that resistive faults generally result from a degradation of

the cable conductor, whereas inductive or capacitive faults result from a superficial degradation of the cable insulation [61]. Therefore, resistive type faults are our main focus in this work.
The types of cable faults, the type of used cables and network topologies are detailed ahead. Any network can thus be modeled in its no-fault and its faulty situations. In the following, the network modeling method is detailed.

1.4 Network Modeling method

The network models are developed in the following so that we can use them later for simulation and for fault detection and localization purposes. Simulations are used to test and validate our fault detection and localization approach on realistic simulated data. The model is also used to study the sensitivity of our health indicators to faults and further to derive the residuals for fault detection and localization.
The modeling of a transmission line can be addressed by two different approaches: the "top-down approach" and the "bottom-up approach". A state of the art on these two approaches to channel modeling can be found in [62]. The studied network is viewed as a "black box" by the top-down approach, whereas the studied network is viewed as a "deterministic quantity" that depends on the network topology and its electrical component by the bottom-up approach. In the top-down approach, extensive measurements of the transmission coefficients between two terminal components of the network must be made to estimate the analytical model parameters using fitting algorithms [63–67]. The top-down approach is more computationally simple than the bottom-up approach and can be useful in case of lack of information about the network topology, electrical components, etc .... The bottom-up approach requires a perfect knowledge of the targeted network such as its topology, the characteristics of the cables used, the impedance of the terminal load, etc...
The chain matrix model that will be detailed in the subsection 1.4.1 is one of the most well-known and used bottom-up approaches [68]. This method is used under the condition of $\lambda_m < l$ with λ_m denoting the wavelength of the highest frequency of the transmitted signal and l denoting the length of the cable.
The Finite Difference Time Domain (FDTD) simulation of the telegraphers' equation in (1.1) does not take into account the variations of the primary parameters R and G with frequency [69]. These issues can be resolved and the modeling process can be made simpler by modeling in the frequency domain.

1.4.1 Chain matrix model

The network is modeled in the frequency domain using the ABCD matrix method or the chain matrix method [70]. The Fourier transform can be applied to the telegraphers' equations in (1.1). The sources are single frequency sinusoids and are assumed to have been applied long enough to be steady state [71]. The time derivative $\frac{\partial}{\partial t}$ is replaced by $j\omega$. The equivalent frequency domain equation of (1.1) is :

$$\begin{cases} \dfrac{\partial V(x)}{\partial x} = -j\omega L I(x) - R I(x) \\ \dfrac{\partial I(x)}{\partial x} = -j\omega C V(x) - G V(x) \end{cases} \tag{1.3}$$

After differentiating (1.3) with respect to x, the resulting equation is:

$$\begin{cases} \dfrac{\partial^2 V(x)}{\partial x^2} = (R + j\omega L)(G + j\omega C) V(x) \\ \dfrac{\partial^2 I(x)}{\partial x^2} = (R + j\omega L)(G + j\omega C) I(x) \end{cases} \tag{1.4}$$

with the propagation constant $\gamma = [(R + j\omega L)(G + j\omega C)]^{\frac{1}{2}}$, the equation (1.4) can be written as:

$$\begin{cases} \dfrac{\partial^2 V(x)}{\partial x^2} = \gamma^2 V(x) \\ \dfrac{\partial^2 I(x)}{\partial x^2} = \gamma^2 I(x) \end{cases} \tag{1.5}$$

The general solution of this equation is:

$$\begin{cases} V(x) = V^+ e^{-\gamma x} + V^- e^{\gamma x} \\ I(x) = \dfrac{V^+}{Z_c} e^{-\gamma x} - \dfrac{V^-}{Z_c} e^{\gamma x} \end{cases} \tag{1.6}$$

The characteristic impedance of the line is denoted by $Zc = (\frac{R+jwL}{G+jwC})^{\frac{1}{2}}$. V^+ and V^- are constants to be determined from the terminal connections. The equation (1.6), is written in matrix form and then used at both bounds at $x = 0$ in (1.7) and $x = l$ in (1.8) where l denotes the length of the line.

$$\begin{bmatrix} V(0) \\ I(0) \end{bmatrix} = \begin{bmatrix} 1 & 1 \\ \frac{1}{Z_c} & \frac{-1}{Z_c} \end{bmatrix} \begin{bmatrix} V^+ \\ V^- \end{bmatrix} \tag{1.7}$$

$$\begin{bmatrix} V(l) \\ I(l) \end{bmatrix} = \begin{bmatrix} e^{-\gamma l} & e^{\gamma l} \\ \frac{e^{-\gamma l}}{Z_c} & -\frac{e^{\gamma l}}{Z_c} \end{bmatrix} \begin{bmatrix} V^+ \\ V^- \end{bmatrix} \tag{1.8}$$

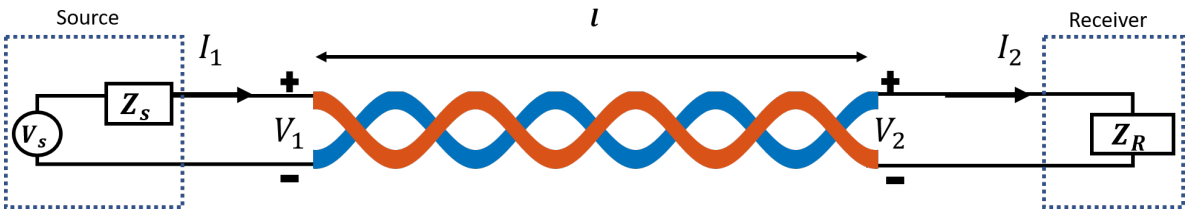

FIGURE 1.7: Simple network.

The chain parameter matrix M form helps us connect the voltage and current at the input of the line to those at the output of the line using the equations above [71] :

$$\begin{bmatrix} V(l) \\ I(l) \end{bmatrix} = M \begin{bmatrix} V(0) \\ I(0) \end{bmatrix} \tag{1.9}$$

$$\text{with } M = \begin{bmatrix} \cosh[\gamma l] & -Z_c \sinh[\gamma l] \\ -\frac{1}{Z_c} \sinh[\gamma l] & \cosh[\gamma l] \end{bmatrix}$$

The ABCD-matrix is defined as the inverse of the chain parameter matrix:

$$\begin{bmatrix} V(0) \\ I(0) \end{bmatrix} = \begin{bmatrix} A & B \\ C & D \end{bmatrix} \begin{bmatrix} V(l) \\ I(l) \end{bmatrix} \tag{1.10}$$

with $A = \cosh[\gamma l]$, $B = Z_c \sinh[\gamma l]$, $C = \frac{1}{Z_c} \sinh[\gamma l]$ and $D = \cosh[\gamma l]$. The ABCD-matrix model is used in the following to model both a simple network and cascaded networks.

1.4.2 Network modeling via ABCD-matrix

At first, a simple network is modeled using the ABCD-matrix model then cascaded networks are modeled.

1.4.2.1 Simple network modeling

The simple network, presented in Fig. 1.7, is modeled in the following using the ABCD model. The equation (1.11) relates the voltage V_1 and the current I_1 at the

input of the network to the voltage V_2 and the current I_2 at the output of the network.

$$\begin{bmatrix} V_1 \\ I_1 \end{bmatrix} = \begin{bmatrix} \cosh[\gamma l] & Z_c \sinh[\gamma l] \\ \frac{1}{Z_c} \sinh[\gamma l] & \cosh[\gamma l] \end{bmatrix} \begin{bmatrix} V_2 \\ I_2 \end{bmatrix} \tag{1.11}$$

From the Fig. 1.7, we have :

- At the source : $V_1 = V_s - Z_s \cdot I_1$.
- At the receiver : $V_2 = Z_R \cdot I_2$.

1.4.2.2 Cascaded network modeling

To model multiple lines cascaded in series, the overall ABCD-matrix is the product of the ABCD-matrix of each individual line where the branches are replaced by an equivalent impedance [72]. The individual line can be a simple network as in 1.4.2.1, a series impedance or a parallel impedance.
A series impedance Z_s is represented by the matrix ϕ_s as in (1.12) :

$$\phi_s = \begin{bmatrix} 1 & Z_s \\ 0 & 1 \end{bmatrix} \tag{1.12}$$

As seen in Table 1.5, a series impedance can represent a soft fault.
A parallel impedance Z_p is represented by the matrix ϕ_p as in (1.13) :

$$\phi_p = \begin{bmatrix} 1 & 0 \\ \frac{1}{Z_p} & 1 \end{bmatrix} \tag{1.13}$$

A parallel impedance can represent all branches connected to a node, where each connected branch can be represented as an impedance. The equivalent impedance $Z_{eq_{i,k}}$ of a branch B_i terminated by an impedance $Z_{R_{i,k}}$ and connected to a node n_k is computed using computed using (1.14) :

$$Z_{eq_{i,k}} = \frac{a_i \cdot Z_{R_{i,k}} + b_i}{c_i \cdot Z_{R_{i,k}} + d_i} \tag{1.14}$$

with a_i, b_i, c_i and d_i are the ABCD parameters of the branch B_i. The impedance Z_{p_k} is the equivalent parallel impedance of several branches connected to the same node

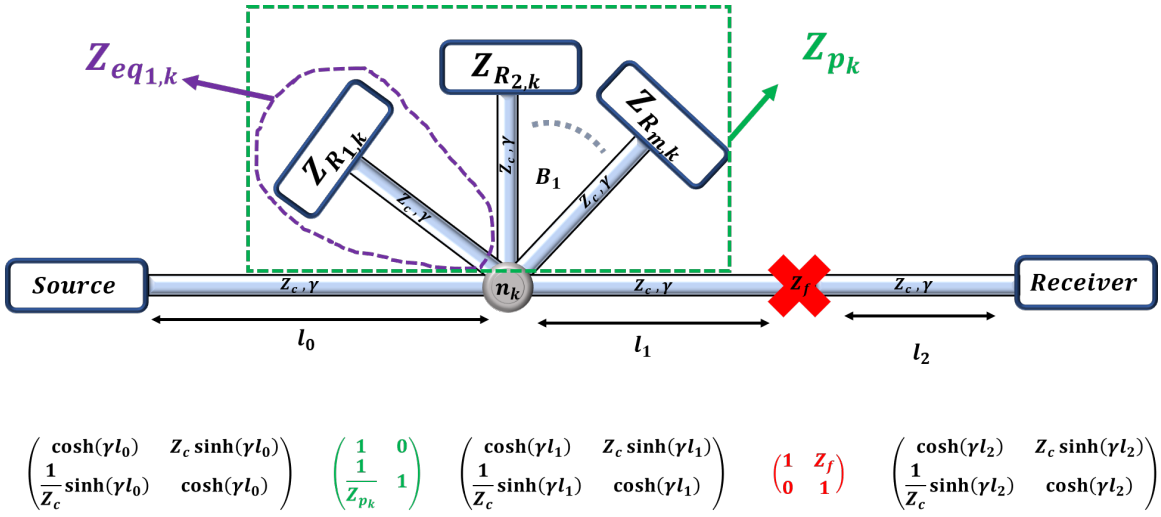

FIGURE 1.8: Cascaded ABCD-matrices.

n_k. It is computed using (1.15) :

$$\frac{1}{Z_{p_k}} = \sum_{i=1}^{i=m_k} \frac{1}{Z_{eq_{i,k}}} \tag{1.15}$$

with $i \in \{1, 2, 3, \ldots, m_k\}$ and m_k is the number of branches connected to the node n_k. An illustration of a cascaded network is presented in Fig. 1.8. In this figure, each part of a network between a source and a receiver is represented by its appropriate matrix. The ABCD-matrix representing the whole network is the product of all the matrices in the Fig. 1.8.

1.4.3 Relationship between ABCD-matrix and S-parameters

As previously mentioned, the model will be used to perform simulations to validate the performance of our method and to study the sensitivity of our health indicators. We will also validate our method with data measured on a test bench. A vector network analyser (VNA) is used to characterize a network by measuring the insertion loss $S_{21}(f)$ between two port of the network under test at each frequency f. The insertion loss $S_{21}(f)$ corresponds to $\frac{2 \cdot V_2}{V_S}$ which corresponds to a factor 2 of the transfer function $H(f)$ also called Transmission Coefficient (TC) [73]. To simplify in the following, we consider that $S_{21}(f)$ and $H(f)$ express the same quantity. The factor 2 which is not considered will have no influence in the following developments.

$$H(f) = S_{21}(f) = \frac{2 \cdot V_2}{V_s} \tag{1.16}$$

$H(f)$ is expressed as function of the ABCD parameters in the following. Using (1.10) in a simple network such presented in Fig. 1.7 :

$$V_1 = A \cdot V_2 + B \cdot I_2 \tag{1.17}$$

$$I_1 = C \cdot V_2 + D \cdot I_2 \tag{1.18}$$

And,

$$H(f) = \frac{2 \cdot V_2}{V_s} = \frac{2 \cdot V_2}{V_1 + Z_s \cdot I_1} \tag{1.19}$$

$$= \frac{2 \cdot V_2}{A \cdot V_2 + B \cdot I_2 + Z_s \cdot (C \cdot V_2 + D \cdot I_2)} \tag{1.20}$$

with $V_2 = Z_R \cdot I_2$ and under the condition of matched impedance [74, 75], $Z_s = Z_R = Z_c$:

$$H(f) = \frac{2 \cdot V_2}{A \cdot V_2 + B \cdot \frac{V_2}{Z_c} + Z_c \cdot (C \cdot V_2 + D \cdot \frac{V_2}{Z_c})} = \frac{2}{A + \frac{B}{Z_c} + Z_c \cdot C + D} \tag{1.21}$$

1.5 Transmission coefficients of different network topologies under no-fault and faulty situations

The transmission coefficients between an electronic control unit acting as a source and another acting as a receiver in different network topologies is expressed below using the ABCD modeling approach.

1.5.1 Point-to-point network

In a point-to-point connection, the network under study is composed of two ECU and a branch of length l connecting them, as shown in the Fig. 1.9. Mesh networks, tree networks and ring networks are all considered as networks with a set of point-to-point connection between their ECU, so the same expressions for the transmission coefficients are obtained for all these networks as for a point-to-point connection. Let us consider that the ECU_0 acts as a source and ECU_1 acts as a

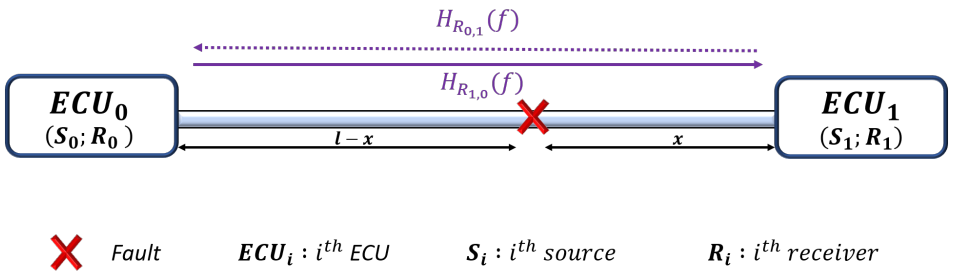

FIGURE 1.9: Representation of a point-to-point network.

receiver. In the following, the no-fault and faulty situations of a point-to-point network are studied.

1.5.1.1 No-fault situation

In the no-fault situation of the network, the network is free of faults. The fault-free branch between the two ECU is represented by the following ABCD matrix:

$$SN^h(l) = \begin{bmatrix} A_S^h & B_S^h \\ C_S^h & D_S^h \end{bmatrix} = \begin{bmatrix} \cosh[\gamma l] & Z_c \cdot \sinh[\gamma l] \\ \frac{1}{Z_c} \cdot \sinh[\gamma l] & \cosh[\gamma l] \end{bmatrix} \tag{1.22}$$

using (1.21), the transmission coefficient between S_0 and R_1 in the no-fault nominal (noise is not considered) situation, $H_{R_{1,0}}^h(f)$, is expressed as follows:

$$H_{R_{1,0}}^h(f) = \frac{2}{A_S^h + \frac{B_S^h}{Z_c} + C_S^h \cdot Z_c + D_S^h} = \frac{1}{e^{\gamma l}} \tag{1.23}$$

1.5.1.2 Faulty situation

Let's consider the situation where the network is faulty, a fault Z_f is located at the branch connecting the two ECU. The faulty branch of length l can be divided into three parts. Each part is represented by an appropriate matrix, so $SN^f(l,x)$ is expressed as the product of these three matrices, with x denoting the distance between the fault position and the ECU_1. The first matrix represents the part of the line of length $l - x$ before the fault position, $SN^h(l-x)$, the second represents a serial fault Z_f and the third matrix represents the part of the line of length x after the fault, $SN^h(x)$.

$$SN^f(l,x) = \begin{bmatrix} A_S^f & B_S^f \\ C_S^f & D_S^f \end{bmatrix} = SN^h(l-x) \cdot \begin{bmatrix} 1 & Z_f \\ 0 & 1 \end{bmatrix} \cdot SN^h(x)$$

which gives :

$$SN^f(l,x) = \begin{bmatrix} \cosh[\gamma l] + \frac{Z_f}{Zc} \cdot \cosh[\gamma(l-x)] \cdot \sinh[\gamma x] & \\ \frac{1}{Z_c} \cdot \sinh[\gamma l] + \frac{Z_f}{Z_c^2} \cdot \sinh[\gamma(l-x)] \cdot \sinh[\gamma x] & \\ & Z_c \cdot \sinh[\gamma l] + Z_f \cdot \cosh[\gamma(l-x)] \cdot \cosh[\gamma x] \\ & \cosh[\gamma l] + \frac{Z_f}{Z_c} \cdot \sinh[\gamma(l-x)] \cdot \cosh[\gamma x] \end{bmatrix} \tag{1.24}$$

In the faulty situation, the transmission coefficient $H^f_{R_{1,0}}(f)$ between S_0 and R_1 is :

$$H^f_{R_{1,0}}(f) = \frac{2}{A_S^f + \frac{B_S^f}{Z_c} + C_S^f \cdot Z_c + D_S^f} \tag{1.25}$$

According to (1.24):

$$\begin{aligned} & A_S^f + \frac{B_S^f}{Z_c} + C_S^f \cdot Z_c + D_S^f \\ & = \cosh\gamma l + \frac{Z_f}{Zc} \cdot \cosh\gamma(l-x) \cdot \sinh\gamma x + \frac{Z_c \cdot \sinh\gamma l + Z_f \cdot \cosh\gamma(l-x) \cdot \cosh\gamma x}{Z_c} \\ & + Z_c \cdot (\frac{1}{Z_c} \cdot \sinh\gamma l + \frac{Z_f}{Z_c^2} \cdot \sinh\gamma(l-x) \sinh\gamma x) + \cosh\gamma l + \frac{Z_f}{Z_c} \cdot \sinh\gamma(l-x) \cdot \cosh\gamma x \\ & = 2 \cdot e^{\gamma l} + \frac{Z_f}{Z_c} \cdot \cosh\gamma(l-x) \cdot \sinh\gamma x + \frac{Z_f}{Z_c} \cdot \cosh\gamma(l-x) \cdot \cosh\gamma x \\ & + \frac{Z_f}{Z_c} \cdot \sinh\gamma(l-x) \cdot \sinh\gamma x + \frac{Z_f}{Z_c} \cdot \sinh\gamma(l-x) \cdot \cosh\gamma x \\ & = 2 \cdot e^{\gamma l} + \frac{Z_f}{Z_c} \cosh\gamma l + \frac{Z_f}{Z_c} \sinh\gamma l = 2 \cdot e^{\gamma l} + \frac{Z_f}{Z_c} \cdot e^{\gamma l} \end{aligned} \tag{1.26}$$

The final expression of $H^f_{R_{1,0}}(f)$ in the faulty situation is :

$$H^f_{R_{1,0}}(f) = \frac{1}{e^{\gamma l} + \frac{Z_f}{2Z_c} \cdot e^{\gamma l}} \tag{1.27}$$

1.5.1.3 Transmission coefficients expressions

The transmission coefficients between the source S_0 and the receiver R_1 of a simple point-to-point network are presented in each situation in table 1.6. The

TABLE 1.6: Transmission coefficients between the source S_0 and the receiver R_1 in the two situations of the network.

	No-fault situation (Reference)	Faulty situation
$H_{R_{1,0}}(f)$	$\frac{1}{e^{\gamma l}}$	$\frac{1}{e^{\gamma l}(1+\frac{Z_f}{2Z_c})}$

transmission coefficient $H^f_{R_{1,0}}(f)$, in the network faulty situation, is a function of the severity of the fault represented by the impedance Z_f. The expressions of the transmission coefficient in a point-to-point network between two ECU shows that it is independent of the fault position. If the impedance of the ECU is matched to the network ($Z_{ECU_0} = Z_{ECU_1} = Z_c$), no reflection will propagate back and forth between the position of the fault x and the end of the cable where the ECU is located.
Considering now that ECU_1 is acting as a source and ECU_0 is acting as receiver, the transmission coefficient $H_{R_{0,1}}(f)$ is estimated at the receiver ECU_0. The expressions of the TC $H_{R_{0,1}}(f)$ are the same as the expressions of the TC $H_{R_{1,0}}(f)$ in the two possible situations of the network.
The expressions of the transmission coefficients in a star-shaped network are expressed in the following.

1.5.2 Star-shaped network

In a star network, all components are individually connected to a central component. The central component can be a hub, a switch, an ECU or even a simple connector [37].
Two different types of star topology are discussed in the following paragraphs: a star communication network (SCN) and a star energy network (SEN).
A SCN is shown in Fig. 1.10a. All ECU designated as slaves are connected to a central or master ECU. A **point-to-point** connection is established between the source S_{m+1} and each of the receivers R_i separately. If one of the ECU wants to communicate with another, it sends the message to the master ECU, which in turn repeats the message and sends it to the target ECU. In this type of network, the same transmission coefficient expressions as in Table 1.6 can be used.

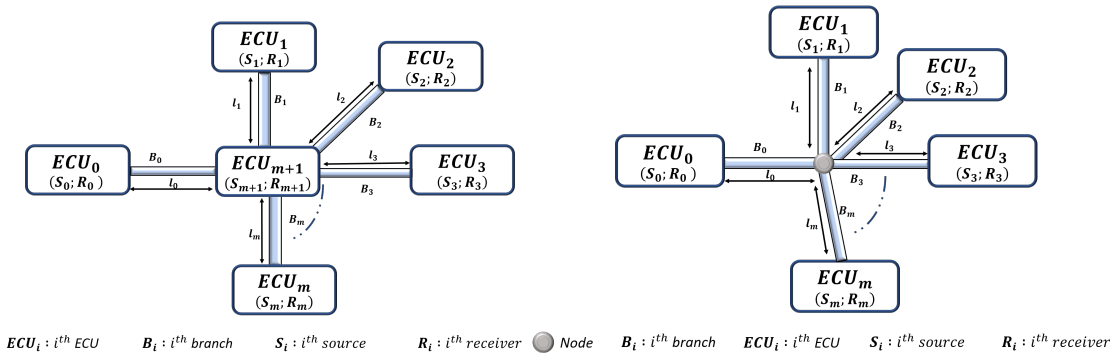

(A) A star communication network (SCN). (B) A star energy network (SEN).

FIGURE 1.10: Star network topologies.

A SEN is shown in Fig. 1.10b. All ECU are connected to a central node. The node is considered as a simple connector. If one ECU wants to communicate with another, the message will be sent directly and will be transmitted to all other ECU.
The three situations of the star energy network are studied:

- The no-fault network : The network is free of faults.
- Faulty source branch : Fault located on the branch directly linked to the ECU acting as a source.
- Faulty receiver branch: Fault located on the branch directly linked to an ECU acting as a receiver.

1.5.2.1 No-fault network

Let's consider the network when it is free of faults. First, consider that ECU_0 is a source and that the other ECU act as receivers. The ABCD matrix between the source S_0 and the ith receiver R_i is the product of three cascaded matrices. The first represents the branch between the source and the node, the second represents all branches extended from the node (except the branch B_i), and the last represents the branch B_i between the node and the receiver R_i. All branches connected to the node can be represented by an equivalent parallel impedance Z_p.

$$Star^h_{R_{i,0}}(l_i) = SN^h(l_0) \cdot \Lambda(Z_p) \cdot SN^h(l_i) \tag{1.28}$$

where $\Lambda(Z_p)$ is the matrix of a parallel impedance Z_p, $SN^h(l_0)$ is the matrix of the branch B_0 and $SN^h(l_i)$ is the matrix of the branch B_i. Z_p is the equivalent parallel

impedance representing all the branches connected to the node except B_i. It can be computed using (1.29).

$$\frac{1}{Z_p} = \sum_{j=1}^{m} \frac{1}{Z_{eq_j}}; \quad j \neq i \tag{1.29}$$

where Z_{eq_j} is the equivalent impedance of the branch B_j connected to the receiver R_j with an impedance Z_{R_j}. It is calculated using (1.30).

$$Z_{eq_j} = \frac{\boldsymbol{a_j} \cdot Z_{R_j} + \boldsymbol{b_j}}{\boldsymbol{c_j} \cdot Z_{R_j} + \boldsymbol{d_j}} \tag{1.30}$$

where $\boldsymbol{a_j}$, $\boldsymbol{b_j}$, $\boldsymbol{c_j}$ and $\boldsymbol{d_j}$ are the parameters of the ABCD-matrix representing the B_j. Under the matched impedance condition ($Z_{R_i} = Z_c \ \forall \ i \in \{1;2;\ldots;m\}$), $Z_{eq_j} = Z_c$ and the equivalent parallel impedance $Z_p = \frac{Z_c}{m-1}$.

$$Star^h_{R_{i,0}} = \begin{bmatrix} \cosh[\gamma l_0] & Z_c \cdot \sinh[\gamma l_0] \\ \frac{1}{Z_c} \cdot \sinh[\gamma l_0] & \cosh[\gamma l_0] \end{bmatrix} \cdot \begin{bmatrix} 1 & 0 \\ \frac{1}{Z_p} & 1 \end{bmatrix} \cdot \begin{bmatrix} \cosh[\gamma l_i] & Z_c \cdot \sinh[\gamma l_i] \\ \frac{1}{Z_c} \cdot \sinh[\gamma l_i] & \cosh[\gamma l_i] \end{bmatrix}$$

$$Star^h_{R_{i,0}} = \begin{bmatrix} \cosh[\gamma(l_0+l_i)] + \frac{Z_c}{Z_p} \cdot \sinh[\gamma l_0] \cdot cosh[\gamma l_i] & \\ \frac{1}{Z_c} \cdot (\sinh[\gamma(l_0+l_i)] + \frac{Z_c}{Z_p} \cdot \cosh[\gamma l_0] \cdot \cosh[\gamma l_i]) & \\ & Z_c \cdot (\sinh[\gamma(l_0+l_i)] + \frac{Z_c}{Z_p} \cdot \sinh[\gamma l_0] \cdot \sinh[\gamma l_i]) \\ & \cosh[\gamma(l_0+l_i)] + \frac{Z_c}{Z_p} \cosh[\gamma l_0] \cdot \cosh[\gamma l_i] \end{bmatrix}$$

$$Star^h_{R_{i,0}} = \begin{bmatrix} \cosh[\gamma(l_0+l_i)] + (m-1) \cdot \sinh[\gamma l_0] \cdot cosh[\gamma l_i] & \\ \frac{1}{Z_c} \cdot (\sinh[\gamma(l_0+l_i)] + (m-1) \cdot \cosh[\gamma l_0] \cdot \cosh[\gamma l_i]) & \\ & Z_c \cdot (\sinh[\gamma(l_0+l_i)] + (m-1) \cdot \sinh[\gamma l_0] \cdot \sinh[\gamma l_i]) \\ & \cosh[\gamma(l_0+l_i)] + (m-1) \cdot \cosh[\gamma l_0] \cdot \sinh[\gamma l_i] \end{bmatrix} \tag{1.31}$$

$$Star^h_{R_{i,0}} = \begin{bmatrix} A^h_{star} & B^h_{star} \\ C^h_{star} & D^h_{star} \end{bmatrix} \tag{1.32}$$

1.5.2.2 Faulty source branch

Let's consider the situation where the fault is located on the branch B_0 directly linked to the ECU acting as source. The faulty branch B_0 of length l_0 can be divided into three parts, a part before the fault position represented by $SN^h(l_0 - x_0)$, another

part representing the fault itself Z_f and a part after the fault position represented by $SN^h(x_0)$ where x_0 is the distance between the fault position and the node. This branch will be represented by the matrix $SN^f(l_0, x_0)$ found in the equation (1.24). The matrix ABCD, representing the network between the source S_0 and the receiver R_i is the product of three matrices: the matrix $SN^f(l_0, x_0)$ representing the faulty branch B_0, the matrix $\Lambda(Z_p)$ representing all the branches extended from the node (except the branch B_i), and the matrix $SN^h(l_i)$ representing the branch B_i between the node and the receiver R_i.

$$\begin{aligned} Star_{R_{i,0}}^{B_0} &= SN^f(l_0, x_0) \cdot \Lambda(Z_p) \cdot SN^h(l_i) \\ Star_{R_{i,0}}^{B_0} &= SN^f(l_0, x_0) \cdot \begin{bmatrix} 1 & 0 \\ \frac{m-1}{Z_c} & 1 \end{bmatrix} \cdot \begin{bmatrix} \cosh[\gamma l_i] & Z_c \cdot \sinh[\gamma l_i] \\ \frac{1}{Z_c} \cdot \sinh[\gamma l_i] & \cosh[\gamma l_i] \end{bmatrix} \end{aligned} \tag{1.33}$$

$$Star_{R_{i,0}}^{B_0} = \begin{bmatrix} A_{star}^{B_0} & B_{star}^{B_0} \\ C_{star}^{B_0} & D_{star}^{B_0} \end{bmatrix} \tag{1.34}$$

$$\begin{aligned} A_{star}^{B_0} = A_{star}^h + \frac{Z_f}{Z_c} \cdot (&\cosh[\gamma(l_0 - x_0)] \sinh[\gamma(l_i + x_0)] + \\ &(m-1) \cdot \cosh[\gamma(l_0 - x_0)] \cosh[\gamma x_0] \cosh[\gamma l_i]) \end{aligned} \tag{1.35}$$

$$\begin{aligned} B_{star}^{B_0} = B_{star}^h + Z_f \cdot (&\cosh[\gamma(l_0 - x_0)] \cosh[\gamma(l_i + x_0)] + \\ &(m-1) \cdot \cosh[\gamma(l_0 - x_0)] \cosh[\gamma x_0] \sinh[\gamma l_i]) \end{aligned} \tag{1.36}$$

$$\begin{aligned} C_{star}^{B_0} = C_{star}^h + \frac{Z_f}{Z_c^2} \cdot (&\sinh[\gamma(l_0 - x_0)] \sinh[\gamma(l_i + x_0)] + \\ &(m-1) \cdot \sinh[\gamma(l_0 - x_0)] \cosh[\gamma x_0] \cosh[\gamma l_i]) \end{aligned} \tag{1.37}$$

$$\begin{aligned} D_{star}^{B_0} = D_{star}^h + \frac{Z_f}{Z_c} \cdot (&\sinh[\gamma(l_0 - x_0)] \cosh[\gamma(l_i + x_0)] + \\ &(m-1) \cdot \sinh[\gamma(l_0 - x_0)] \cosh[\gamma x_0] \sinh[\gamma l_i]) \end{aligned} \tag{1.38}$$

1.5.2.3 Faulty receiver branch

The situation where the fault is located on the branch B_i directly linked to the ECU acting as receiver R_i is now discussed. The faulty branch B_i of length l_i can be divided into three parts, a part before the fault position represented by $SN^h(x_i)$, another part representing the fault itself Z_f and a part after the fault position represented by $SN^h(l_i - x_i)$ where x_i is the distance between the fault position and the node. This branch will be represented by the matrix $SN^f(l_i, x_i)$ found in the equation (1.24). The matrix ABCD, representing the network between the source S_0 and the receiver R_i is the product of three matrices: the matrix $SN^h(l_0)$ representing the branch B_0, the matrix $\Lambda(Z_p)$ representing all the branches extended from the node (except the faulty branch B_i) and the matrix $SN^f(l_i, x_i)$ representing the faulty branch B_i between the node and the receiver R_i.

$$\begin{aligned} Star_{R_{i,0}}^{B_i} &= SN^h(l_0) \cdot \Lambda(Z_p) \cdot SN^f(l_i, x_i) \\ Star_{R_{i,0}}^{B_i} &= \begin{bmatrix} A_{star}^{B_i} & B_{star}^{B_i} \\ C_{star}^{B_i} & D_{star}^{B_i} \end{bmatrix} = SN^h(l_0) \cdot \begin{bmatrix} 1 & 0 \\ \frac{m-1}{Z_c} & 1 \end{bmatrix} \cdot SN^f(l_i, x_i) \end{aligned} \tag{1.39}$$

$$\begin{aligned} A_{star}^{B_i} = A_{star}^h + \frac{Z_f}{Z_c} \cdot (&\sinh[\gamma(l_i - x_i)] \cosh[\gamma(l_0 + x_i)] + \\ &(m-1) \cdot \sinh[\gamma l_0] \cosh[\gamma x_i] \sinh[\gamma(l_i - x_i)]) \end{aligned} \tag{1.40}$$

$$\begin{aligned} B_{star}^{B_i} = B_{star}^h + Z_f \cdot (&\cosh[\gamma(l_0 + x_i)] \cosh[\gamma(l_i - x_i)] + \\ &(m-1) \cdot \cosh[\gamma(l_i - x_i)] \cosh[\gamma x_i] \sinh[\gamma l_0]) \end{aligned} \tag{1.41}$$

$$\begin{aligned} C_{star}^{B_i} = C_{star}^h + \frac{Z_f}{Z_c^2} \cdot (&\sinh[\gamma(l_0 + x_i)] \sinh[\gamma(l_i - x_i)] + \\ &(m-1) \cdot \sinh[\gamma(l_i - x_i)] \cosh[\gamma x_i] \cosh[\gamma l_0]) \end{aligned} \tag{1.42}$$

$$\begin{aligned} D_{star}^{B_i} = D_{star}^h + \frac{Z_f}{Z_c} \cdot (&\sinh[\gamma(l_0 + x_i)] \cosh[\gamma(l_i - x_i)] + \\ &(m-1) \cdot \cosh[\gamma(l_i - x_i)] \cosh[\gamma x_i] \cosh[\gamma l_0]) \end{aligned} \tag{1.43}$$

Now the situation where the receiver R_j is situated on the branch B_j different from the faulty branch B_i is discussed. The ABCD-matrix, representing the network between the source S_0 and the receiver R_j with $j \neq i$ is the product of three matrices: the matrix $SN^h(l_0)$ representing the branch B_0, the matrix $\Lambda(Z_p^f)$ representing all the branches extended from the node (except the branch B_j), and the matrix $SN^h(l_j)$ representing the branch B_j between the node and the receiver R_j.

$$\begin{aligned} Star_{R_{j,0}}^{B_j} &= SN^h(l_0) \cdot \Lambda(Z_p^f) \cdot SN^h(l_j) \\ Star_{R_{j,0}}^{B_j} &= \begin{bmatrix} A_{star}^{B_j} & B_{star}^{B_j} \\ C_{star}^{B_j} & D_{star}^{B_j} \end{bmatrix} = SN^h(l_0) \cdot \begin{bmatrix} 1 & 0 \\ \frac{1}{Z} & 1 \end{bmatrix} \cdot SN^h(l_j) \end{aligned} \tag{1.44}$$

$$A_{star}^{B_j} = A_{star}^h + (\frac{Z_c}{Z} - (m-1)) \cdot (\sinh[\gamma l_0] \cosh[\gamma l_j]) \tag{1.45}$$

$$B_{star}^{B_j} = B_{star}^h + Z_c \cdot (\frac{Z_c}{Z} - (m-1)) \cdot (\sinh[\gamma l_0] \sinh[\gamma l_j]) \tag{1.46}$$

$$C_{star}^{B_j} = C_{star}^h + \frac{1}{Z_c} \cdot (\frac{Z_c}{Z} - (m-1)) \cdot (\cosh[\gamma l_0] \cosh[\gamma l_j]) \tag{1.47}$$

$$D_{star}^{B_j} = D_{star}^h + (\frac{Z_c}{Z} - (m-1)) \cdot (\cosh[\gamma l_0] \sinh[\gamma l_j]) \tag{1.48}$$

with the equivalent impedance Z in the form of (A0.2.3):

$$\frac{1}{Z} = \frac{1}{Z_c} \cdot \frac{2(m-1)Z_c + Z_f((m-1) + (m-3)e^{-2\gamma x_i})}{2Z_c + Z_f(1 + e^{-2\gamma x_i})} \tag{1.49}$$

1.5.2.4 Transmission coefficients expressions :

The transmission coefficients between the source S_0 and each receiver of the star-shaped network are presented in each situation in table 1.7. They are obtained using the equation (1.21) and the ABCD parameters representing the star-shaped network in its no-fault and faulty situations. Interested readers can refer to section A0.2 in the appendices for the development of the expression.

The Y-shaped network, a special case of the star energy network, in which the number of branches is limited to three branches is detailed in the following.

TABLE 1.7: Transmission coefficients between the source S_0 and each receiver, R_i, in all the possible single faulty cases of the SEN.

	No-fault situation Reference	Faulty B_0	Faulty B_i (Connected to R_i)	Faulty B_j ($j \neq i$)
$H_{R_{i,0}}(f)$	$\frac{2}{(m+1)\cdot e^{\gamma(l_0+l_i)}}$	$\frac{2}{e^{\gamma(l_0+l_i)}\cdot((m+1)+A(x_0))}$	$\frac{2}{e^{\gamma(l_0+l_i)}\cdot((m+1)+A(x_i))}$	$\frac{2}{e^{\gamma(l_0+l_i)}\cdot((m+1)+B(x_j))}$

With $A(x_i) = \frac{Z_f}{2\cdot Z_c}\cdot(2+(m-1)(1+e^{-2\cdot\gamma\cdot x_i}))$, $B(x_j) = -\frac{2Z_f\cdot e^{-2\gamma x_j}}{2Z_c+Z_f(1+e^{-2\gamma x_j})}$

where $i, j \in \{1;2;\ldots;m\}$ and $i \neq j$

1.5.3 Y-shaped network

A Y-shaped network, as shown in Fig. 1.11, consists of three ECU, denoted by ECU_i with $i \in \{0;1;2\}$, one node and three branches.

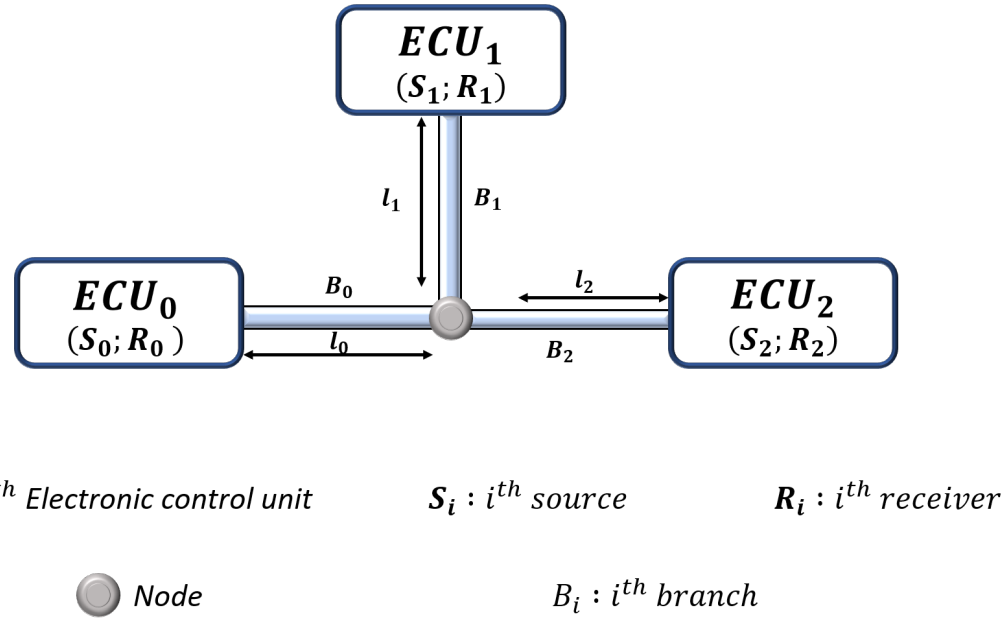

FIGURE 1.11: Y-shaped network.

A fault can occur in any of the three branches B_0, B_1 and B_2, so three situations, including the no-fault situation, of the network are explored in the following using the chain matrix model:

- No-fault network.
- Faulty source branch : Fault on the branch directly linked to the ECU acting as a source.

- Faulty receiver branch: Fault on one of the branches directly linked to a ECU acting as a receiver.

In the following, the ECU are considered to be matched ($Z_{ECU_0} = Z_{ECU_1} = Z_{ECU_2} = Z_c$). The ECU_0 plays the role of source S_0 and the other two ECU play the role of receivers R_1 and R_2.

1.5.3.1 No-fault network

Let's consider the network when it is free of faults. This network is considered as a special situation of the star network with $m = 2$ ECU acting as receivers.
The ABCD matrix of a Y-shaped network in its no-fault situation is obtained by replacing m by 2 in the equation (1.31) :

$$Y^h_{R_{i,0}} = \begin{bmatrix} \cosh[\gamma(l_0+l_i)] + \sinh[\gamma l_0]\cdot cosh[\gamma l_i] & Z_c\cdot(\sinh[\gamma(l_0+l_i)] + \sinh[\gamma l_0]\cdot\sinh[\gamma l_i]) \\ \frac{1}{Z_c}\cdot(\sinh[\gamma(l_0+l_i)] + \cosh[\gamma l_0]\cdot\cosh[\gamma l_i]) & \cosh[\gamma(l_0+l_i)] + \cosh[\gamma l_0]\cdot\sinh[\gamma l_i] \end{bmatrix} \tag{1.50}$$

$$Y^h_{R_{i,0}} = \begin{bmatrix} A^h_Y & B^h_Y \\ C^h_Y & D^h_Y \end{bmatrix} \tag{1.51}$$

1.5.3.2 Faulty source branch

In a situation where the fault is on the branch B_0 directly linked to the ECU acting as a source, the ABCD matrix is obtained by replacing m by 2 in the equations (1.35), (1.36),(1.37) and (1.38) :

$$A^{B_0}_Y = A^h_Y + \frac{Z_f}{Z_c}\cdot(\cosh[\gamma(l_0-x_0)]\sinh[\gamma(l_i+x_0)] + \cosh[\gamma(l_0-x_0)]\cosh[\gamma x_0]\cosh\gamma l_i]) \tag{1.52}$$

$$B^{B_0}_Y = B^h_Y + Z_f\cdot(\cosh[\gamma(l_0-x_0)]\cosh[\gamma(l_i+x_0)] + \cosh[\gamma(l_0-x_0)]\cosh[\gamma x_0]\sinh[\gamma l_i]) \tag{1.53}$$

$$C_Y^{B_0} = C_Y^h + \frac{Z_f}{Z_c^2} \cdot (\sinh[\gamma(l_0 - x_0)] \sinh[\gamma(l_i + x_0)] + \sinh[\gamma(l_0 - x_0)] \cosh[\gamma x_0] \cosh[\gamma l_i]) \tag{1.54}$$

$$D_Y^{B_0} = D_Y^h + \frac{Z_f}{Z_c} \cdot (\sinh[\gamma(l_0 - x_0)] \cosh[\gamma(l_i + x_0)] + \sinh[\gamma(l_0 - x_0)] \cosh[\gamma x_0] \sinh[\gamma l_i]) \tag{1.55}$$

1.5.3.3 Faulty receiver branch

In a situation where the fault is on the branch B_i with $i \in \{1;2\}$, the ABCD matrix, representing the network between the source S_0 and the receiver R_i is obtained by replacing m by 2 in the equations (1.40), (1.41), (1.42) and (1.43) :

$$A_Y^{B_i} = A_Y^h + \frac{Z_f}{Z_c} \cdot (\sinh[\gamma(l_i - x_i)] \cosh[\gamma(l_0 + x_i)] + \sinh[\gamma l_0] \cosh[\gamma x_i] \sinh[\gamma(l_i - x_i)]) \tag{1.56}$$

$$B_Y^{B_i} = B_Y^h + Z_f \cdot (\cosh[\gamma(l_0 + x_i)] \cosh[\gamma(l_i - x_i)] + \cosh[\gamma(l_i - x_i)] \cosh[\gamma x_i] \sinh[\gamma l_0]) \tag{1.57}$$

$$C_Y^{B_i} = C_Y^h + \frac{Z_f}{Z_c^2} \cdot (\sinh[\gamma(l_0 + x_i)] \sinh[\gamma(l_i - x_i)] + \sinh[\gamma(l_i - x_i)] \cosh[\gamma x_i] \cosh[\gamma l_0]) \tag{1.58}$$

$$D_Y^{B_i} = D_Y^h + \frac{Z_f}{Z_c} \cdot (\sinh[\gamma(l_0 + x_i)] \cosh[\gamma(l_i - x_i)] + \cosh[\gamma(l_i - x_i)] \cosh[\gamma x_i] \cosh[\gamma l_0]) \tag{1.59}$$

The ABCD matrix, representing the network between the source S_0 and the receiver R_j is obtained by replacing m by 2 in the equation (1.45) :

$$A_Y^{B_j} = A_Y^h + (\frac{Z_c}{Z} - 1) \cdot (\sinh[\gamma l_0] \cosh[\gamma l_j]) \tag{1.60}$$

$$B_Y^{B_j} = B_Y^h + Z_c \cdot (\frac{Z_c}{Z} - 1) \cdot (\sinh[\gamma l_0] \sinh[\gamma l_j]) \tag{1.61}$$

$$C_Y^{B_j} = C_Y^h + \frac{1}{Z_c} \cdot (\frac{Z_c}{Z} - 1) \cdot (\cosh[\gamma l_0] \cosh[\gamma l_j]) \tag{1.62}$$

$$D_Y^{B_j} = D_Y^h + (\frac{Z_c}{Z} - 1) \cdot (\cosh[\gamma l_0] \sinh[\gamma l_j]) \tag{1.63}$$

The equivalent impedance Z is obtained from the equation (1.49) by replacing m by 2, it is expressed as follows:

$$\frac{1}{Z} = \frac{1}{Z_c} \cdot \frac{2Z_c + Z_f(1 - e^{-2\gamma x_i})}{2Z_c + Z_f(1 + e^{-2\gamma x_i})} \tag{1.64}$$

1.5.3.4 Transmission coefficients expressions

The transmission coefficients between the source S_0 and each receiver of the Y-shaped network are presented in each situation in table 1.8. They are obtained using the equation (1.21) and the ABCD parameters representing the Y-shaped network in its no-fault and faulty situations found in 1.5.3. Interested readers can refer to section A0.1 in the appendices for more details. As it can be seen in the table 1.8, the transmission coefficients

TABLE 1.8: Transmission coefficients between the source S_0 and each receiver in the four situations of the network.

	No-fault situation (Reference)	Faulty B_0	Faulty B_1	Faulty B_2
$H_{R_{1,0}}(f)$	$\frac{2}{3 \cdot e^{\gamma \cdot (l_0 + l_1)}}$	$\frac{2}{e^{\gamma(l_0+l_1)} \cdot (3 + A(x_0))}$	$\frac{2}{e^{\gamma(l_0+l_1)} \cdot (3 + A(x_1))}$	$\frac{2}{e^{\gamma(l_0+l_1)} \cdot (3 + B(x_2))}$
$H_{R_{2,0}}(f)$	$\frac{2}{3 \cdot e^{\gamma \cdot (l_0 + l_2)}}$	$\frac{2}{e^{\gamma(l_0+l_2)} \cdot (3 + A(x_0))}$	$\frac{2}{e^{\gamma(l_0+l_2)} \cdot (3 + B(x_1))}$	$\frac{2}{e^{\gamma(l_0+l_2)} \cdot (3 + A(x_2))}$

With $A(x_i) = \frac{Z_f}{2 \cdot Z_c} \cdot (3 + e^{-2 \cdot \gamma \cdot x_i})$, where $i \in \{0; 1; 2\}$

$B(x_i) = \frac{-2 \cdot Z_f e^{-2\gamma x_i}}{2Z_c + Z_f(1 + e^{-2\gamma x_i})}$

between the source and each receiver in a faulty network situation are a function of the severity of the fault represented by its impedance Z_f and the distance between the fault position and the position of the node x_i in the branch B_i. The expressions of $H_{R_{1,0}}(f)$ and $H_{R_{2,0}}(f)$ in the faulty B_0 (faulty source branch) situation are identical. However, these expressions are different in the faulty B_1 or B_2 (faulty receiver branch) situations.

It should be noted that if we change the source, the expressions of the TC are the same:

$H_{R_{0,1}}(f) = H_{R_{1,0}}(f)$. The expressions of $H_{R_{1,0}}(f)$ have the same form if one of the branches B_0 or B_1, located on the direct path between the ECU_0 and ECU_1, is faulty. What changes is the position of the fault noted x_0 or x_1. In fact, if we have a fault on B_0 (Z_f, x_0), and S_0 is the source, we have the expression in the cell (1,2) of the table. If we change the source to S_1, the same fault will be on a branch connected to a receiver at a distance of x_0 from the node. We can therefore use the expression in cell (1,3) of the table which is similar to the cell (1,2).

In a real application, the transmission coefficient $H(f)$ can be either measured by a vector network analyser or estimated using dedicated signals. Power line communication (PLC) system is a special technology that requires the estimation of $H(f)$ using a multi-carrier modulation scheme. The introduction of the PLC technology and the estimation procedure is presented in the following section.

1.6 Power Line Communication : basics and interests

1.6.1 Introduction

The objective here is to briefly introduce the concept of PLC and to highlight the estimation of the transmission coefficient $H(f)$ required in the PLC receiver for communication purpose. PLC is a technology that transmits information over power lines [5, 76, 77]. This technology is divided into two main families: narrowband PLC and broadband PLC. A comparison between the two technologies is presented in Table 1.9.

TABLE 1.9: Comparison between different types of PLC

PLC	Frequency bandwidth	Rate	Range	Technologies (Standards)
Narrowband	$3 - 500$ kHz	Up to 500 kbps	Several kilometers	PRIME [78], G3-PLC [30], IEEE 1901.2, ITU-T G.hnem, IEC 61334, ISO/IEC14908-3, KONNEX EN50065, X-10
Wideband	$1.8 - 250$ MHz	Up to 2024 Mbps	Up to hundreds of meters	HomePlug AV PHY, IEEE P1901, HomePlug Green PHY, HD-PLC, H.hn (G.9960), HomePlug AV2

Smart grid applications, home automation, automotive industry [6] use currently PLC technology. All the transportation domain could benefit from the use of PLC to reduce wire

bundles, allowing the reduction of the wire costs, of the vehicle weight and thus of the CO2 emission rate. Since the electronic control units (ECU) and sensors used are all powered by power transmission cables, using these cables for data transmission is an ideal solution for reducing the amount of wiring in vehicles.

The new generation of multimedia applications such as HD television, internet protocol television, interactive gaming, whole-home audio, security monitoring, and smart grid management requires high data rate. As a solution, some wideband technology such as HomePlug AV2 (HPAV2) are proposed to support applications with high bandwidth, $[1.8 : 86.13]\ MHz$, and improved data rates up to $2Gbit/s$ [79–81]. Hence, in our work, the upper limit of the considered bandwidth of interest is set to $100MHz$. In most PLC systems, data transmission is carried out using orthogonal frequency division multiplexing (OFDM) modulation scheme. The principle of the OFDM process is highlighted in the following.

1.6.2 Orthogonal frequency division multiplexing

OFDM is the technology behind many wireless broadband systems such as WiFi (IEEE 802.11a, g, n, ac), WiMAX (IEEE 802.16) and fourth generation mobile communications 4G (LTE) and many wireline systems such as ADSL (Asymmetric Digital Subscriber Line), MoCA (Multi-media over Coas Alliance), PLC [82]. OFDM is a modulation process involving multi-carrier transmission techniques. OFDM can be seen as a simultaneous transmission of N subcarriers using a subchannel efficiently spaced (Example of 5 subcarriers in Fig. 1.12). The available transmission bandwidth BW is divided into several orthogonal subchannel Δf.

The Figure 1.13 represents the OFDM modulator which is the sum of N different modulated signals.

Each of the subcarriers is modulated using quadrature amplitude modulation (QAM) [83]. QAM can refer to different digital modulation methods as Binary Phase Shift Keying (BPSK), Quadrature Phase Shift Keying (QPSK), 16QAM (16-state QAM), 32QAM (32-state QAM). For example, 4-state QAM modulation (or QPSK) transmits data with a carrier waves whose amplitude and phase can take 4 states depending of the value of the binary data. The

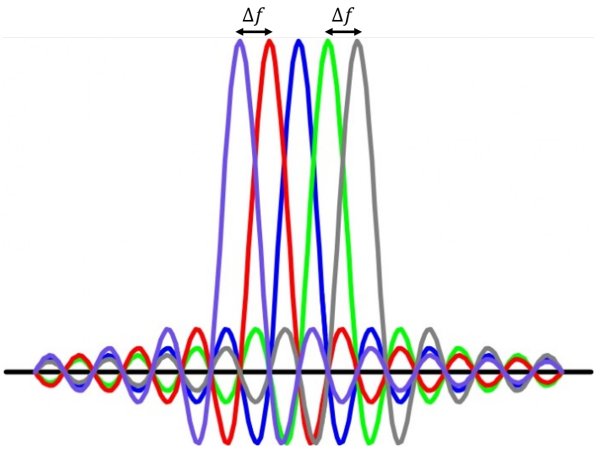

FIGURE 1.12: Five orthogonal subcarriers.

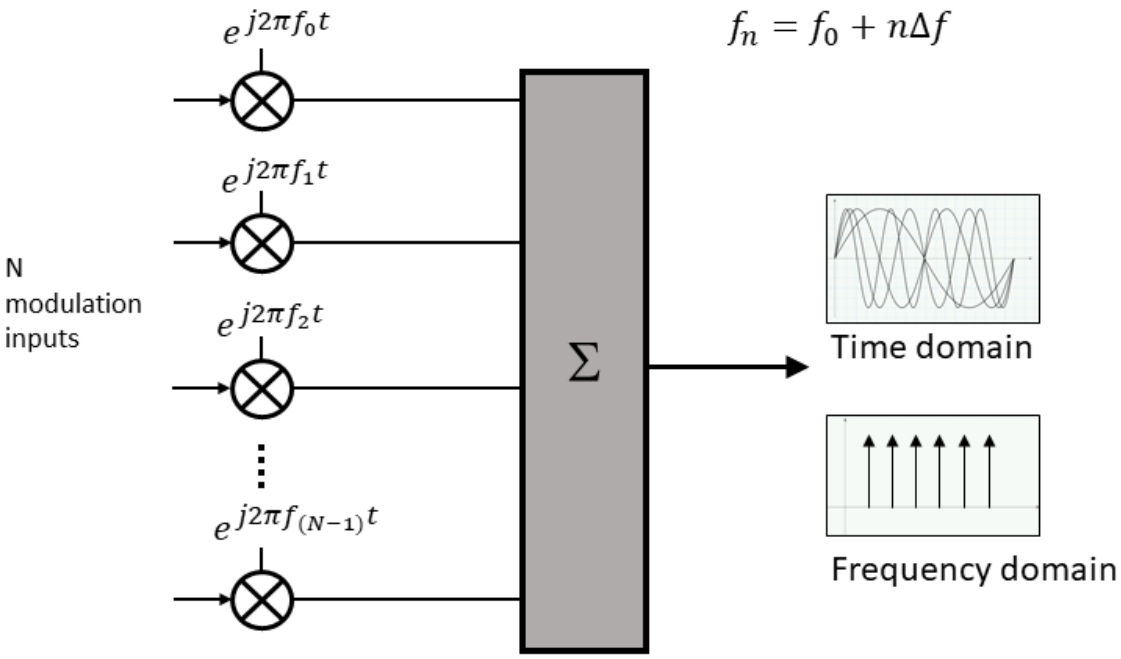

FIGURE 1.13: OFDM modulator.

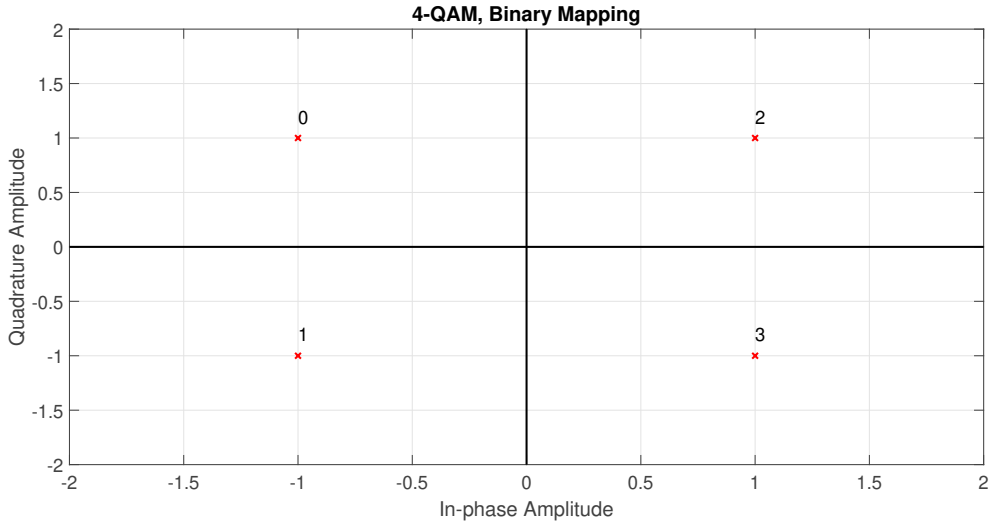

FIGURE 1.14: 4-QAM constellation map.

QAM constellation map in Fig. 1.14 shows the state (amplitude, phase) of the carrier wave depending of the binary data (0, 1, 2 or 3).

The OFDM symbol $x(t)$ is defined as the sum of the signals representing the N modulated sub-carriers :

$$x(t) = \sum_{k=1}^{N} x_k(t) = \sum_{k=1}^{N} X_k \cdot e^{j2\pi f_k t} \quad with \quad t \in [0 : T_s] \; and \; f_k = \frac{k}{T_s}. \tag{1.65}$$

The equations above are continuous functions but OFDM systems are implemented in discrete form. The signal $x(t)$ is sampled with the sampling period $T_e = \frac{T_s}{N}$. At each sampling time $t = n \cdot T_e$ with $n \in [1 : N]$, the sampled signal $x(n \cdot T_e)$ is as follows :

$$x(n \cdot T_e) = x(n) = \sum_{k=1}^{N} X_k \cdot e^{j2\pi \frac{k}{T_s} \cdot n \cdot T_e} = \sum_{k=1}^{N} X_k \cdot e^{j2\pi \frac{k \cdot n}{N}} \tag{1.66}$$

x_n denotes the set of complex symbols of the baseband signal. As we can see in the formula (1.66), the sampled signal is the result of the Inverse Discret Fourrier Tranform of the X_k symbol. That's why in real OFDM system, the Inverse Fast Fourier Transform (IFFT) is used at the transmitter to efficiently create the time domain waveform from the array of modulated subcarriers $\{X_k\}$. $\{x_n\}$ forms the OFDM symbol. At the receiver, the FFT is used to transform the time domain signal back to the array of subcarriers carrying QAM modulation $\{Y_k\}$ in the frequency domain. Figure 1.15 shows the Baseband OFDM system

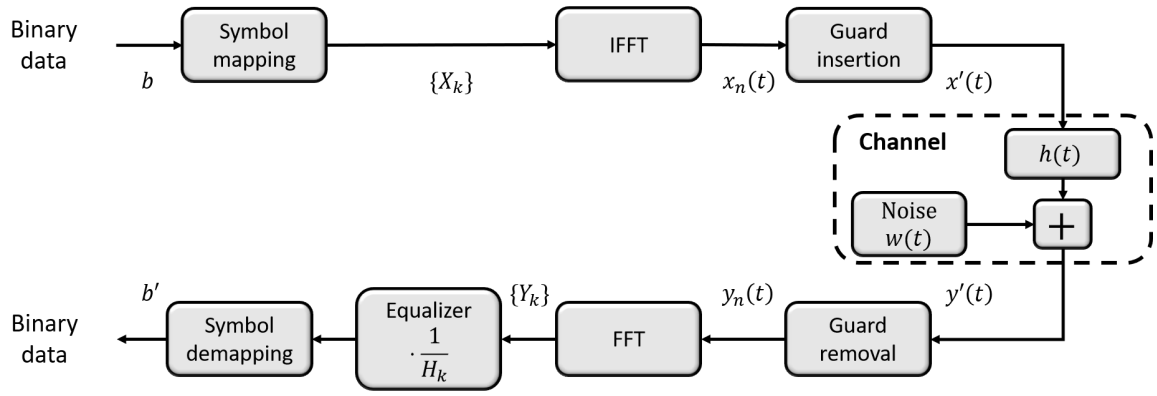

FIGURE 1.15: Baseband OFDM system.

including the transmitter part, the receiver part and the channel. A guard interval is inserted between each OFDM symbol to provide time separation between symbols. This is a simple method to prevent multipath propagation in the channel from causing interference between symbols. This type of interference is due to the multipath effect, which causes the transmitted signal to be duplicated and received several times as an echo. In general a copy of the end of the symbol is inserted into its beginning. This operation is known as cyclic prefixing and prevents also the Intercarrier Interference (ICI) . Its duration must be two to four times the effective delay spread [84] in wireless communication for example. The resulting signal is denoted $x'(t)$.

The transmission channel is represented by the impulse response $h(t)$ and the additive noise $w(t)$. The signal at the output of the channel is denoted as $y'(t) = h(t) * x'(t) + w(t)$ in the time domain. If we assume that the intersymbol interference (ISI) and ICI are cancelled thanks to the insertion of the guard interval, in the frequency domain, the previous equation can be written as $Y_k = H_k \cdot X_k + W_k$ with H_k the transmission coefficient between a source and a receiver at the k^{th} sub-carrier. H_k can be estimated at the receiver.

At the receiver, the signal attenuation and delay caused by the channel is compensated thanks to the equalizer. The symbols $\{Y_k\}$ are simply multiplied by C_k, the inverse of the transmission coefficient.

$$C_k = \frac{1}{\hat{H}_k} \tag{1.67}$$

In the OFDM process, the channel transmission coefficient H_k is required at the receiver part to equalize the signal. To estimate H_k [85], a reference signal (or pilot signal) known by the receiver is used. The transmitter sends the pilot symbols X_{pilot} and the receiver received

Y_{pilot}. Using the Least Square (LS) estimator technique [82, 86], the estimation process computes for each sub-carrier k, an average value of estimated N_p symbols in order to reduce the influence of noise. The estimation of the transmission coefficient at the k^{th} sub-carrier is given by :

$$\hat{H}_k = \frac{1}{N_p} \sum_{n=1}^{N_p} \frac{Y_{k,n}^{pilot}}{X_{k,n}^{pilot}} \tag{1.68}$$

1.7 Conclusion

In this chapter, a state of the art on networks, on their characteristics, and on modeling methods was made. These networks are used to connect electronic control units together for communication and power supply. Since networks are deployed in harsh environments, they are prone to faults. The faults effects are represented as series impedances. The ABCD modeling approach is used in this chapter to model different network topologies in the presence and in the absence of faults. Afterwards, the expressions of the transmission coefficients of these networks between an ECU acting as a source and others acting as receivers are given. In PLC systems, these transmission coefficients can be obtained using OFDM scheme that was also detailed in this chapter. From the TC expressions, fault-sensitive health indicators are proposed in chapter 2. From the health indicators, residuals that will be used for our proposed transferometry-based fault detection and localization are proposed.

Chapter 2

General principle of the diagnosis method based on the transmission coefficients: Validation on a Y-shaped network

---

This chapter is divided into five main sections. First, the general concepts of diagnosis are introduced. Next, a state of the art of the wired networks fault diagnosis methods is presented and discussed with a particular focus on reflectometry-based and transferometry-based methods. Then, our proposed diagnosis method based on the transmission coefficients is detailed. Residuals are proposed to detect a local degradation (or soft fault), to locate the faulty branch and to monitor the evolution of its degradation. Finally, the proposed monitoring method is validated on real measurements extracted from a Y-shaped network test bench. To obtain many different faulty situations, realistic simulation-based data are also used to study the sensitivity of the residuals to soft fault characteristics (level of degradation i.e. soft fault severity and position) and to noise.

2.1 General concept of diagnosis

Real-world engineering systems, such as transportation systems, smart grids, nuclear power plants and chemical plants, are prone to faults. Faults tend to degrade system performance and lead to serious consequences. Therefore, it is important to have a monitoring system that can follow the physical conditions of the system by collecting data, recognizing and reporting any abnormal behavior [87, 88]. The reliability, safety and efficiency of these systems can be improved by using fault detection and diagnosis methods which were the subject of intensive research [89–93]. By monitoring a system and taking appropriate action in case of early detection of a fault, it is possible to plan maintenance operations to avoid total system failure and reduce repair expenses. The general principle of the diagnosis process is duplication and comparison techniques that can be based on hardware redundancy, analytical redundancy or signal-based/data-based approaches [94, 95]:

- The **hardware redundancy** approach is based on comparing duplicate measurements from different sets of identical sensors, and then a voting process is used to detect and isolate the faulty sensor [96]. Unfortunately, this approach leads to increased weight, cost and energy consumption.
- The **analytical redundancy** approach is based on the use of the analytical relationships between the input and output signals given by dynamic process models under given hypothesis (no-fault or fault) of the target system. Residual signals are generated by comparing the actual measured outputs on the system and the respective estimated outputs using the model. Residuals are close to zero in the no-fault conditions and non-zero in the faulty conditions [97, 98]. These techniques are based on parity equations [99], state observers [100], parameter/state estimation [101].
- The **signal-based or data-based** approach consists in extracting signal or data characteristics (frequency, time, shape, position...) from measurements or available data. These characteristics are thus compared to *a priori* known characteristics of the system under no-fault and fault hypotheses [102, 103].

The diagram in Fig. 2.1 summarizes the basic concepts of the three diagnosis approaches described above.

The faults considered in the literature are distinguished as sensor, actuator, process component and controller faults [46]. Most of these elements are

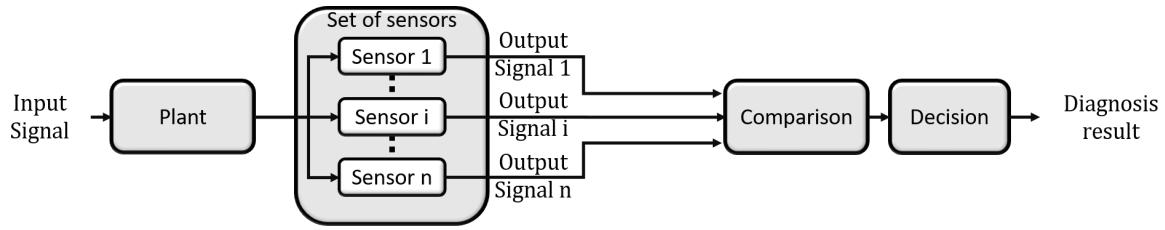

(A) Hardware redundancy

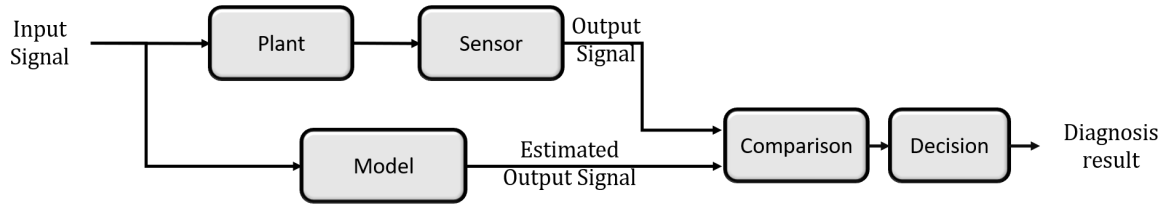

(B) Analytical redundancy

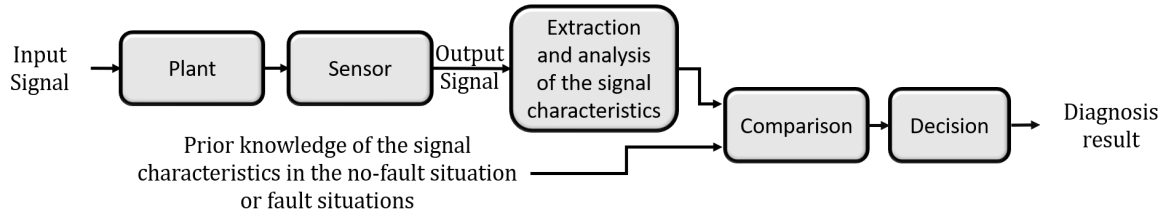

(C) Signal-based or data-based methods

FIGURE 2.1: General principle of the diagnosis process.

interconnected by wired networks that are used for data routing and power supply. These networks are generally assumed to operate in a no-fault condition and the methods of sensor/actuator/component fault diagnosis are applicable under this assumption. However, the embedded wired networks are prone to soft faults that can evolve into hard faults (cf. definitions 1 and 2). The following section is devoted to the wireframe diagnosis methods found in the literature.

2.2 Wireframe diagnosis methods

The power supply of electronic components and the exchange of information between them in transportation systems, in smart grids and in industrial applications are done mainly via cables. This results in a great complexity of the wired network which must be maintained in optimal operation. Therefore, the implementation of a monitoring system for the wired network is needed. This system must be able to detect, locate and identify soft faults before they lead to more serious faults (short circuits or open circuits) that make the cable unusable.
By deploying a monitoring system capable of detecting soft faults, it is therefore

possible to reconfigure the communication system to avoid the faulty branch, leading to a fault-tolerant network [104]. This monitoring system can also provide maintenance support to directly repair the faulty cable which would reduce the repair costs.
By browsing the literature, one can find different wireline diagnosis methods such as:

- Visual inspection [105].
- X-ray [106].
- Guided ultrasonic waves [107, 108].
- Infrared thermal imaging [109].
- High-pot [110].
- Reflectometry-based methods [111].
- Transferometry-based methods [3].

The majority of these methods are signal-based methods. A comparison between the previously mentioned methods is made in [69] resulting that the most used methods for fault diagnosis in wired networks are reflectometry-based methods. The advantages and disadvantages of the diagnosis methods are summarised in the table 2.1. The reflectometry-based methods are presented and discussed in the next subsection. Transferometry-based method will be detailed in section 2.2.2.

2.2.1 Reflectometry-based methods

These methods use the same principle as a radar. A dedicated signal is injected into the network, and at each impedance discontinuity (e.g. node, faults, mismatched load, etc...) a fraction of the injected signal is reflected back to the injection point. The general principle of the methods, illustrated in Fig.2.2, is to analyze reflected signals. To distinguish the reflections due to faults from reflections due to other types of impedance discontinuity, the reflectogram of the network is compared to a reference reflectogram constructed when the network is in the no-fault condition. Therefore, these diagnosis methods are considered to be signal-based methods (see section 2.1). These methods are divided into two main families: Frequency Domain Reflectometry (FDR) and Time Domain Reflectometry (TDR) according to the type of signal which is injected and the processing method of the reflected signal [113,

TABLE 2.1: Comparison of diagnosis methods [69, 112]

Method	Advantages	Disadvantages
Visual inspection	Detects hard and soft faults. Provides location information.	Detects only visible soft fault. Depends on the operator. Not suitable for online diagnosis.
X-Rays	Detects hard and soft faults.	Requires complex systems.
Guided ultrasonic wave	Detects insulator faults.	Not suitable for complex networks.
Infrared thermal imaging	Provides location information.	Detects only faults creating a hot spot.
High Pot	Detects insulator faults.	Requires complex systems. Can damage the tested cable.
Reflectometry	Detects soft and hard faults. Can provide exact position information.	Blind zone problem. Requires installation of dedicated instruments for diagnosis purpose. Need powerful data processing techniques. Limitations to detect soft faults.
Transferometry	Detects soft and hard fault. Use the existing components. Support online implementation. Provide location information.	Increases the computational and communication costs.

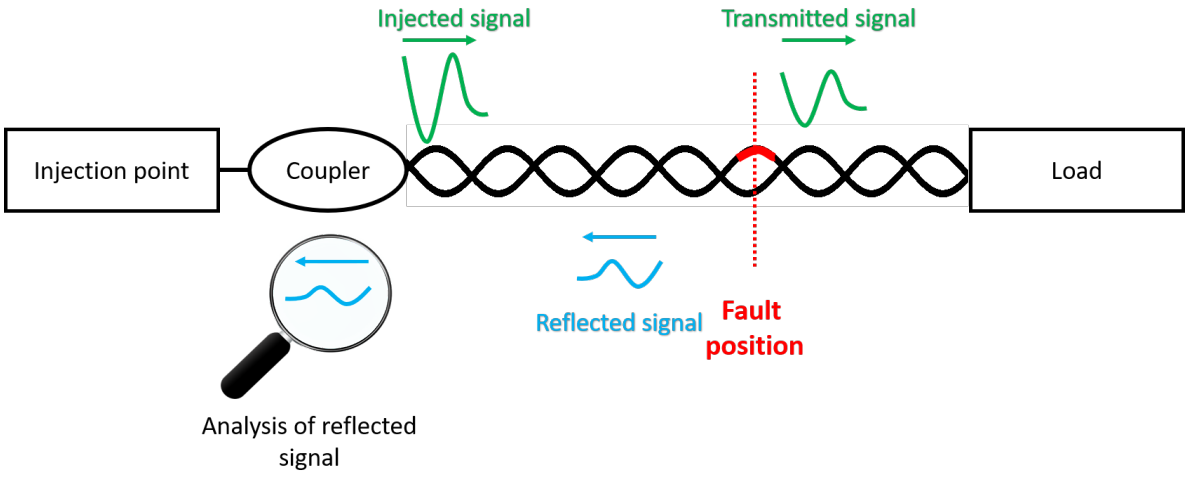

FIGURE 2.2: General principle of Reflectometry-based methods.

114].
In FDR methods, the injected signal is known as a "chirp" signal which is a set of sine waves whose frequency varies linearly with time. Three types of FDR are commonly used: standing wave reflectometry (SWR), frequency modulated continuous wave (FMCW) and frequency domain reflectometry with phase detection (PDFDR) [115].
In conventional TDR methods, the injected signal is a Gaussian pulse. As the injected signal can disturb the electronic components connected to the cable to be tested, the classical TDR methods are not used online. That's why several methods derived from TDR such as Sequence TDR (STDR), Spread Spectrum TDR (SSTDR), Multi-Carrier TDR (MCTDR), Orthogonal Multi-Tone TDR (OMTDR) inspired by OFDM, Noise DR (NDR), chaos TDT (CTDR) and Binary TDR (BTDR) have emerged [116–118]. A review of existing reflectometry-based methods is presented in [47].
Reflectometry-based methods detect and can locate hard faults. However, these methods may have difficulty in detecting small reflections generated by soft faults due to attenuation and distortion of the signal during propagation. They can be limited by the ambiguity of the location of the faulty branch and the blind spot problem [69]. The signature of soft faults can be masked by noise, and reflections due to soft faults can be masked by those caused by nodes [119]. To overcome some of these problems, distributed reflectometry methods were proposed [120–122]. In these methods, several reflectometers are installed in complex networks and a data fusion algorithm between all reflectograms is applied to obtain the final diagnosis result. To avoid the use of too many reflectometers, a combination between distributed reflectometry with Principal Component Analysis (PCA) was proposed in [112]. Reflectometry methods are continuously being studied, particularly for the detection and localisation of soft faults in complex networks. These methods, however, only rely on the analysis of the signals they inject, not the other signals that are present in the network. To benefit from the additional information provided by the signals sent from and to *ECU*, transferometry-based methods are proposed [3]. These methods discussed in the following subsection can be seen as complementary to the reflectometry methods.

2.2.2 Transferometry-based methods

Instead of analyzing the reflected signals, the transmitted signals received by the receiver may be analyzed as shown in Fig. 2.3. The general principle of a transmission-based (or transferometry-based) monitoring method is the

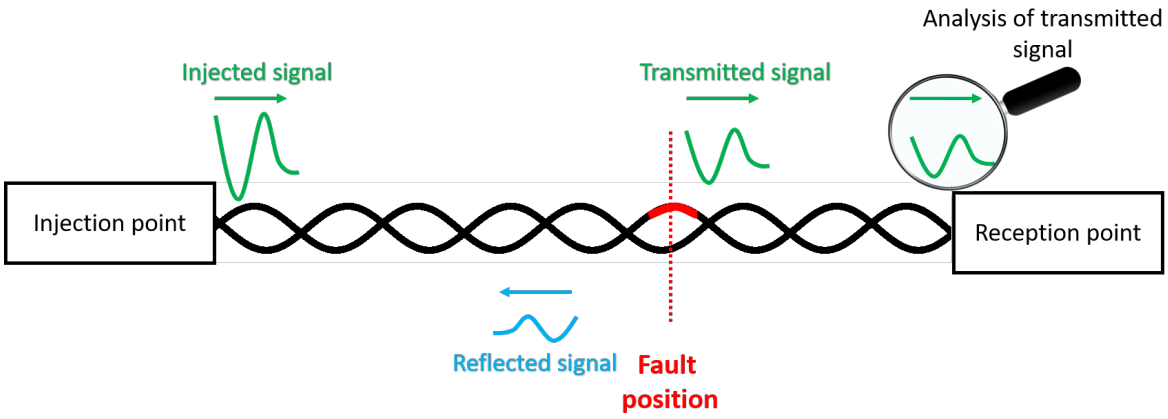

FIGURE 2.3: General principle of Transferometry-based methods.

comparison between a reference Transmission Coefficient (TC), estimated when the network is supposed to be in the no-fault situation, and the successive TCs estimated online. In [123], the difference between the compared TC is detected by comparing the values and positions of the TC peaks and notches of reference TC with successive online estimated TC. This comparison was performed in [124–126] using different machine learning techniques (support vector machine - regression) by selecting multiple features, namely the mean, variance, skewness and kurtosis of the channel TC over the operating bandwidth of 2 to 30 MHz or using neural networks to avoid any manual feature extraction process in [127]. By employing frequency domain deconvolution between a reference TC and an online estimated TC, soft faults in a point-to-point connection of two power line devices can be detected [128]. In order to compare the reference TC and successive TC measurements, Euclidean distance is used in [129]. In all the previous investigations, the considered networks are simple point-to-point connections.
However, to our knowledge several points have never been studied :

- Detecting and locating soft faults (i.e. local degradation) in complex networks for which the communication system can still operate correctly.
- Tracking the degradation process along the time.
- Study the influence of the fault characteristics (level of degradation or severity and position of the fault) on the transmission coefficients.

To answer these challenging questions, a transferometry-based diagnosis method is proposed in the following section.

Remark 1 *The use of PLC technology is a great advantage for transferometry-based methods, because no additional measurement instrument will be required to get the TC [130].*

2.3 Proposed transferometry-based diagnosis methodology

2.3.1 Expressions of the transmission coefficients in function of the network parameters

As explained in chapter 1, section 1.6.2, PLC technology aims to use energy cables for data communication. In PLC-type transmission systems, the transmission coefficients, between ECU acting as sources and others acting as receivers, are estimated online for communication purposes. The estimation procedure is detailed in chapter 1, section 1.6.2. This estimation constitutes the first step of our method based on monitoring the transmission coefficients. The expressions of the transmission coefficients in function of the ABCD model parameters are recalled in the Tables 2.2, 2.3 and 2.4 for point-to-point, Y-shaped and star-shaped energy network (SEN) topologies respectively. In what follows, Z_c denotes the characteristic impedance of the studied network and Z_f denotes the added impedance representing the fault.

TABLE 2.2: Transmission coefficients between the source and the receiver in the two situations of the point-to-point network of length l.

	No-fault situation (Reference)	Faulty situation
$H_{R_{1,0}}(f) = H_{R_{0,1}}(f)$	$\frac{1}{e^{\gamma l}}$	$\frac{1}{e^{\gamma l}(1+\frac{Z_f}{2Z_c})}$

These expressions are useful to express the influence of the fault on the transmission coefficients. From these expressions, we will generate health indicators and residuals that are fault-sensitive. The proposed health indicators are detailed in the following.

TABLE 2.3: Transmission coefficients between the source S_0 and each receiver, R_i, in all the possible single faulty cases of the SEN.

	No-fault situation Reference	Faulty B_0	Faulty B_i (Connected to R_i)	Faulty B_j ($j \neq i$)
$H_{R_{i,0}}(f)$	$\frac{2}{(m+1)\cdot e^{\gamma(l_0+l_i)}}$	$\frac{2}{e^{\gamma(l_0+l_i)}\cdot((m+1)+A(x_0))}$	$\frac{2}{e^{\gamma(l_0+l_i)}\cdot((m+1)+A(x_i))}$	$\frac{2}{e^{\gamma(l_0+l_i)}\cdot((m+1)+B(x_j))}$

$$\text{With } A(x_i) = \frac{Z_f}{2\cdot Z_c}\cdot(2+(m-1)(1+e^{-2\cdot\gamma\cdot x_i})),\ B(x_j) = -\frac{2Z_f\cdot e^{-2\gamma x_j}}{2Z_c+Z_f(1+e^{-2\gamma x_j})},$$
$$\text{where } \ i,j \in \{1;2;\ldots;m\} \text{ and } i \neq j$$

TABLE 2.4: Transmission coefficients between the source S_0 and each receiver in the four situations of the Y-shaped network.

	No-fault situation (Reference)	Faulty B_0	Faulty B_1	Faulty B_2
$H_{R_{1,0}}(f)$	$\frac{2}{3\cdot e^{\gamma\cdot(l_0+l_1)}}$	$\frac{2}{e^{\gamma(l_0+l_1)}\cdot(3+A(x_0))}$	$\frac{2}{e^{\gamma(l_0+l_1)}\cdot(3+A(x_1))}$	$\frac{2}{e^{\gamma(l_0+l_1)}\cdot(3+B(x_2))}$
$H_{R_{2,0}}(f)$	$\frac{2}{3\cdot e^{\gamma\cdot(l_0+l_2)}}$	$\frac{2}{e^{\gamma(l_0+l_2)}\cdot(3+A(x_0))}$	$\frac{2}{e^{\gamma(l_0+l_2)}\cdot(3+B(x_1))}$	$\frac{2}{e^{\gamma(l_0+l_2)}\cdot(3+A(x_2))}$

$$\text{With } A(x_i) = \frac{Z_f}{2\cdot Z_c}\cdot(3+e^{-2\cdot\gamma\cdot x_i}),\ B(x_i) = \frac{-2\cdot Z_f e^{-2\gamma x_i}}{2Z_c+Z_f(1+e^{-2\gamma x_i})},$$
$$\text{where } i \in \{0;1;2\}$$

2.3.2 Health indicators

2.3.2.1 Definition of the health indicators

Definition 3 *The health indicator, $I_{R_{i,s}}(f)$, computed locally for the frequency f, at the receiver R_i when S_s is the source, is:*

$$I_{R_{i,s}}(f) = \frac{\left|H^{Reference}_{R_{i,s}}(f)\right|}{\left|H_{R_{i,s}}(f)\right|} - 1 \ \ \forall\, f \in BW \tag{2.1}$$

where $\left|H^{Reference}_{R_{i,s}}(f)\right|$ is the module of the network transmission coefficient between S_s and R_i in no-fault nominal situation, supposed to be known. $\left|H_{R_{i,s}}(f)\right|$ is the module of the transmission coefficient that is estimated online and BW is the bandwidth that is chosen accordingly to the application.

This work is intended to be applied in PLC systems, and more particularly HPAV2 standards that operates in the bandwidth of $\{1.8 : 86.13\}MHz$. Therefore, our

proposed method will be validated with measured data in the bandwidth $BW = \{0.25 : 100\}MHz$ with 1601 frequency components which includes the bandwidth used in the HPAV2 technology [80, 81].
In the following, the expressions of the health indicators are obtained in the three different topologies, point-to-point, Y-shaped and Star-shaped Energy Networks (SEN) in their no-fault and faulty situations.

2.3.2.2 Expression of the health indicators for a point-to-point network

The expressions of the health indicators are studied in the two situations of the point-to-point network using (2.1) and the expressions of the transmission coefficients found in Table 2.2. In what follows, f is the frequency in the given bandwidth BW.
In a point-to-point network with two terminal ECU, each ECU can act as a source, the other ECU acts as a receiver. The two TC obtained in the two configurations are the same as it is recalled in Table 2.2. Thus the two health indicators $I_{R_{1,0}}(f)$ and $I_{R_{0,1}}(f)$ are identical in fault-free and faulty situations.

- No-fault network:
  In a no-fault situation, the estimated transmission coefficient is the same as the reference transmission coefficient. Therefore, the health indicator is equal to zero $\forall\ f \in BW$:
  $$I_{R_{1,0}}(f) = I_{R_{0,1}}(f) = 0 \tag{2.2}$$

- Faulty branch network:
  If a fault is located at the branch connecting the two ECU, the estimated transmission coefficient is different from the reference transmission coefficient. Therefore, the health indicator is different from zero. The expression of the health indicator is the following :
  $$\begin{aligned} I_{R_{1,0}}(f) = I_{R_{0,1}}(f) &= \frac{\left|H_{R_{1,0}}^{Reference}(f)\right|}{\left|H_{R_{1,0}}(f)\right|} - 1 = \frac{\left|\frac{1}{e^{\gamma l}}\right|}{\left|\frac{1}{e^{\gamma l}(1+\frac{Z_f}{2Z_c})}\right|} - 1 \\ &= \left|1 + \frac{Z_f}{2 \cdot Z_c}\right| - 1 \end{aligned} \tag{2.3}$$
  where Z_f is the impedance of the fault.

A signature matrix as shown in Table 2.5 can be constructed for a point-to-point network. This matrix is based on the theoretical expressions of the health indicator. A 0 indicates that the health indicator is null and a 1 indicates a non-zero value.

TABLE 2.5: Point-to-point network signature matrix.

	No-fault situation (Reference)	Faulty situation
$I_{R_{1,0}}(f) = I_{R_{0,1}}(f)$	0	1

0 indicates that the health indicator is equal to zero
1 indicates that the health indicator is different from zero.

2.3.2.3 Expression of the health indicators for a Y-shaped network

In this section, we consider a Y-shaped network represented in Figure 2.4. The expression of the health indicators are derived in function of the fault characteristics (impedance Z_f and position of the fault in each branch).

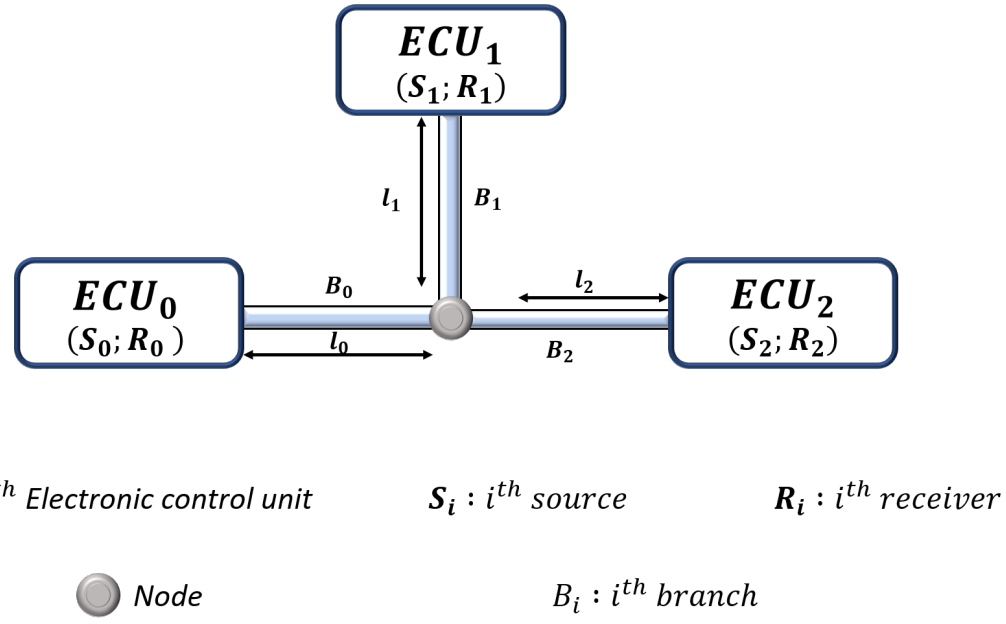

FIGURE 2.4: Y-shaped network.

We first consider that ECU_0 is the source that transmits the pilot signal to estimate the TC at the receivers R_1 and R_2. The expressions of the health indicators, as functions of the frequency $f \in BW$, are given in the no-fault and all faulty situations of the Y-shaped network:

- No-fault network:
  In a nominal no-fault situation, the TC at each receiver is equal to the reference TC. Thus the two health indicators equal zero:

$$I_{R_{1,0}}(f) = I_{R_{2,0}}(f) = 0 \ \ \forall f \ \in BW \tag{2.4}$$

- Faulty source branch B_0:
  The expressions of the health indicators, when the fault is located at the branch B_0 are obtained using (2.1) and the expressions of the transmission coefficients found in Table 2.4. It gives

$$\begin{aligned} I_{R_{1,0}}(f) = I_{R_{2,0}}(f) &= \frac{\left|H_{R_{1,0}}^{Reference}(f)\right|}{\left|H_{R_{1,0}}(f)\right|} - 1 = \frac{\left|\frac{2}{3\cdot e^{\gamma\cdot(l_0+l_1)}}\right|}{\left|\frac{2}{e^{\gamma(l_0+l_1)}\cdot(3+\frac{Z_f}{2\cdot Z_c}\cdot(3+e^{-2\cdot\gamma\cdot x_0}))}\right|} - 1 \\ &= \left|\frac{6\cdot Z_c + Z_f\cdot(3+e^{-2\gamma x_0})}{6\cdot Z_c}\right| - 1 \end{aligned} \tag{2.5}$$

  where x_0 is the distance between the fault position and the node. The term $Z_f \cdot (3 + e^{-2\gamma x_0})$ is different from zero. As a consequence, we have

$$I_{R_{1,0}}(f) = I_{R_{2,0}}(f) \neq 0 \tag{2.6}$$

- Faulty receiver branch B_i:
  The expressions of the health indicators, when a fault is located at the branch B_i ($i \in 1;2$), are obtained using (2.1) and the expressions of the transmission coefficients found in Table 2.4.

  It gives

$$\begin{aligned} I_{R_{i,0}}(f) &= \frac{\left|H_{R_{i,0}}^{Reference}(f)\right|}{\left|H_{R_{i,0}}(f)\right|} - 1 = \frac{\left|\frac{2}{3\cdot e^{\gamma\cdot(l_0+l_i)}}\right|}{\left|\frac{2}{e^{\gamma(l_0+l_i)}\cdot(3+\frac{Z_f}{2\cdot Z_c}\cdot(3+e^{-2\cdot\gamma\cdot x_i}))}\right|} - 1 \\ &= \left|\frac{6\cdot Z_c + 3\cdot Z_f + Z_f\cdot e^{-2\gamma x_i}}{6\cdot Z_c}\right| - 1 \end{aligned} \tag{2.7}$$

Remark 2 *The expression of the health indicator $I_{R_{i,0}}(f)$ when the branch B_i is faulty*

is identical to the expressions of the health indicators $I_{R_{1,0}}(f)$ and $I_{R_{2,0}}(f)$ when the branch B_0 is faulty. These expressions differ by the position of the fault x_i or x_o respectively. This is normal because the fault is located at the direct path between the source S_0 and the receiver R_i in both situations.

The expression of the other health indicator computed at receiver R_j ($j \in \{1;2\}, j \neq i$), which is not directly connected to the faulty branch R_i is

$$I_{R_{j,0}}(f) = \frac{\left|H_{R_{j,0}}^{Reference}(f)\right|}{\left|H_{R_{j,0}}(f)\right|} - 1 = \frac{\left|\frac{2}{3 \cdot e^{\gamma \cdot (l_0 + l_j)}}\right|}{\left|\frac{2}{e^{\gamma(l_0+l_j)} \cdot (3 + \frac{-2 \cdot Z_f e^{-2\gamma x_i}}{2 \cdot Z_c + Z_f (1 + e^{-2\gamma x_i})})}\right|} - 1 \tag{2.8}$$

$$= \left|\frac{6 \cdot Z_c + 3 \cdot Z_f + Z_f \cdot e^{-2 \cdot \gamma \cdot x_i}}{6 \cdot Z_c + 3 \cdot Z_f + 3 \cdot Z_f \cdot e^{-2\gamma x_i}}\right| - 1 \tag{2.9}$$

From the previous expressions, we deduce that the two health indicators $I_{R_{i,0}}(f)$ and $I_{R_{j,0}}(f)$ with $i \neq j$ are different:

$$I_{R_{i,0}}(f) \neq I_{R_{j,0}}(f) \tag{2.10}$$

In summary, if a fault is located at the branch connected to the source, the health indicators calculated at the receivers are equal. Otherwise, the health indicators are different from each other.

The expressions of the health indicators have been obtained by considering that the ECU_0 is acting as the source which transmits the pilot signal. The two other ECU : ECU_1 and ECU_2 can also play the role of the source. In a Y-shaped network composed of three ECU, a total of six health indicators (two per receiver) can be computed.

If we consider that ECU_1 is the source S_1. The same expressions as previously are obtained by making a circular rotation of the indices : replacing the index 0 by 1, the index 2 by 0, the index 1 by 2.

If we consider that ECU_2 is the source S_2. The same expressions as previously are obtained by making an inverse circular rotation of the indices : replacing the index 0 by 2, the index 2 by 1, the index 1 by 0.

A characterization of the 6 health indicators, considering the sources S_0, S_1, S_2, in the four possible network situations is summarized in Table 2.6.

TABLE 2.6: Characterization of the health indicators in a Y-shaped network.

Source	No-fault network	Faulty B_0	Faulty B_1	Faulty B_2
S_0	$I_{R_{1,0}}(f) = I_{R_{2,0}}(f) = 0$	$I_{R_{1,0}}(f) = I_{R_{2,0}}(f)$	$I_{R_{1,0}}(f) \neq I_{R_{2,0}}(f)$	$I_{R_{1,0}}(f) \neq I_{R_{2,0}}(f)$
S_1	$I_{R_{0,1}}(f) = I_{R_{2,1}}(f) = 0$	$I_{R_{0,1}}(f) \neq I_{R_{2,1}}(f)$	$I_{R_{0,1}}(f) = I_{R_{2,1}}(f)$	$I_{R_{0,1}}(f) \neq I_{R_{2,1}}(f)$
S_2	$I_{R_{0,2}}(f) = I_{R_{1,2}}(f) = 0$	$I_{R_{0,2}}(f) \neq I_{R_{1,2}}(f)$	$I_{R_{0,2}}(f) \neq I_{R_{1,2}}(f)$	$I_{R_{0,2}}(f) = I_{R_{1,2}}(f)$

Remark 3 *We can express the following general result. A Y-shaped network consists of a node that connects a source S_s and a set of receivers $\{R_j; R_k\}$ with $s, j, k \in \{1;2;3\}$ and $s \neq j \neq k$. If the fault is on the source branch B_s, the health indicators computed at the receivers R_j and R_k are equal. If the fault is on one of the other branches (receiver-side branches B_j or B_k) all the health indicators are different. This general result will be used when considering bus networks in chapter 3.*

The health indicators are computed at the receivers by using the estimated TC with the pilot signal. The computed health indicators (N_f values, where N_f is the number of frequencies in the BW) are sent to the corresponding source to be compared. To perform the comparison of two health indicators, we will propose different comparison methods in Section 2.4.

2.3.2.4 Expression of the health indicators for a star energy network

The expressions of the transmission coefficients are given in Table 2.3 in all possible situations of the star energy network shown in Fig.2.5.
Let us consider that the ECU_0 is acting as a source and the other ECU are acting as receivers. One health indicator per receiver, $I_{R_{i,0}}(f)$, with $i \in \{1;2;\ldots;m\}$, is computed. Several situations may be encountered:

- As in the previous studied topologies, in the no-fault situation, all the health indicators are equal to zero,

$$I_{R_{i,0}}(f) = 0 \; \forall i \in \{1;2;\ldots;m\}, \; \forall f \; \in BW \tag{2.11}$$

- Faulty source branch : A fault is located at the branch directly connected to the source and all the other branches are fault-free. The expressions of the health indicators in this case are obtained using 2.1 and the expressions of the TC

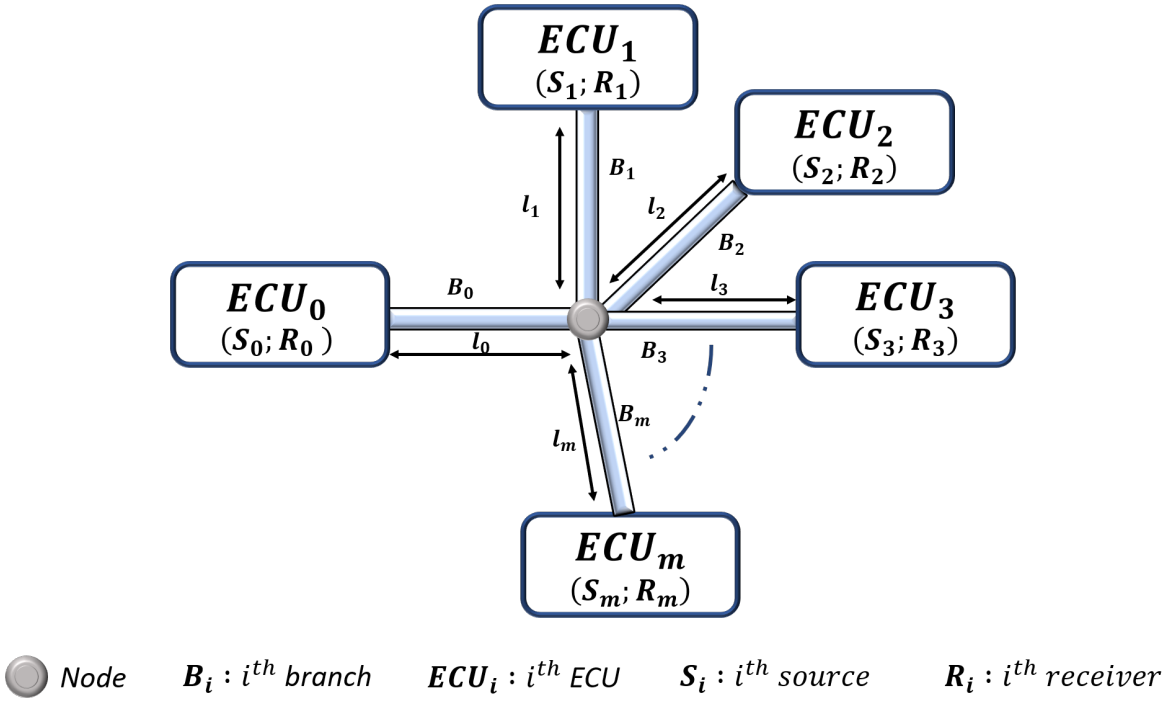

FIGURE 2.5: A star energy network (SEN).

found in table 2.3 $\forall\, i, j \in \{1; 2; \ldots; m\}$.

$$
\begin{aligned}
I_{R_{i,0}}(f) = I_{R_{j,0}}(f) &= \frac{\left|H^{Reference}_{R_{i,0}}(f)\right|}{\left|H_{R_{i,0}}(f)\right|} - 1 \\
&= \frac{\left|\frac{2}{(m+1)\cdot e^{\gamma(l_0+l_i)}}\right|}{\left|\frac{2}{e^{\gamma(l_0+l_i)}\cdot((m+1)+\frac{Z_f}{2\cdot Z_c}\cdot(2+(m-1)(1+e^{-2\cdot\gamma\cdot x_0})))}\right|} - 1 \\
&= \left|1 + \frac{Z_f}{2\cdot Z_c}\cdot\left(1 + \frac{m-1}{m+1}\cdot e^{-2\cdot\gamma\cdot x_0}\right)\right| - 1 \neq 0
\end{aligned}
\tag{2.12}
$$

All the health indicators are equal when the fault is located at the branch directly connected to the source. Since the term $\frac{Z_f}{2\cdot Z_c}\cdot\left(1+\frac{m-1}{m+1}\cdot e^{-2\cdot\gamma\cdot x_0}\right)$ is different from zero, the health indicators are not null.

- Faulty receiver branch : A fault is located at a branch directly connected to one receiver, R_j, and all the other branches are fault-free. The expressions of the health indicators in this case are obtained using 2.1 and the expressions of the TC found in table 2.3. Two expressions of the health indicators are obtained, depending on the faulty branch:

– The expression of the health indicator computed at the receiver directly connected to the faulty branch is

$$I_{R_{j,0}}(f) = \frac{\left|H_{R_{j,0}}^{Reference}(f)\right|}{\left|H_{R_{j,0}}(f)\right|} - 1 = \frac{\left|\frac{2}{(m+1)\cdot e^{\gamma(l_0+l_j)}}\right|}{\left|\frac{2}{e^{\gamma(l_0+l_j)}\cdot((m+1)+\frac{Z_f}{2\cdot Z_c}\cdot(2+(m-1)(1+e^{-2\cdot\gamma\cdot x_j})))}\right|} - 1$$
$$= \left|1 + \frac{Z_f}{2\cdot Z_c}\cdot(1+\frac{m-1}{m+1}\cdot e^{-2\cdot\gamma\cdot x_j})\right| - 1, \quad \forall f \in BW \tag{2.13}$$

– The expression of the health indicators computed at the receivers that are not connected to the faulty branch is

$$I_{R_{i,0}}(f) = \frac{\left|H_{R_{i,0}}^{Reference}(f)\right|}{\left|H_{R_{i,0}}(f)\right|} - 1 = \frac{\left|\frac{2}{(m+1)\cdot e^{\gamma(l_0+l_i)}}\right|}{\left|\frac{2}{e^{\gamma(l_0+l_i)}\cdot((m+1)+\frac{-2Z_f\cdot e^{-2\gamma x_j}}{2Z_c+Z_f(1+e^{-2\gamma x_j})})}\right|} - 1 \tag{2.14}$$
$$= \left|1 + \frac{-2Z_f\cdot e^{-2\gamma x_j}}{(m+1)(2Z_c+Z_f(1+e^{-2\gamma x_j}))}\right| - 1$$
$$\forall\, i \in \{1;2;\ldots;m\} - \{j\},\ \forall f \in BW$$

From the previous expressions, all health indicators, with the exception of one, are equal and different from zero. The health indicator associated to the receiver R_j directly connected to the faulty branch is different from all others.

In all the previous networks, each receiver computes locally the health indicators before sending the values to the ECU source. Then, a method of comparing these health indicators is performed by the ECU source. Different comparison methods are detailed in the following.

2.4 Health indicators comparison methods

2.4.1 Correlation-based comparison method

Each health indicator is composed of frequency-dependent variables. Correlation metrics can be used to compare such variables [131]. They allow a global decision over the entire bandwidth instead of comparing frequency-dependent variables at each frequency.

Remark 4 *Correlation metrics can be defined as a measure of consistency (degree of linearity) between frequency-dependent variables [132].*

Several correlation metrics can be found in the literature such as:

- Pearson's coefficient [133] which is normalized between -1 and + 1.
- Frequency Response Assurance Criterion (FRAC) [134] which is normalized between 0 and +1.
- Frequency Response Function Root Mean Square (FRFRMS) [135] which is not normalized and is a log magnitude comparison.

A review of the different correlation metrics is presented in [132, 136, 137], where the FRAC metric is reported as one of the simplest and most popular metrics.

Definition 4 *The Frequency Response Assurance Criterion (FRAC) reported in [132] is a correlation metric used to compare between two frequency response functions. It is defined as follows :*

$$FRAC(X,Y) = \frac{|\sum_k X(f_k) \cdot Y^*(f_k)|^2}{\sum_k X(f_k) \cdot X^*(f_k) \sum_k Y(f_k) \cdot Y^*(f_k)} \tag{2.15}$$

X and Y denote the two frequency-dependent variables to be compared. J^* denotes the conjugate of J and $|J|$ is the module of J. f_k denotes the k^{th} frequency component.

To take into account the magnitude difference between the two compared functions, $X(f)$ and $Y(f)$, the Modified Frequency Response Assurance Criterion (MFRAC) is proposed.

Definition 5 *The Modified Frequency Response Assurance Criterion is defined in [137] as:*

$$MFRAC(X,Y) = P_{ratio} \cdot FRAC(X,Y) \text{ with } P_{ratio} = \frac{min(P_{X(f_k)}, P_{Y(f_k)})}{max(P_X, P_Y)} \tag{2.16}$$

P_{ratio} is the power ratio of the two compared frequency response functions and $P_J = \sum_k |J(f_k)|^2$ is the overall power over the bandwidth of interest.

Any two frequency response functions can be compared using FRAC or MFRAC metrics [132]. MFRAC metric quantifies the existence or absence of a linear relationship between the two compared frequency response functions. It provides a value between 0 and 1, where 1 denotes a perfect correlation between the compared functions and 0 denotes an absence of correlation between the two compared functions.
To compare the results of FRAC and MFRAC metrics, three different situations are presented in the Fig. 2.6. In the first case, both correlation metrics FRAC and MFRAC are calculated on two sinus signals with different amplitude and offset. The FRAC value is 1 considering that the two signals are strongly correlated. Due to the normalization, the MFRAC value is 0.25 considering that the two signals are not similar. In our application to compare the equality or the non equality of the health indicators, MFRAC metric seems to be more suitable than FRAC.
In the second case, the metrics are applied to compare two same sinus signals, one of them being noisy. The correlation metrics FRAC and MFRAC provide a value of 0.98, revealing an excellent similarity between the signals. In the last case, two white Gaussian noises are compared. The FRAC and MFRAC metrics provide logically a value of 0, confirming the absence of correlation between two noises. The health indicators in the no-fault situation equal zero in absence of noise, and are random signals in presence of noise. The correlation metrics between two health indicators will thus indicate that they are not correlated, and thus that they are different, even if they are theoretically equal. To avoid this wrong indication, and consequently a wrong decision, another comparison method, based on residuals, is proposed in the following.

2.4.2 Residuals based comparison method

In a point-to-point network, the health indicators are either equal or different from zero. In a Y-shaped or star-shaped networks, the health indicators are either equal to zero, equal to or different from each other for all frequencies f. To compare between

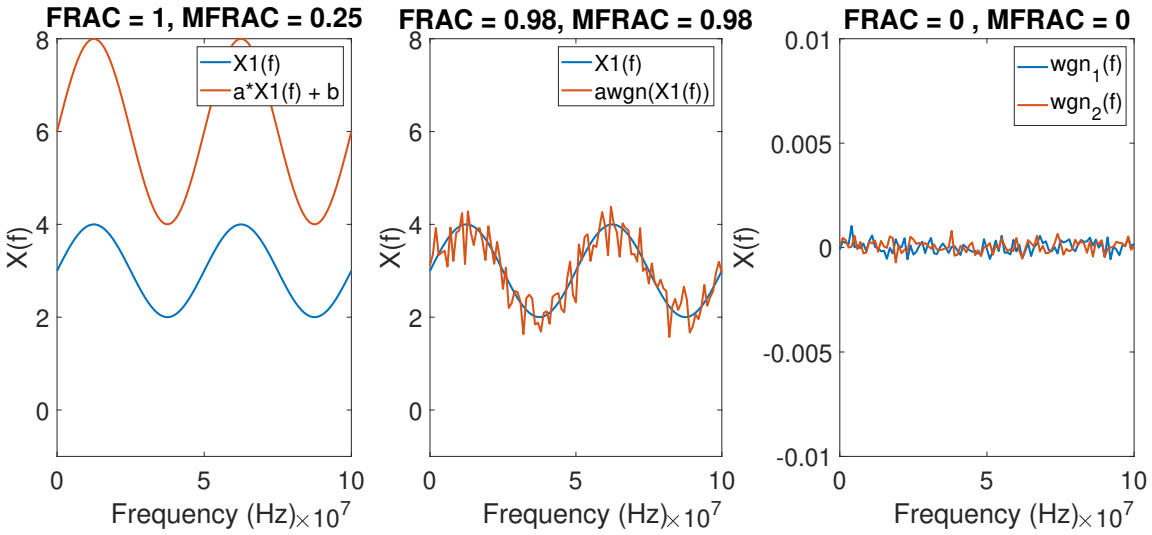

FIGURE 2.6: Illustration of FRAC and MFRAC metrics.

these health indicators to zero or to each other, residuals r_p and r_s are proposed in the following.

The residual r_p is proposed for networks with point-to-point connections between ECU and the residual r_s is proposed for Y-shaped and star-shaped networks. These residuals allow a global decision over the entire bandwidth instead of comparing health indicators at each frequency.

2.4.2.1 Residual for a point-to-point network

Definition 6 *The residual r_p is defined as:*

$$r_p = \frac{1}{N_f} \sum_{f_1}^{f_{N_f}} |I_{R_{i,s}}(f)| \quad with\ f \in BW = [f_1 : \Delta_f : f_{N_f}] \tag{2.17}$$

where $I_{R_{i,s}}(f)$, is the health indicator computed online, BW is the frequency bandwidth. N_f is the number of frequency components (sub-carriers).

The residual r_p is either equal to zero or different from zero. If the residual is equal to zero, the network is in the no-fault nominal situation. Otherwise, the network is considered to be faulty.

$$r_p \begin{cases} = 0 & \text{network is in the no-fault nominal situation.} \\ \neq 0 & \text{network is in a faulty nominal situation.} \end{cases} \tag{2.18}$$

2.4.2.2 Residual for a Y-shaped network

In a Y-shaped network, each source receives a pair of health indicators from the receivers. To decide whether the network is considered to be faulty or not and to locate the faulty branch, a comparison between the two health indicators is performed for all the frequencies in the BW. To avoid a separate comparison at each frequency f, a global comparison is proposed through structured residuals.

Definition 7 *The residual r_s is defined as:*

$$r_s = \frac{1}{N_f} \sum_{f_1}^{f_{N_f}} |I_{R_{i,s}}(f) - I_{R_{j,s}}(f)| \quad with\ f \in BW = [f_1 : \Delta_f : f_{N_f}] \tag{2.19}$$

where BW is the frequency bandwidth, N_f is the number of frequency components (sub-carriers), s is the index of the ECU source, i and j are the indices of the ECU receivers with $s \neq i \neq j \in \{0,1,2\}$. The residual r_s is computed at the source S_s and the pair of health indicators, $I_{R_{i,s}}(f)$ and $I_{R_{j,s}}(f)$, are computed respectively at the receivers R_i and R_j.

By computing the residuals, we only have one number to test instead of several indicators to compare for many frequencies. Table 2.7 presents the signature matrix, based on these residuals. This matrix is used to detect the presence of a fault and to locate the faulty branch.

TABLE 2.7: Residual-based Y-shaped network signature matrix.

r_s	No-fault	Faulty B_0	Faulty B_1	Faulty B_2
r_0	0	0	1	1
r_1	0	1	0	1
r_2	0	1	1	0

0 indicates that r_s is equal to zero.
1 indicates that r_s is different from zero.

In a Y-shaped network, one residual per ECU can be computed which leads to three residuals r_0, r_1 and r_2. The residuals form a structured residual set. The residuals values can be represented in the 3-dimensional residual space [138]. According to the signature matrix in table 2.7, for each faulty situation, only a fault-specific subset of residuals becomes different from zero.

Consider the faulty B_0 situation, the residual r_0 is null and the residuals in the subset $\{r_1; r_2\}$ are different from zero. The health indicators $I_{R_{1,0}}(f)$ and $I_{R_{2,0}}(f)$ are

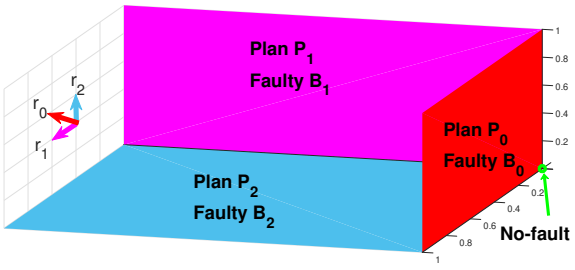

FIGURE 2.7: Structured residuals.

equal. Since $I_{R_{0,1}}(f)$ is equal to $I_{R_{1,0}}(f)$ and $I_{R_{2,0}}(f)$ is equal to $I_{R_{0,2}}(f)$, therefore $I_{R_{0,1}}(f)$ is equal to $I_{R_{0,2}}(f)$.

Using (2.19), let us consider the residual r_1:

$$r_1 = \frac{1}{N_f} \sum_{f_1}^{f_{N_f}} |I_{R_{0,1}}(f) - I_{R_{2,1}}(f)| \quad with\ f \in BW$$

Replacing $I_{R_{0,1}}(f)$ by $I_{R_{0,2}}(f)$ and $I_{R_{2,1}}(f)$ by $I_{R_{1,2}}(f)$ leads to

$$r_1 = r_2 = \frac{1}{N_f} \sum_{f_1}^{f_{N_f}} |I_{R_{0,2}}(f) - I_{R_{1,2}}(f)| \quad with\ f \in BW$$

By analogy to the faulty B_0 situation, each fault-specific subset produces two non-zero equal residuals in the faulty B_1 and faulty B_2 situations. Geometrically, the residual vector is confined in a subspace spanned by a subset of coordinate vectors as seen in Fig. 2.7 :

1. The origin (0;0;0) represents a no-fault situation.
2. If the fault is located at the branch B_0, the residual vector is located in the plane P_0 spanned by the residuals r_1 and r_2.
3. If the fault is located at the branch B_1, the residual vector is located in the plane P_1 spanned by the residuals r_0 and r_2.
4. If the fault is located at the branch B_2, the residual vector is located in the plane P_2 spanned by the residuals r_0 and r_1.

In conclusion, in a Y-shaped network, the soft fault detection and localization procedure requires the estimation of six transmission coefficients, the computation of six health indicators and three residuals.

Remark 5 *The three residuals r_0, r_1, and r_2 are used to form the signature matrix seen in Table 2.7 (one residual per source). The hamming distance between each network situation's signature is equal to two. Two residuals are sufficient to distinguish between the different fault signatures. However, with only two residuals, the hamming distance between two signatures will be equal to 1. In presence of noise, the residuals are random variables and a decision procedure has to be applied to decide if the residual is zero or not. This will inevitably generate wrong decisions (false alarm or missed detection). To have a more robust decision the three residuals are kept in the following.*

2.4.3 Communication between ECU

The communication mechanism is out of the scope of this work, but the *ECU* in the network must exchange information in order to compute the residuals required for the proposed fault detection and localization approach. The estimation of the transmission coefficients is the initial step in our fault localization and detection process. This step is not included in the messages needed for diagnosis because it is necessary for both communication and diagnosis.
After the estimation procedure, each of the three *ECU* computes the health indicators locally. They must be then transmitted through the network in order to compute the residuals. In order to accomplish this, a supervisor organizes the messages dedicated to monitor the network.
Let's consider that the ECU_0 of the Y-shaped network is the supervisor. A time window will be assigned for monitoring, during which the ECU_0 will send out a message to the two other *ECU* informing them the start of the monitoring procedure. Once this message is received, each *ECU* will reply to this message by sending their health indicators to the supervisor. ECU_0 will receive the health indicators $I_{R_{1,0}}(f)$ and $I_{R_{1,2}}(f)$ from ECU_1 and the health indicators $I_{R_{2,0}}(f)$ and $I_{R_{2,1}}(f)$ from ECU_2. Upon receiving the four health indicators, the three residuals are computed by ECU_0 and the final diagnosis result is obtained.

2.4.4 Summary of the fault detection and localization method

The fault detection and localization method is summarized in Fig. 2.8. It consists of three main steps :

1. Estimation of the transmission coefficients (TC) through pilot signals by the receivers.

2. Computation of the health indicators for all frequencies in the BW by the receivers. The indicators values are sent to the source via PLC link.
3. Computation of the residuals by the sources.
4. Comparison of the residuals with the preconstructed signature matrix.

A point in the residuals space represents the state of the targeted network. The effect of a fault in a particular branch will shift the point from the origin (0;0;0) to one of the three planes.

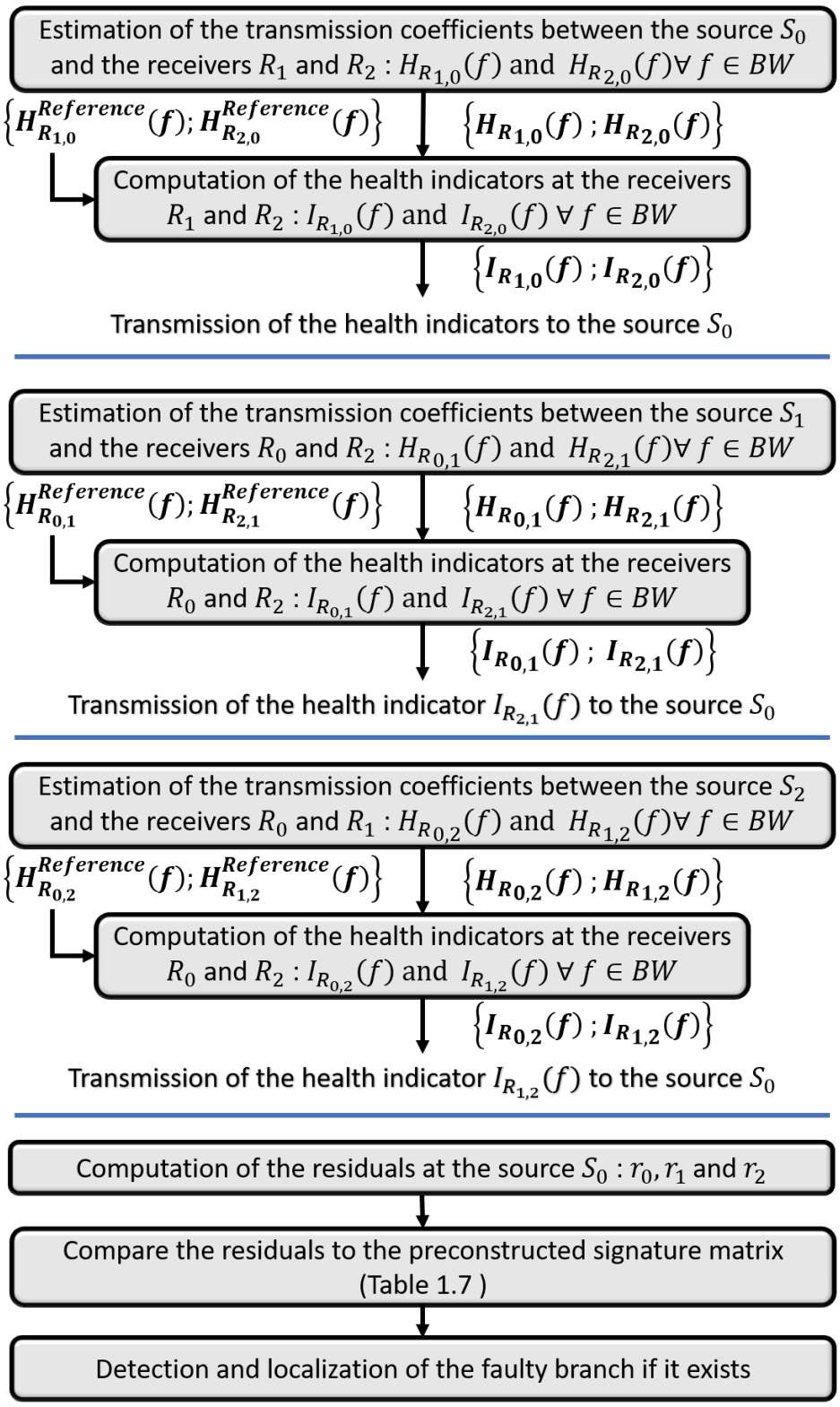

FIGURE 2.8: Fault detection and localization method (Y-shaped network).

FIGURE 2.9: Test bench.

2.5 Validation on a Y-shaped network

2.5.1 Test-bench description

A test bench, shown in Fig. 2.9, has been set up to test the efficiency of the proposed PLC-based fault detection and localization method. The test bench is a Y-shaped network similar to the one represented in Fig. 2.10. The three branches are connected with a node as shown in Fig.2.11b. The installed cables consist of unshielded twisted pair cables of type DRB 18 with a characteristic impedance of nearly 120 Ω surrounded by 6 AWG14 single wires (single wires are not loaded).

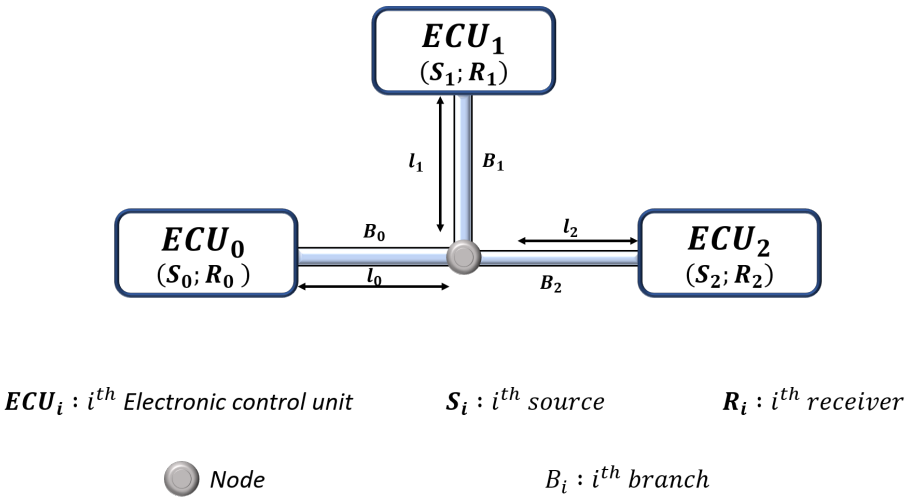

FIGURE 2.10: Y-shaped network.

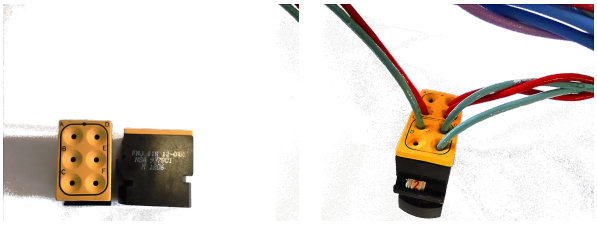

(A) (B)

FIGURE 2.11: Crossroads of the branches of the Y-shaped network. (A) Node, (B) Connection of three cables.

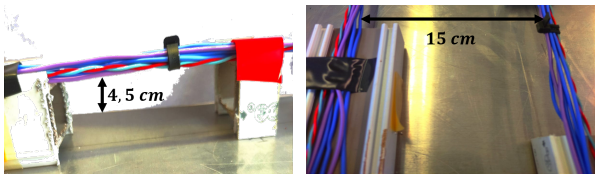

(A) (B)

FIGURE 2.12: Installation of the twisted cables. (A) Distance from the aluminum ground plane, (B) Distance between two sections of cables.

The diameters of the conductor and on the insulation of the DRB 18 are 1.2 mm and 1.6 mm respectively. Those of the conductor and on the insulation of the monowires are 1.1 mm and 2.3 mm respectively. The cables are placed above an aluminium ground plane at a height of 4.5 cm and the distance between each straight section of cable is 15 cm as shown in Fig. 2.12b.

This bench was built to be easily manipulated for fault diagnosis purpose. A fault represented by an impedance $Z_f \in \{5\Omega\,; 10\Omega\,; 47\Omega\,; 100\Omega\}$ can be inserted in series and removed in three different positions. The length of the branches B_0, B_1 and B_2 are respectively $l_0 = 4.25\ m$, $l_1 = 5\ m$ and $l_2 = 5.1\ m$. The distance between the fault positions and the node in each branch is $x_0 = 1.75\ m$, $x_1 = 2.5\ m$ and $x_2 = 1.5\ m$.

Our initial goals were to prove the validity of diagnosis method's and to study the robustness and sensitivity of the proposed residuals as a proof-of-concept. Thus, the ECU's programming requirements and the communication protocols used to transmit pilot signals from the sources to the receivers in order to estimate the TC were not our priorities. So we opted not to concentrate on this aspect but to use a measuring instrument to measure the TC, and to directly control the communications. The instrument is a 4 ports Vector Network Analyser (VNA E5071C). It is used to inject a signal with a power of $P_{inj} = 0\ dBm$ into the network and to measure the transmission coefficients between each source and each two end lines in the frequency band of $[0.25 : 100]\ MHz$ which is traditionally used in smart grids applications with 1601 frequency components (Inter Frame BandWidth, $IFBW = 10\ kHz$).

Since the input and outputs of the VNA have an impedance of 50Ω different to that of the lines, 3 baluns as shown in Fig.2.13 are used to match the measurement instrument to the network. The transmission coefficients between each pair of baluns are then measured by the VNA and transmitted to a computer for data processing via MATLAB®. In order to not take into account the baluns and the connections between the baluns and the VNA in the measurements, a calibration of the VNA is required before each measurement between two baluns.

To consider the background noise of a vehicle [139] and to approach real installation conditions and test the robustness of the proposed residuals, Additive White

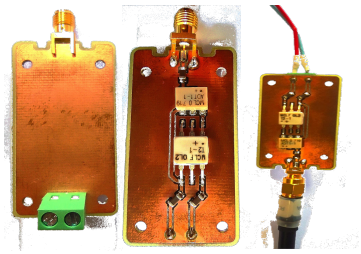

(A) (B) (C)

FIGURE 2.13: Balun. (A) Back side, (B) Front side, (C) Balun connection.

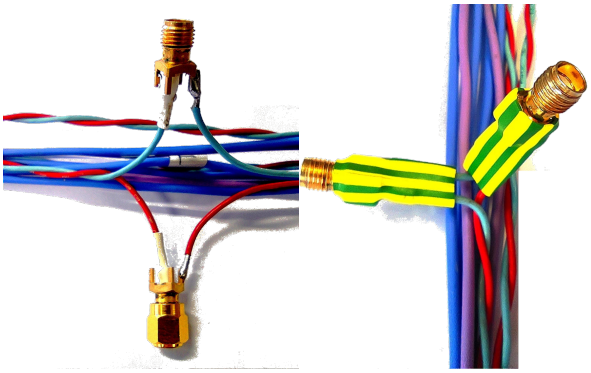

(A) (B)

FIGURE 2.14: Cable connected to female connector straight. (A) without heat shrink tubing, (B) with heat shrink tubing.

Gaussian Noise with a signal to noise ratio of 100 dB is added via MATLAB® to the measured TC.
In the following, the different fault samples implementation are described. To insert and remove faults from each cable, the cables are cut and reconnected to a RS PRO female coaxial connector Straight, 50Ω solder connection PCB mount as seen in Fig. 2.14. To protect the connection between the cable and the connector, a heat shrink tubing is added as shown in Fig. 2.13b.

The cable can be either in a no-fault situation or in a faulty situation depending on the SMA plug connected to the female coaxial connector :

- To represent a no-fault situation, a straight SMA RF terminator is connected to the female coaxial connector. This connection represents a short circuit, so it is as if the cable had never been cut.
- To represent a faulty situation, a resistive impedance $Z_f = \{5; 10; 47; 100\}\Omega$ is connected to a straight adapter plug plug. Then this adapter is connected to the female connector. This connection represents an insertion of a resistive impedance in series.

2.5.2 Validation of the proposed diagnosis method

The proposed fault detection and localization method detailed in section 2.3 is tested on the Y-shaped test-bench in the four different situations :

- No-fault situation : The network is fault-free.
- Faulty B_0 : The fault is located at the branch B_0.
- Faulty B_1 : The fault is located at the branch B_1.
- Faulty B_2 : The fault is located at the branch B_2.

In the three faulty situations, the fault severity represented by the added impedance Z_f can take four different values with $Z_f = \{5;\ 10;\ 47;\ 100\}\ \Omega$. In total, 13 different cases (1 fault-free and 12 faulty) of the network are tested. A transmission coefficient is measured over the entire bandwidth by the VNA and is composed of 1601 frequency components in the bandwidth $[250kHz : 62.3kHz : 100MHz]$.
The modules of the measured transmission coefficients in the no-fault and faulty B_0 situations are presented in Fig. 2.15. Since the health indicators are just a function of the modules of the TC, we were not interested in the phase of the TC. After

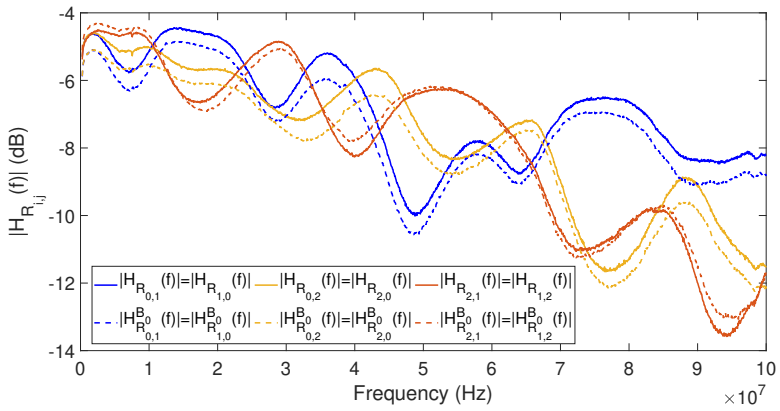

FIGURE 2.15: Module of the transmission coefficients (no-fault, faulty B_0 with $Z_f = 10\Omega$).

acquiring the transmission coefficients, the health indicators are calculated using (2.1) in the 13 cases of the network.

For the faulty cases, the transmission coefficients and health indicators, obtained when the fault severity $Z_f = 10\ \Omega$, are first discussed in this part :

1. The health indicators in the no-fault situation are presented in Fig. 2.16. Theoretically, the health indicators are null in the no-fault situation. Due to

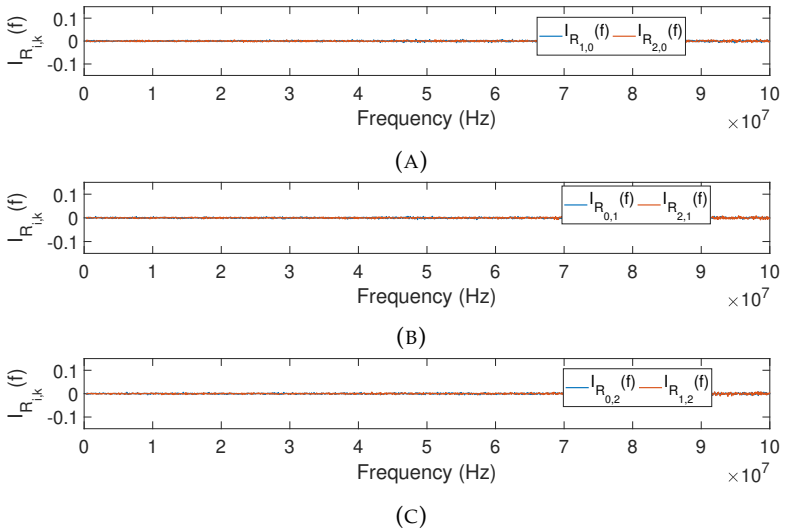

FIGURE 2.16: Variation of the health indicators (No-fault network).

noise, they take a value close to zero with a mean value of $5e^{-6}$ and a standard deviation of 0.002.

2. In the faulty B_0 situation : Theoretically, when S_0 is transmitting, the 2 health indicators computed at the receivers R_1 and R_2 are equal, i.e. $I_{R_{1,0}}(f) = I_{R_{2,0}}(f)$. When S_1 (resp. S_2) is transmitting, the health indicators computed at the receivers R_0 and R_2 (resp. R_0 and R_1) are different, i.e $I_{R_{0,1}}(f) \neq I_{R_{2,1}}(f)$ (resp. $I_{R_{0,2}}(f) \neq I_{R_{1,2}}(f)$).

   The experimental health indicators are presented in Fig. 2.17. As it can be seen in Fig. 2.17a, the health indicators $I_{R_{1,0}}(f)$ and $I_{R_{2,0}}(f)$ are quite similar ($I_{R_{1,0}}(f) \approx I_{R_{2,0}}(f)$), while the health indicators $I_{R_{0,1}}(f)$ and $I_{R_{2,1}}(f)$ (resp. $I_{R_{0,2}}(f)$ and $I_{R_{1,2}}(f)$) are clearly different which can be seen in Fig. 2.17b and Fig. 2.17c. Moreover, as $I_{R_{0,1}}(f) = I_{R_{1,0}}(f)$ and $I_{R_{0,2}}(f) = I_{R_{2,0}}(f)$, the four health indicators $I_{R_{0,1}}(f)$, $I_{R_{1,0}}(f)$, $I_{R_{2,0}}(f)$ and $I_{R_{0,2}}(f)$ are superimposed in Fig. 2.17.

   All these experimental results confirm what was expected theoretically.

3. In the faulty B_1 situation : Theoretically, when S_1 is transmitting, the health indicators, computed at the receivers R_0 and R_2 are equal ($I_{R_{0,1}}(f) = I_{R_{2,1}}(f)$). When S_0 (resp. S_2) is transmitting, the health indicators computed at the receivers R_1 and R_2 (resp. R_0 and R_1) are different from each others ($I_{R_{1,0}}(f) \neq I_{R_{2,0}}(f)$ and $I_{R_{0,2}}(f) \neq I_{R_{1,2}}(f)$).

   The experimental health indicators are presented in Fig. 2.18. As it can be seen in Fig. 2.18b, the health indicators, $I_{R_{0,1}}(f)$ and $I_{R_{2,1}}(f)$, are quite similar ($I_{R_{0,1}}(f) \approx I_{R_{2,1}}(f)$) and the health indicators $I_{R_{1,0}}(f)$ and $I_{R_{2,0}}(f)$ (respectively $I_{R_{0,2}}(f)$ and $I_{R_{1,2}}(f)$) are clearly different.

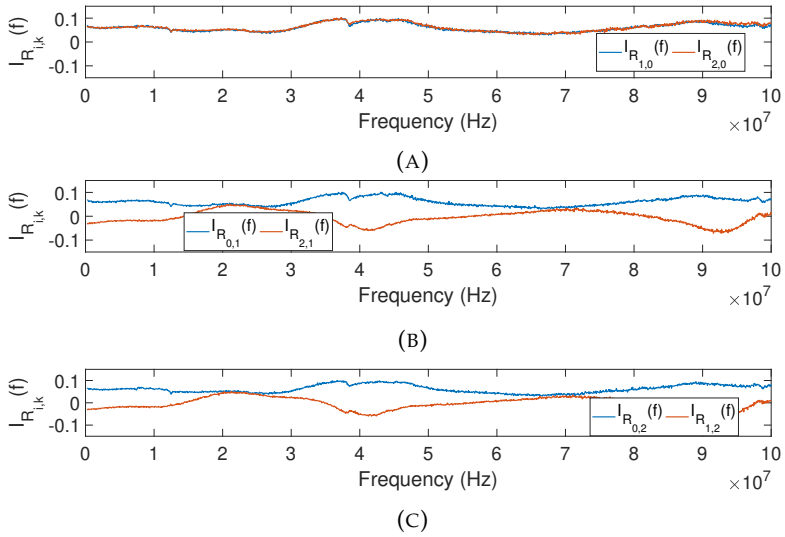

FIGURE 2.17: Variation of the health indicators (Faulty B_0, $Z_f = 10\Omega$).

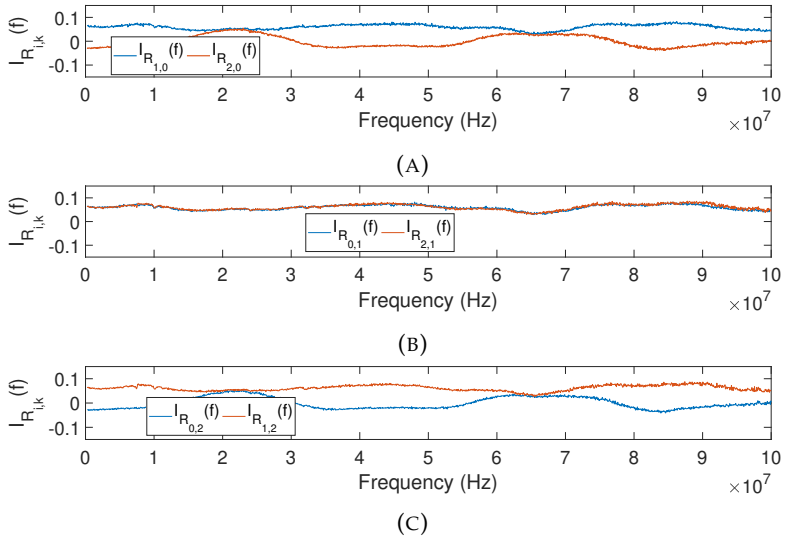

FIGURE 2.18: Variation of the health indicators (Faulty B_1, $Z_f = 10\Omega$).

All these experimental results confirm what was expected theoretically.

4. In the faulty B_2 situation : Theoretically, when S_2 is transmitting, the health indicators computed at the receivers R_0 and R_1, are equal ($I_{R_{0,2}}(f) = I_{R_{1,2}}(f)$) and when S_0 (resp. S_1) is transmitting, the health indicators computed at the receivers R_1 and R_2 (resp. R_0 and R_2) are different ($I_{R_{1,0}}(f) \neq I_{R_{2,0}}(f)$ and $I_{R_{0,1}}(f) \neq I_{R_{2,1}}(f)$).

   The experimental health indicators are presented in Fig. 2.19. The experimental health indicators are in accordance with the theory: the health indicators $I_{R_{0,2}}(f)$ and $I_{R_{1,2}}(f)$ are quite equal ($I_{R_{0,2}}(f) \approx I_{R_{1,2}}(f)$) while the health indicators $I_{R_{1,0}}(f)$ and $I_{R_{2,0}}(f)$ (resp. $I_{R_{0,1}}(f)$ and $I_{R_{2,1}}(f)$) are clearly different.

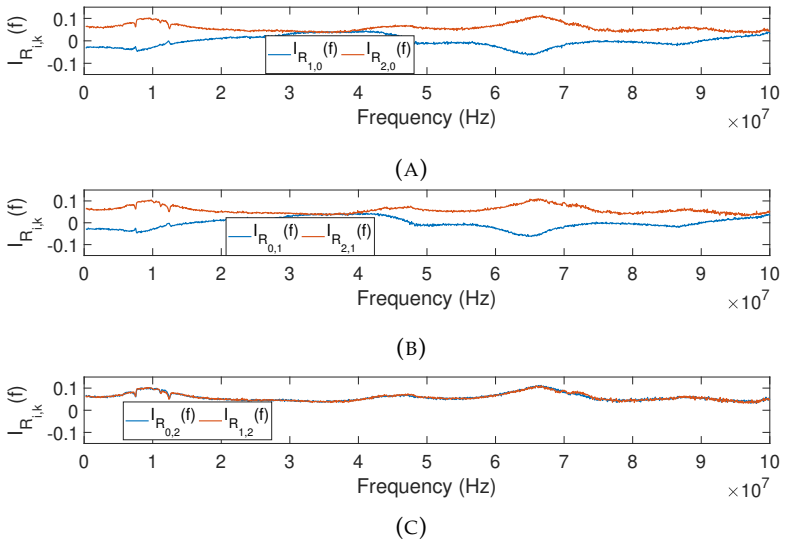

FIGURE 2.19: Variation of the health indicators (Faulty B_2, $Z_f = 10\Omega$).

All these experimental results confirm what was expected theoretically.

2.5.2.1 Residuals generation

The residuals r_0, r_1 and r_2, between each pair of health indicators, are computed using (2.20), (2.21) and (2.22).

$$r_0 = \frac{1}{1601} \sum_{250kHz}^{100MHz} |I_{R_{1,0}}(f) - I_{R_{2,0}}(f)| \quad with\ f \in BW = [250kHz : 62.3kHz : 100MHz] \tag{2.20}$$

$$r_1 = \frac{1}{1601} \sum_{250kHz}^{100MHz} |I_{R_{0,1}}(f) - I_{R_{2,1}}(f)| \quad with\ f \in BW = [250kHz : 62.3kHz : 100MHz] \tag{2.21}$$

$$r_2 = \frac{1}{1601} \sum_{250kHz}^{100MHz} |I_{R_{0,2}}(f) - I_{R_{1,2}}(f)| \quad with\ f \in BW = [250kHz : 62.3kHz : 100MHz] \tag{2.22}$$

13 different cases (1 fault-free and 12 faulty cases) are considered in the experimental network. The 12 faulty cases correspond to four different fault severities (4 added resistances) located in the 3 branches B_0, B_1 and B_2.

A transmission coefficient (TC) is measured by the VNA for each case and all frequencies in $BW = [250kHz : 62.3kHz : 100MHz]$. Then, MATLAB® is used to add a white Gaussian noise to the TC values with a signal to noise ratio of $100dB$

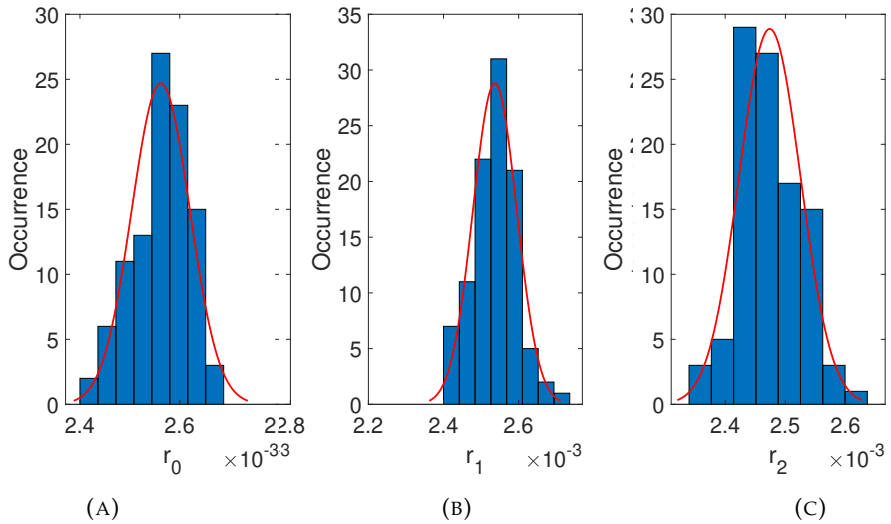

(A) (B) (C)

FIGURE 2.20: Distribution of the residuals. (A) r_0, (B) r_1 and (C) r_2.

to get closer to the experimental conditions in an embedded system. 100 noisy TC values per case are generated and 100 residual values are computed. The residuals are plotted in the residual space (r_0 , r_1, r_2).
In the no-fault situation of the network, the distribution of the computed residuals is shown in Fig. 2.20 and according to a Chi-square goodness-of-fit test [140], it approaches a Normal distribution with a 5% significance level. Their mean values μ_k and their standard deviations σ_k, where $k \in \{1;2;3\}$ represents the residual index, are computed and listed in Table 2.8.

TABLE 2.8: Statistical features of the residuals in the no-fault situation.

	r_0	r_1	r_2
μ_k	$2.6e^{-3}$	$2.5e^{-3}$	$2.5e^{-3}$
σ_k	$5.8e^{-3}$	$5.8e^{-3}$	$5.1e^{-3}$

Since the distribution of the three residuals approximates a Normal distribution, it means that 99.73% of their values are in the range of $[\psi_k^-, \psi_k^+]$, where $\psi_k^- = \mu_k - 3\sigma_k$ and $\psi_k^+ = \mu_k + 3\sigma_k$ with $k \in \{0;1;2\}$.

Definition 8 *A sample is defined by a set of residual values r_k where $k \in 0, 1, ..N-1$. It is represented by a point in the residual space of dimension N.*

In case of a Y-shaped network, a sample is defined by $N = 3$ residual values $(r_0; r_1; r_2)$.

Definition 9 *A cluster is a set of samples (a set of points in the residual space) where each residual value r_k of the samples belongs to the interval $[\psi_k^- \psi_k^+]$. A cluster is thus a statistical*

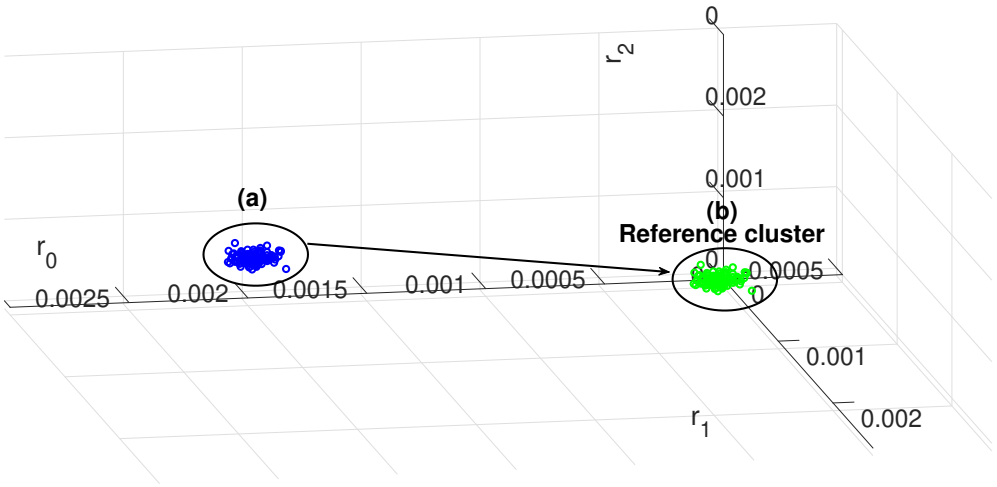

FIGURE 2.21: Residuals in the no-fault situation (Before and after centering at the origin).

distribution of residuals (each residual is a random variable) which is limited to the interval $[\psi_k^- \psi_k^+]$.

Remark 6 *Theoretically, in the ideal situation (no-fault and no noise), the residuals values are centered at the origin of the residual space. In presence of noise on the TC, as it is seen in Table 2.8 each residual in no-fault situation follows a statistical distribution whose mean value is not zero. This is shown by the blue cluster in Fig. 2.21 which is not centered at the origin. The non-zero mean is due to the fact that the additive noise that affects the transmission coefficients is injected non-linearly in the health indicators, and further in the residuals.*

In order to simplify the decision making, the residuals are centered at the origin. The mean values (μ_0, μ_1 and μ_2) of the first 50 residuals are subtracted to all residuals values. As a consequence, a new cluster (in green colour in Fig. 2.21) centered at the origin is obtained.

Definition 10 *The reference cluster is the cluster formed by the residuals in the no-fault situation of the network. The reference cluster is centered at the origin to simplify the decision making.*

The residuals are computed in the 13 cases of the network (no-fault, faults with four different fault severities in B_0, B_1 and B_2). Each residual is modified by subtracting the mean value of the first 50 residual values. The obtained residuals are presented in

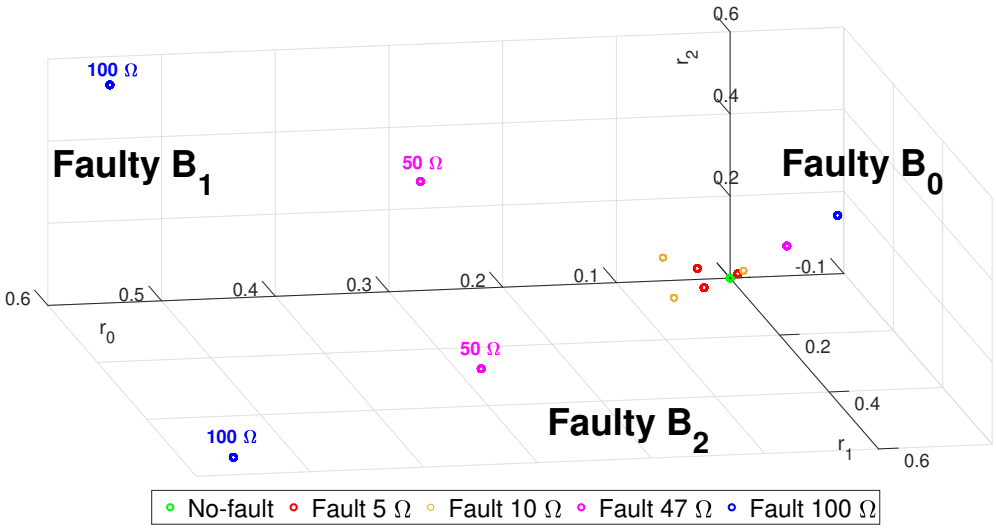

FIGURE 2.22: Residuals in different network situations.

Fig. 2.22. We can see that the distances between the faulty clusters and the reference clusters depend on the severity of the fault. The more severe the fault is, the greater the distance to the reference cluster is.

In accordance to the signature matrix of structured residuals presented in the Table 2.7, the cluster obtained for each faulty branch should belong to the expected plane. This is not exactly the case as it will shown in the following.

The faulty B_0 and the faulty B_1 situations are analysed, the analysis of the faulty B_2 situation may be deduced :

1. **Faulty B_0 :** According to the signature matrix presented in the table 2.7, if the branch B_0 is faulty, the residual r_0 should be equal to zero, i.e., the cluster representing this case should be in the plane P_0 spanned by the residuals r_1 and r_2. In the plane P_1 spanned by the residuals r_0 and r_2, the cluster representing this case should be on the r_2 axis. In the plane P_2 spanned by the residuals r_0 and r_1, the cluster representing this case should be on the r_1 axis.
   The residuals are presented in Fig. 2.23a and in Fig. 2.23b in the planes P_0 and P_2 for different situations of fault represented by the resistance, $Z_f = \{5; 10; 47; 100\}\ \Omega$, inserted at the branch B_0. In the figure, the residuals in the no-fault situation are in green color whereas the residuals in the faulty situation are in red color.

   In the plane P_0, the green cluster is around (0;0). The distance between the red clusters and the green cluster increases with the severity of the inserted fault Z_f.
   In the plane P_2, in which the r_0-axis has been expanded, we observe that the

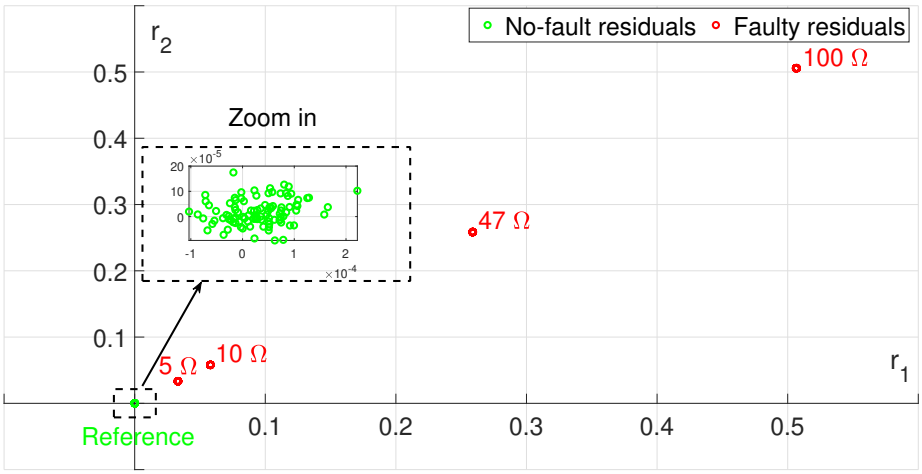

(A) Plane P_0

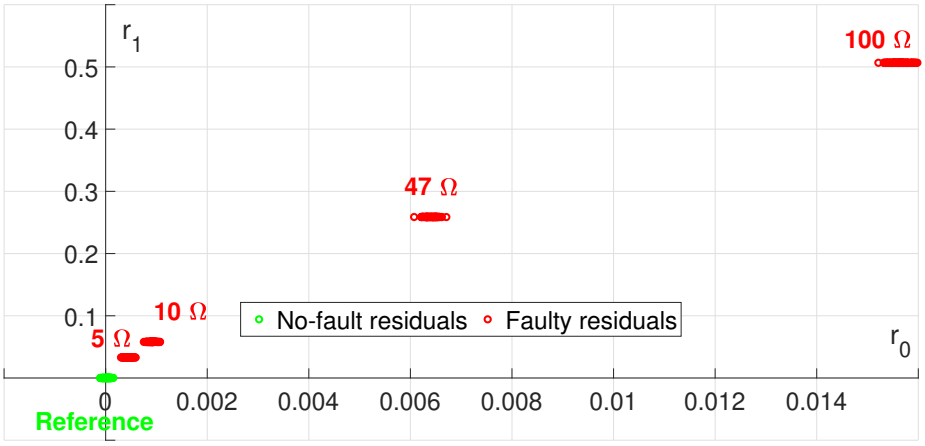

(B) Plane P_2

FIGURE 2.23: Residuals in the planes P_0 and P_2, faulty B_0, four fault severities.

residuals r_0 are not exactly equal to zero. As pointed out previously for the no-fault situation, this is due to the additive noise on the transmission coefficients that influence non-linearly the health indicators, and further the residuals. It is also observed that this small but non-zero component depends on the fault severity.

2. **Faulty B_1 :** Theoretically, if the branch B_1 is faulty, the residual r_1 should be equal to zero, i.e., the cluster representing this case should be in the plane P_1 spanned by the residuals r_0 and r_2. In the plane P_0 spanned by the residuals r_1 and r_2, the cluster representing this case should be on the r_2 axis. In the plane P_2 spanned by the residuals r_0 and r_1, the cluster representing this case should be on the r_0 axis.
   The residuals are presented in Fig. 2.24a and in Fig. 2.24b in the planes P_0 and P_1 respectively.
   In the plane P_0, the residuals r_1 are not exactly equal to zero and depend on the severity of the fault as it has been seen in the previous case.
   In the plane P_1, the green cluster is around (0;0). The distance between the red clusters and the green cluster increases with the severity of the inserted fault Z_f.

Theoretically, we have proved that a cluster in the plane P_i (i.e., $r_i = 0$) indicates that the fault is located at the branch B_i. As we have pointed out previously, the experimental results show that the residuals that should be equal to zero are not exactly zero. The obtained small values depend of the severity of the fault. We propose in the following a modification of the residual to better meet the expected properties.

2.5.2.2 Improving the residuals in presence of noise

The residuals, proposed in subsection 2.4.2, are sensitive to soft fault. According to the signature matrix presented in Table 2.7, the sensitivity of each residual depends on the network situation (no-fault, faulty B_0, faulty B_1 and faulty B_2). For example, if the soft fault is located on the branch B_0, the residuals r_1 and r_2 are non-zero (fault-sensitive) and the residual r_0 should be strictly equal to zero.
Due to noise or external disturbances, the residuals r_0 will deviate from zero as seen in Fig.2.23b. Hence, it is necessary to improve these residuals to facilitate the decision making.

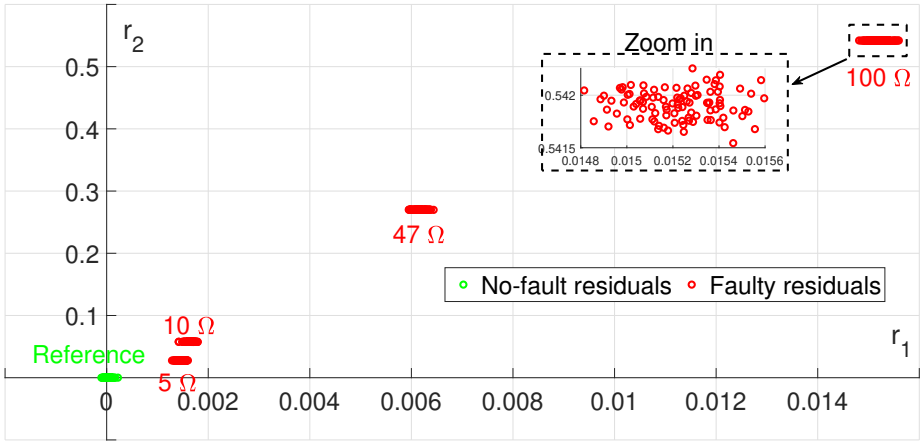

(A) Plane P_0.

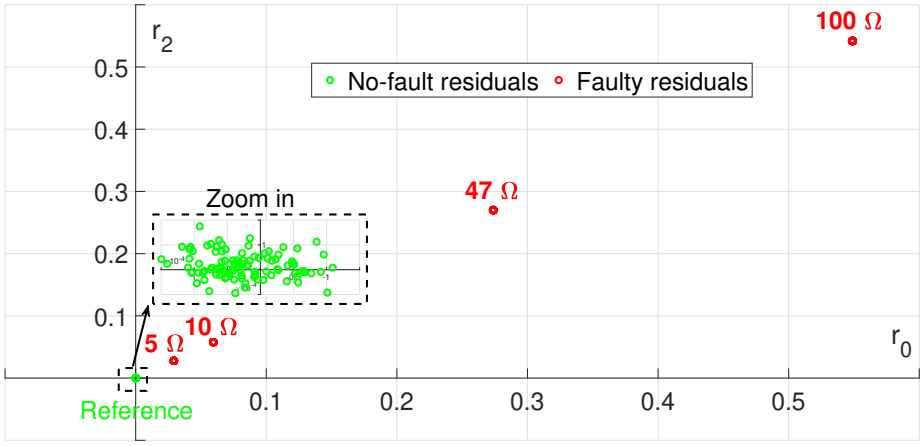

(B) Plane P_1.

FIGURE 2.24: Residuals in the planes P_0 and P_1, faulty B_1, four fault severities.

We propose to combine the correlation and the residuals to cope with the effects of noise. The modified improved residuals are called practical residuals.

Definition 11 *Practical residuals are the product of the residuals defined in* (2.19) *with a weight derived from the correlation coefficient defined in* (2.15),

$$\rho_s = (1 - MFRAC(I_{R_{i,s}(f)}, I_{R_{j,s}(f)})) \cdot r_s \tag{2.23}$$

The same signature matrix is obtained when the initial residuals are replaced by the practical residuals:

- In the no-fault situation : health indicators are stochastic variables with zero mean. The correlation coefficient $MFRAC(I_{R_{i,s}(f)}, I_{R_{j,s}(f)})$ between these signals is near zero, therefore the weighting factor $1 - MFRAC(I_{R_{i,s}(f)}, I_{R_{j,s}(f)})$ is near one and has thus no impact on the calculation of the residuals. This result is illustrated in Fig. 2.25, where the residuals (in the configuration of Fig. 2.16) and the practical residuals are both shown. The points in the new cluster seems to be superimposed with the points of the previous cluster. The two sets of residuals $\{r_0; r_1; r_2\}$ and $\{\rho_0; \rho_1; \rho_2\}$ have the same mean values of $\{0.0025; 0.0040; 0.0026\}$ and the same standard deviations of $\{0.0147; 0.0102; 0.0098\}$.
- In a faulty situation, two cases may occur :
  1. If two health indicators are strongly correlated, their correlation coefficient is close to one. Therefore, the weighting factor is close to zero, and the values of the new residuals are close to zero. An illustration is done in Fig. 2.26a, Fig. 2.26b and Fig. 2.26c where the residuals in red color and the practical residuals in blue color are presented in the planes P_0, P_1 and P_2 respectively and in the presence of four different severities of the fault Z_f in the branch B_0. In this situation, the two health indicators $I_{R_{1,0}}(f)$ and $I_{R_{2,0}}(f)$ are strongly correlated like in Fig 2.17a. As a consequence, the values of the residuals ρ_0 are near zero. The four new clusters in blue are located on the r_2 axis in the plane P_1 or on the r_1 axis in the plane P_2.
  2. If two health indicators are poorly correlated (i.e. they are strongly different), their correlation coefficient is close to zero. Therefore, the weighting factor is close to one, and the values of the new residuals are close to the initial residuals. The residuals and the practical residuals in the faulty B_2 situation are presented in Fig. 2.27a, Fig. 2.27b and in Fig.

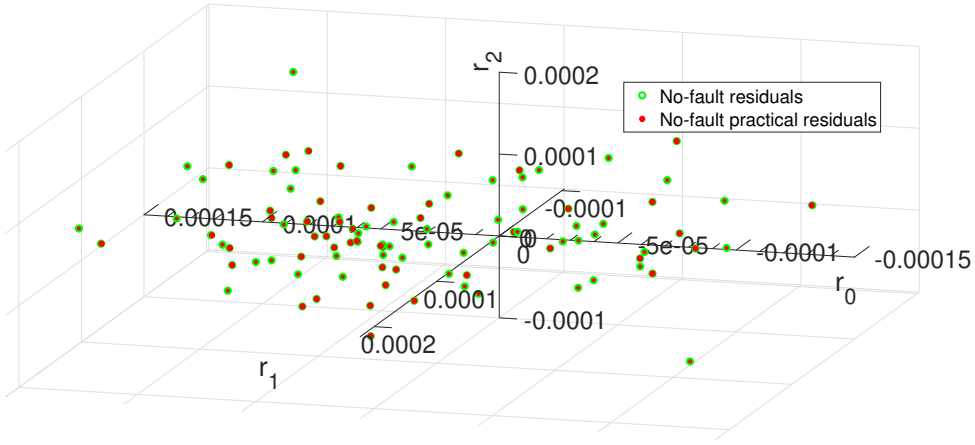

FIGURE 2.25: Residuals and practical residuals representations - no-fault situation.

2.27c respectively in the planes P_0, P_1 and P_2. In this situation, the two health indicators $I_{R_{0,2}}(f)$ and $I_{R_{1,2}}(f)$ are strongly correlated as it can be seen in Fig. 2.19c. Therefore, the weighting factor is close to zero, and the values of the practical residuals ρ_2 are near zero. Hence, the points in the four new clusters in blue are located on the r_1 axis in the plane P_0 or on the r_0 axis in the plane P_1.

To conclude, if there is a fault in the branch B_i, the proposed practical residual ρ_i is near zero. In the previous examples, we can see that the fault has an influence on the residuals, thus a robustness and sensitivity analysis of the residuals is made in the following.

2.5.3 Robustness and sensitivity analysis of the residuals

Two issues are addressed in this part :

1. The influence of the noise on the residuals.
2. The influence of the fault characteristics (position and severity of the fault) on the residuals.

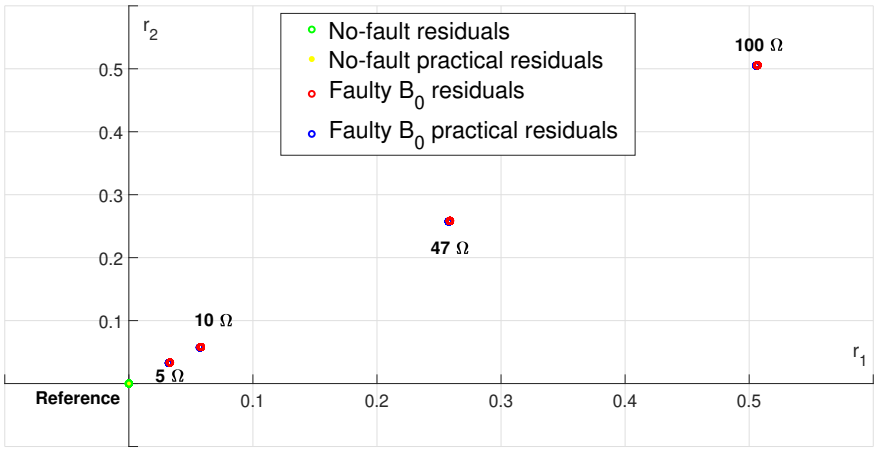

(A) Plane P_0.

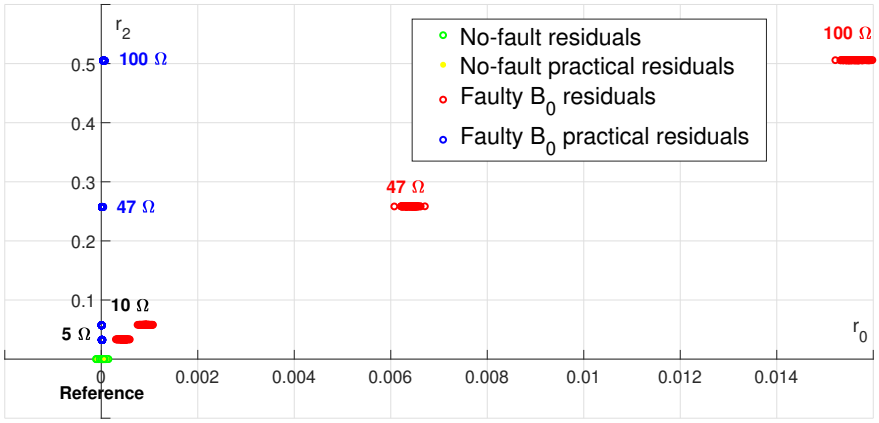

(B) Plane P_1.

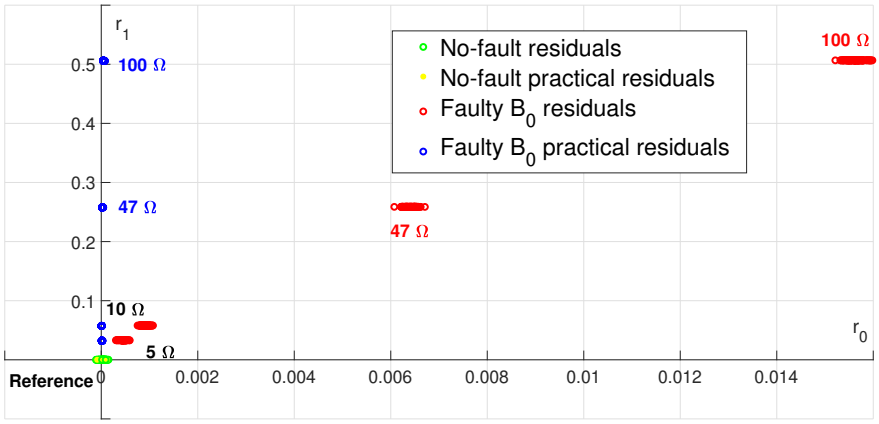

(C) Plane P_2.

FIGURE 2.26: Residuals and practical residuals (Faulty B_0).

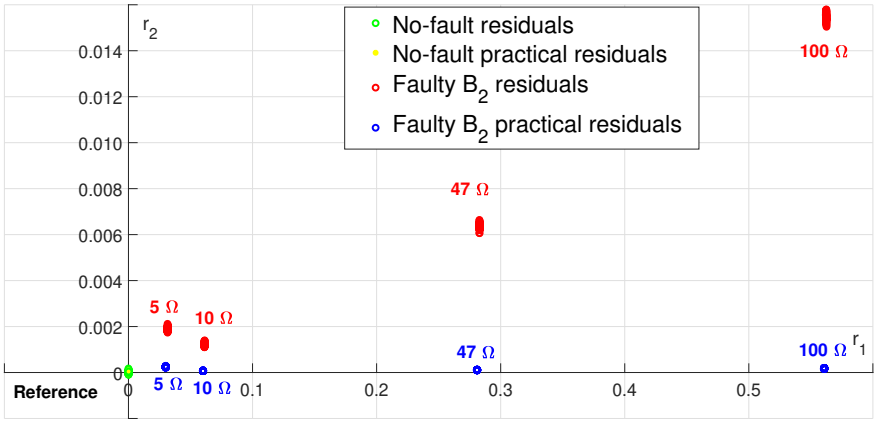

(A) Plane P_0.

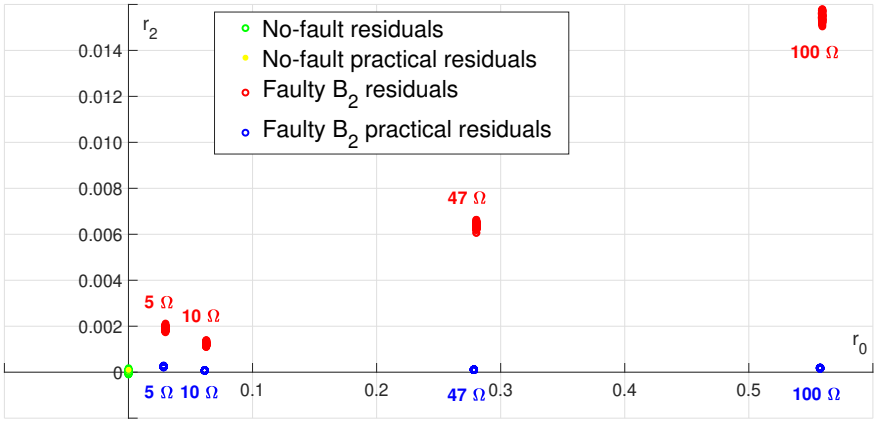

(B) Plane P_1.

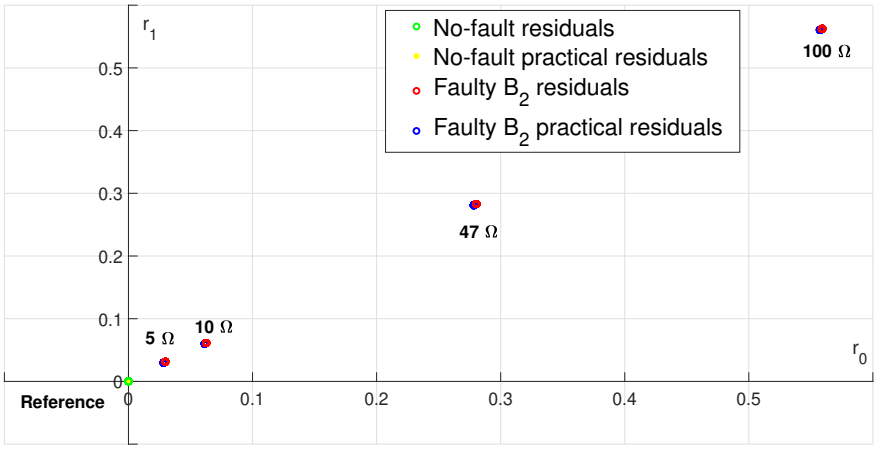

(C) Plane P_2.

FIGURE 2.27: Residuals and practical residuals (Faulty B_2).

2.5.3.1 Influence of the noise

The objective is to study the robustness of the residuals. In this study, the TC data are obtained from measurements on the test bench, and white Gaussian noise are added via MATLAB® to the values of the measured TC to get closer to the experimental conditions in an embedded system. Three SNR values are considered, $SNR = \{50\ dB; 30\ dB; 10\ dB\}$. The no-fault and the faulty B_2 situations of the network are considered. The fault severity is set to 5 Ω and the position of the fault is fixed in the test bench to $x_2 = 1.5\ m$ in the branch B_2.
The results are reported in Fig. 2.28 in the plane P_2. In Fig. 2.28a, the no-fault and faulty clusters are shown for two different SNR values (50 dB and 30 dB). As it can be seen, the cluster sizes increase when the SNR decreases and the faulty clusters become closer to the reference cluster. In Fig. 2.28b, the residuals are shown for a SNR value of 10 dB. As it can be seen, at this SNR value, the no-fault and the faulty clusters overlap. These two clusters can not be easily distinguished. In conclusion, the clusters size increases and its distance from the reference cluster decreases with an increasing noise level making it difficult to detect the soft fault.

2.5.3.2 Influence of the fault characteristics

To study the influence of the fault characteristics on the residuals, simulated-based data are used. Data are generated using intensive realistic simulations based on the ABCD matrix modeling method (Detailed in 1.4.1). One hundred simulated transmission coefficient per case are generated. The network shown in Fig. 2.10 is simulated via MATLAB® in the bandwidth of $[100kHz : 62,43kHz : 100MHz]$ with $l_0 = 4\ m$, $l_1 = 10\ m$ and $l_2 = 7\ m$, the lengths of the branches B_0, B_1 and B_2 respectively.
The primary parameters of the network R, L, C and G are computed using the expressions found in the section 1.2.2 [34]. The characteristic impedance Z_c of each branch is equal to 120Ω. White Gaussian noise is added to the simulated TC and a signal-to-noise-ratio of 100 dB is set.
The influence of the fault characteristics on the residuals is studied by changing :

- The severity of the fault Z_f from 0 Ω to 10 Ω with a step of 0.2 Ω.
- The distance x_i between the position of the fault and the position of the node from 0.1 m to 3.9 m with a step of 0.2 m.

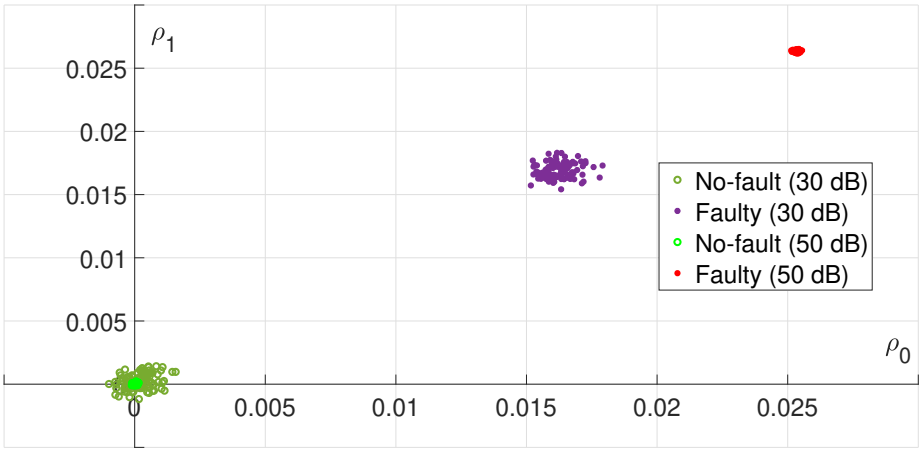

(A) $SNR = \{50\ ;\ 30\}\ dB$

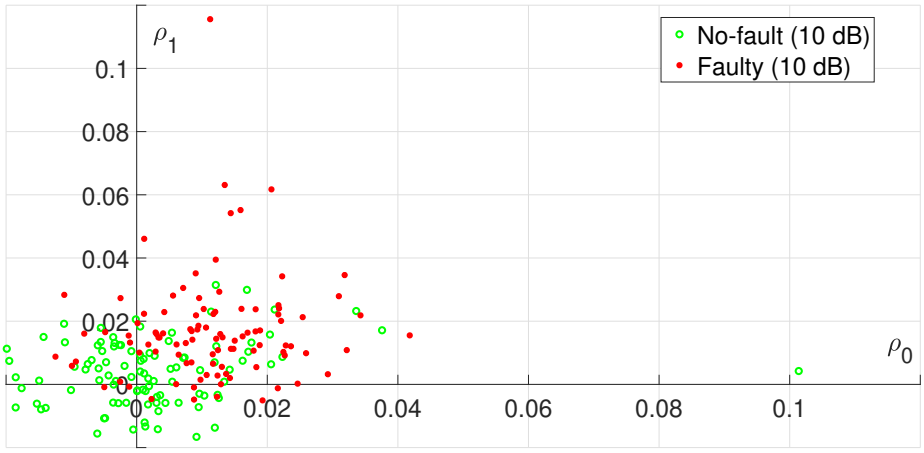

(B) $SNR = 10\ dB$

FIGURE 2.28: Variation of clusters with respect to the noise level (Faulty B_2, $Z_f = 5\Omega$, $x_2 = 1.5m$).

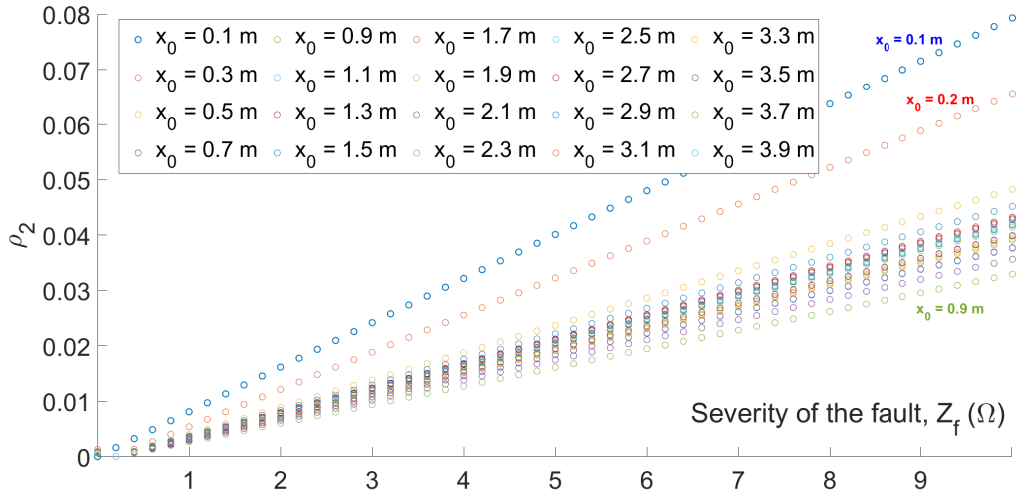

FIGURE 2.29: Variation of the residual ρ_2 with respect to the fault position x_0 and the fault severity Z_f.

In the faulty B_0 situation, the residual ρ_0 is null and the residuals ρ_1 and ρ_2 are equal and are different from zero. Thus, the influence of the fault characteristics on the residual ρ_2 is studied and presented in the Fig. 2.29 with respect to the fault characteristics (position and severity). For each fault position x_0, the residual value evolves quite linearly in function of the fault and slope changes accordingly to the position of fault x_0. This is a qualitative result obtained from experimental data. At this stage, this result has not been proved theoretically. This is one of the challenging perspectives of this thesis. In conclusion, we observe through experiments that wherever the fault is located, the distance between the no-fault and the faulty clusters evolves with the severity of the fault. Additionally, it is not possible to determine the position and severity values from a specific residual value.

2.6 Conclusion

A method for soft fault detection and localization in wired networks is proposed in this chapter. This method is based on monitoring the transmission coefficients between the distributed ECU in the network. The transmission coefficients can be measured via VNA or can be estimated by PLC using the OFDM scheme. Fault sensitive health indicators are then proposed. These health indicators are calculated locally from these transmission coefficients by the ECU acting as receivers and are sent to the ECU sources, in which the residuals are computed. Residuals allow to

compare the health indicators and perform the detection of the soft fault and the localization of the faulty branch thanks to a signature matrix. In practical applications, these residuals are enhanced by weighting them with correlation coefficients between the compared health indicators.

This fault diagnosis method is validated using measurements extracted from a Y-shaped test bench where the transmission coefficients were measured directly using a VNA. The fault is represented in the test bench by the insertion of a resistance in series with the cable, the impedance value represents the severity of the fault. Then, realistic intensive simulations were used to study the robustness and the sensitivity of the proposed residuals by changing the signal-to-noise ratio, the severity of the fault represented by its impedance and its position on the faulty cable. It was found that regardless of the position of the fault, the residual values rise with fault severity. The distance between the fault position and the node position has a slightly smaller influence on the residuals. The more noise there is, the more difficult it is to separate between non-faulty and faulty clusters since the clusters formed by the residuals are enlarged and become more dispersed so that the non-faulty and faulty clusters overlap.

In general, a soft fault does not appear suddenly, so it is possible to follow a local degradation of the network using the residuals. Studying the influence of fault characteristics and the influence of the noise on the residuals can help to determine a minimum detectable fault. An extension of the proposed fault detection and localization method to complex networks and in particular to bus network is proposed in the next chapter.

Chapter 3

Diagnosis method for a complex network

In this chapter, the fault detection and localization method applied to a Y-shaped network in chapter 2 is extended to more complex networks. The first studied network is the bus network. The extended fault detection and localization method results in a great number of residuals to be computed for such networks. Therefore, a hierarchical method is proposed to reduce the number of required residuals. The proposed methodology reduces both communication and computation costs. Afterwards, the diagnosis principle is extended to other network topologies such as hybrid networks. The diagnosis method is validated on realistic simulated data of a bus network.

3.1 Transmission-based fault diagnosis in a bus network

3.1.1 Bus network description

A bus network consists of a main branch to which all electronic control units (ECU) are connected. In a bus network, a node connects only three branches and at least one of these three branches is connected to an ECU. A bus network with $N+1$ ECU (with $N > 2$) has $N-1$ nodes and $2N-1$ branches (see Fig. 3.1). There are $N+1$ branches B_i directly connected to an ECU and $N-2$ branches B_{b_i} located between

two successive nodes. The fault detection and localization method in a bus network is detailed in the following.

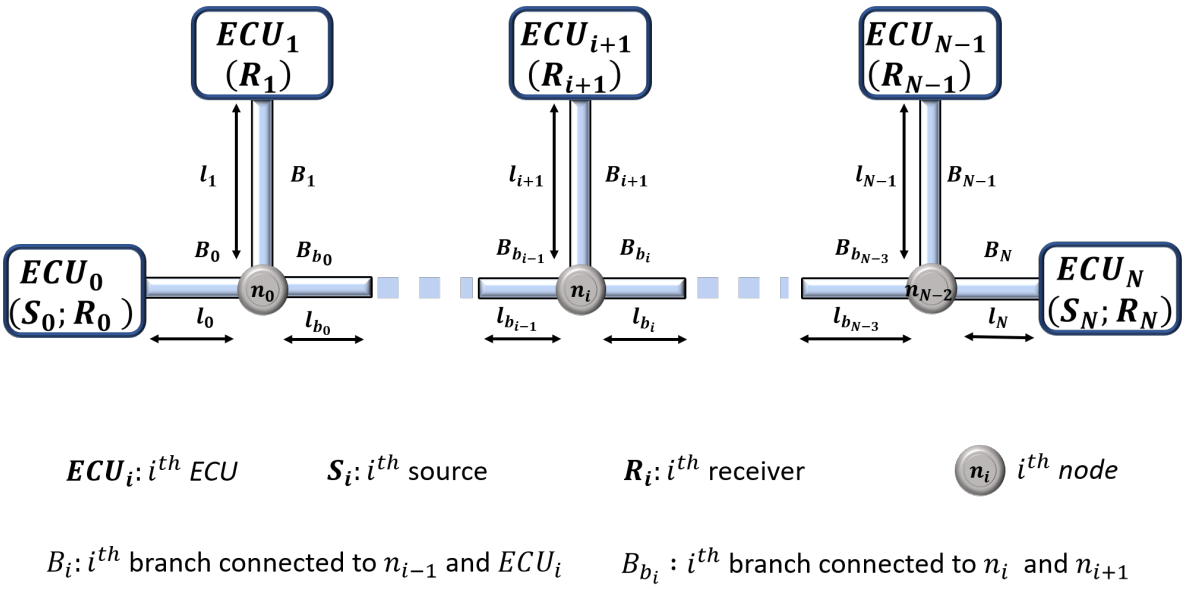

FIGURE 3.1: Bus network

3.1.2 Three Fault detection and localization methods

Let us first recall the main principles of the fault detection and localization method described in Chapter 2 for a Y-shaped network.

The three branches B_0, B_1 and B_2 of the Y-shaped network are either a source branch or receiver branches. The source branch refers to the branch that connects the node to the *ECU* acting as a source. The receiver branches refer to the branches that connect the node to the *ECU* acting as receivers. Two health indicators are computed on the two receivers. These health indicators have the following characteristics :

- If the fault is located in the source branch, the 2 health indicators computed by the receivers are equal for all frequencies in the considered bandwidth : $BW = [f_1 : \Delta_f : f_{N_f}]$.
- If the fault is located at one of the receiver branches, the 2 health indicators computed at the receivers are different for all frequencies in the considered BW.

Residuals are thus introduced to quantify the global difference on the BW between two health indicators.

The same principle is extended for fault detection and localization in a bus network. The proposed method is also discussed in terms of computation and communication costs.

3.1.2.1 Fault detection and localization method applied on a bus network - Method I

In the bus network shown in Fig. 3.1, ECU_0 is acting as a source and all the other ECU are acting as receivers. The branches connected to a node n_i are divided into two sets of branches:

- The source-side branches set $\{B_{S_i}\}_{S_0}$.
  This set contains the branches situated between the source S_0 and the node n_i:
  $\{B_{S_i}\}_{S_0} = \{B_0; B_1; \ldots; B_i\} \cup \{B_{b_0}; B_{b_1}; \ldots; B_{b_{i-1}}\}$.
- The receiver-side branches set $\{B_{R_i}\}_{S_0}$.
  This set contains the branches from the other sides of the node n_i,
  $\{B_{R_i}\}_{S_0} = \{B_{i+1}; B_{i+2}; \ldots; B_N\} \cup \{B_{b_i}; B_{b_{i+1}}; \ldots; B_{b_{N-3}}\}$.

The distinction between source-side and receiver-side branches, when the source is S_0, with respect to a node n_i is shown in the Fig. 3.2.

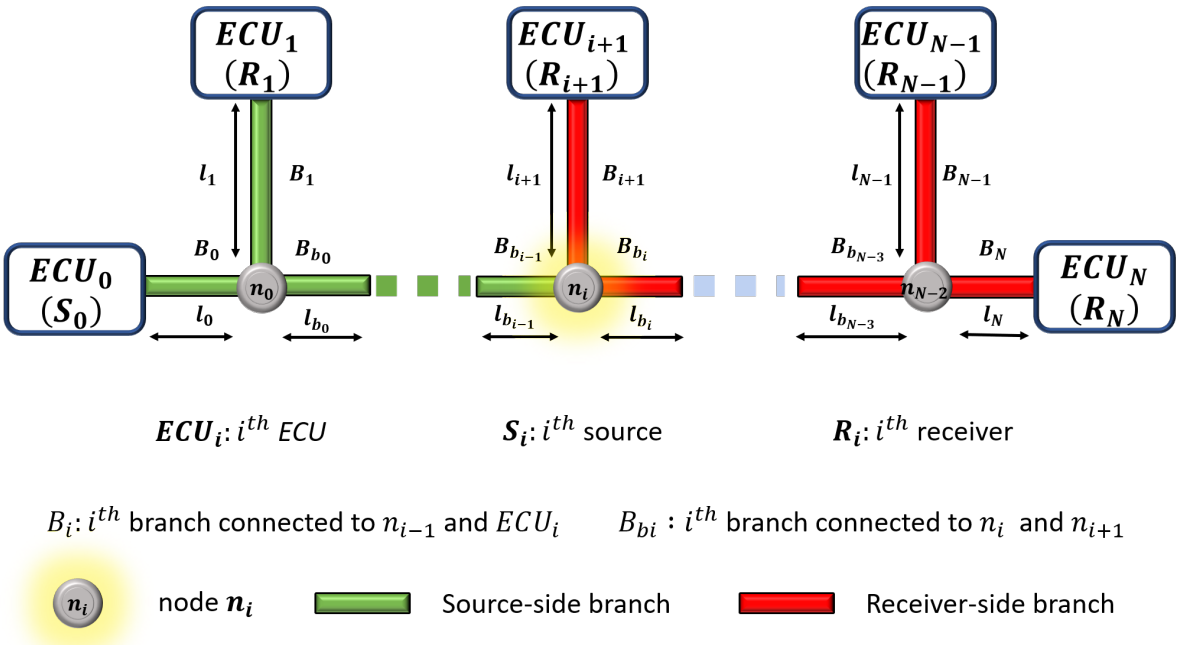

FIGURE 3.2: Source-side and receiver-side branches in a bus network with source S_0.

This bus network can be represented as a Y-shaped network with a node n_i connecting the set of branches B_{i+1}, the set of branches $\{B_{S_i}\}_{S_0} - \{B_{i+1}\}$ and the branch $\{B_{R_i}\}_{S_0}$ as shown in Fig. 3.3. This illustration can be useful for extending the fault detection and localization methodology from a Y-shaped network to a bus network.

The first step in the fault detection and localization procedure for a bus network is the estimation of the transmission coefficients (TC) between the source S_0 and the receivers R_i, with $i \in \{1;2;\cdot;N\}$. From the reference TC estimated when the network is considered in the no-fault situation and the TC estimated online, the health indicators $I_{R_{i,0}}(f) \quad \forall i \in \{1;2;\cdot;N\}$ and $\forall f \in BW = [f_1 : \Delta_f : f_{N_f}]$ are computed locally at each receiver R_i.
As a direct extension of the health indicators' characteristics for a Y-shaped network, we have the following :

- When the network is not faulty, all the reference TC and the corresponding estimated TC are equal, which results in all health indicators computed at the receivers, being zero.

  Thus we have

  $I_{R_{i,0}}(f) = 0$

  $\forall\, i \in \{1;2;\cdot;N\}, \forall f \in BW = [f_1 : \Delta_f : f_{N_f}]$.

- A faulty situation results in different values of the transmission coefficients, resulting in non-zero health indicators. The non-zero health indicators values depend on the position of the fault in the network, i.e. which branch is faulty. If a branch B_i, $i \in \{0;1;\cdot;N\}$ or $B_{b_{i-1}}, i \in \{1;2;\cdot;N-2\}$ is faulty:

  - The health indicators computed at the receivers connected to the branches of the receiver-side branches set $\{B_{R_i}\}_{S_0}$ are such that :

    $I_{R_j}(f) = I_{R_k}(f) = I(f) \neq 0$

    $\forall\, j,k \in [i+1 : N], \forall f \in BW = [f_1 : \Delta_f : f_{N_f}]$.

  - The health indicators computed at the receivers connected to the branches of the source-side branches set $\{B_{S_i}\}_{S_0}$ are such that :

    $I_{R_j}(f) \neq 0$ and $I_{R_k}(f) \neq 0$

    $I_{R_j}(f) \neq I_{R_k}(f) \neq 0$

    $I_{R_j}(f) \neq I(f)$ and $I_{R_k}(f) \neq I(f)$

    $\forall\, j \in [1 : i]$ and $k \in [1 : N]$(with $j \neq k$), $\forall f \in BW = [f_1 : \Delta_f : f_{N_f}]$:

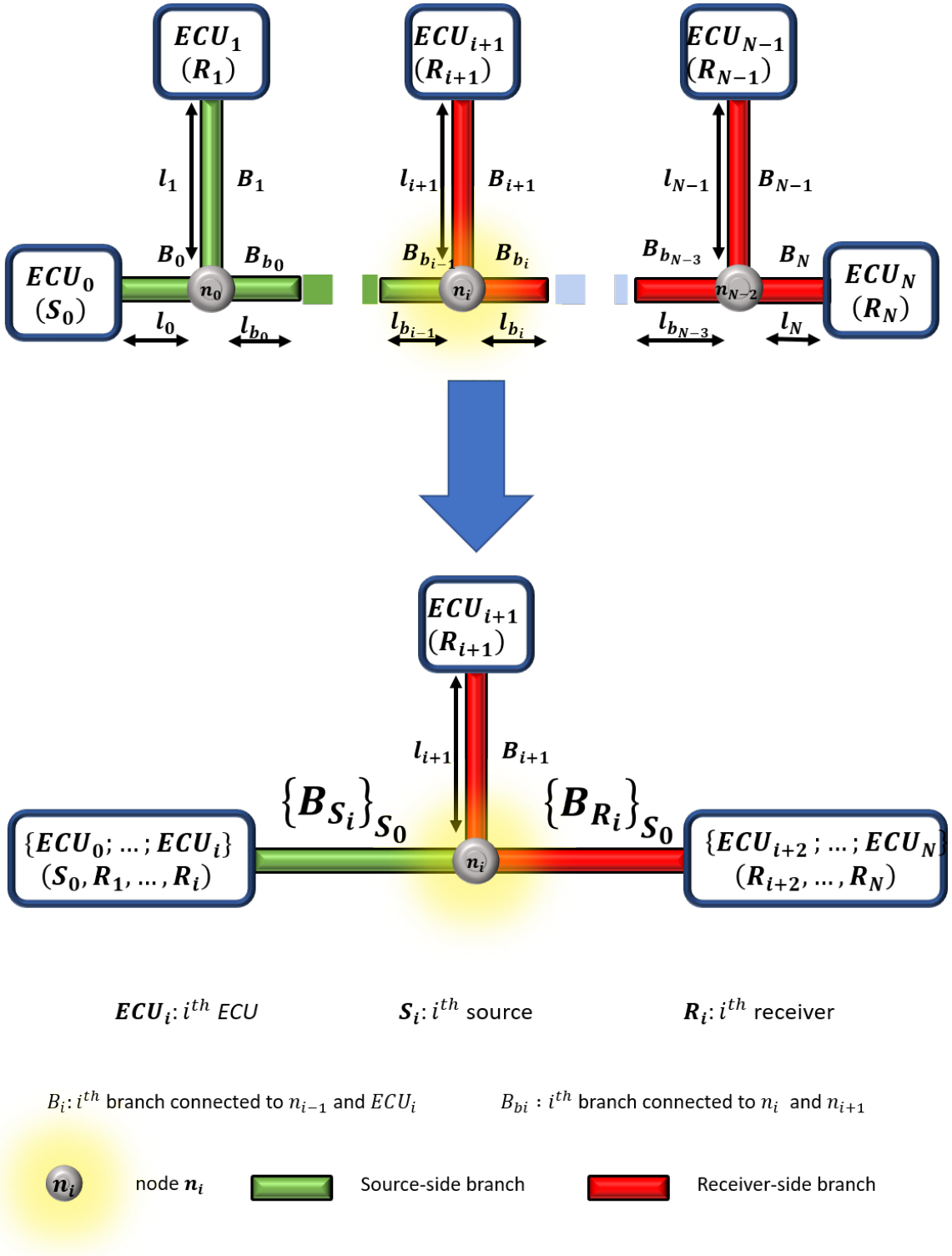

FIGURE 3.3: Representation of a bus network as a Y-shaped network.

TABLE 3.1: Residual-based bus network signature matrix (residual $r_0^{N,i}$).

r_k	No-fault	Faulty B_0	Faulty B_1	Faulty B_{b_0}	...	Faulty B_i	Faulty $B_{b_{i-1}}$	...	Faulty B_{N-1}	Faulty B_N
$r_0^{N,1}$	0	0	1	1		1	1	...	1	1
$r_0^{N,2}$	0	0	0	0	...	1	1	...	1	1
⋮	⋮	⋮	⋮	⋮	...	⋮	⋮	...	⋮	⋮
$r_0^{N,i}$	0	0	0	0	...	1	1	...	1	1
$r_0^{N,i+1}$	0	0	0	0	...	0	0	...	1	1
⋮	⋮	⋮	⋮	⋮	...	⋮	⋮	...	⋮	⋮
$r_0^{N,N-1}$	0	0	0	0	...	0	0	...	1	1

0 indicates that $r_k^{j,i}$ is equal to zero.
1 indicates that $r_k^{j,i}$ is different from zero.

Each receiver estimates the transmission coefficient between the source and itself, resulting in N estimated transmission coefficients. Then the N health indicators are computed locally at each receiver for each frequency carrier in the bandwidth BW. The health indicator values are then sent to S_0, where the residuals are computed. The source S_0 computes $N-1$ residuals to compare the health indicators. Using these residuals, the fault may be detected and the faulty branch located.
Let's define the residual $r_0^{N,i}$:

$$r_0^{N,i} = \frac{1}{N_f} \sum_{f_1}^{f_{N_f}} |I_{R_{i,0}}(f) - I_{R_{N,0}}(f)|$$
$$with\ f \in BW = [f_1 : \Delta_f : f_{N_f}]\ and\ i \in \{1; 2; \ldots; N-1\} \tag{3.1}$$

This residual is used to compare between the two health indicators $I_{R_{N,0}}(f)$ computed at the receiver R_N and $I_{R_{i,0}}(f)$ computed at the receivers R_i when S_0 is the source.
A signature matrix, shown in Table 3.1, is constructed based on the residuals $r_0^{N,i}$ with $i = \{1, 2, \ldots, N-1\}$.

Remark 7 *The receiver R_N is the farthest receiver from the source S_0 which means that the number of nodes between R_N and S_0 is maximum. Whatever the selected node, the receiver-side branches set includes the branch B_N connected to R_N. A faulty branch, B_{i+1} or B_{b_i}, is connected to a node n_i. All the health indicators computed at the receivers R_j where $i < j < N$ are equal to the $I_{R_{N,0}}(f)$. Hence, $I_{R_{N,0}}(f)$ and $I_{R_{i,0}}(f)$ are compared with the objective to construct a signature matrix with the fewest possible ambiguities.*

The health indicators' characteristics in no-fault and faulty situations lead to the following characteristics of the signature table 3.1:

- All health indicators are null in the no-fault situation, and all health indicators are equal in the faulty B_0 situation. Therefore, in both situations, the residuals computed to compare $I_{R_{N,0}}(f)$ and $I_{R_{i,0}}(f)$ are null. Hence, the signature of the no-fault situation is identical to the signature of the faulty B_0 situation.
- The health indicators $I_{R_{k,0}}(f)\ \forall k \in \{i+1;\ldots;N\}$ are equal to each other and the health indicators $I_{R_{j,0}}(f)\ \forall j \in \{1;\ldots;i\}$ are different from each other in the faulty B_i and $B_{b_{i-1}}$ situations. Therefore, in both situations the residuals $r_0^{N,k}$ are null and the residuals $r_0^{N,j}$ are non-zero. Hence, the signature of the faulty B_i situation is identical to the signature of the faulty $B_{b_{i-1}}$ situation, with $i \in \{1,2,3,\ldots,N-2\}$.
- All health indicators are different from each other in the faulty B_N and the faulty B_{N-1} situations. Therefore, the residuals computed to compare $I_{R_{N,0}}(f)$ and $I_{R_{i,0}}(f)\ \forall i$ are non-zero. Hence, the signature of the faulty B_{N-1} situation is identical to the signature of the faulty B_N situation.

To remove the ambiguity caused by identical signatures, it is necessary to compute additional residuals by setting another ECU as a source.
Any other ECU can *a priori* plays the role of a new source. The two branches B_N and B_{N-1} are connected to the same node n_{N-2}. Therefore, these two branches will always be included in the receiver-side branches unless ECU_N or ECU_{N-1} is chosen as the new source. Hence, in order to remove the ambiguity between the faulty B_N and faulty B_{N-1} situations and to assign one of them to the source-side branches and the other to the receiver-side branches, it is necessary to chose one of the ECU, ECU_N or ECU_{N-1}, as the new source.
Let us choose ECU_N as the new source S_N. The branches connected to any node n_i can be divided into two sets of branches:

- The source-side branches set $\{B_{S_i}\}_{S_N}$:
  It contains the branches situated between the source S_N and the node n_i, $\{B_{S_i}\}_{S_N} = \{B_{i+2}; B_{i+3}; \ldots; B_N\} \cup \{B_{b_i}; B_{b_{i+1}}; \ldots; B_{b_{N-3}}\}$.
- The receiver-side branches set $\{B_{R_i}\}_{S_N}$:
  It contains the branches of the other sides of the node n_i, $\{B_{R_i}\}_{S_N} = \{B_0; B_1; \ldots; B_{i+1}\} \cup \{B_{b_1}; B_{b_2}; \ldots; B_{b_{i-1}}\}$.

The distinction between source-side and receiver-side branches, when the source is S_N, with respect to a node n_i is shown in the Fig. 3.4. To compute the residuals, the

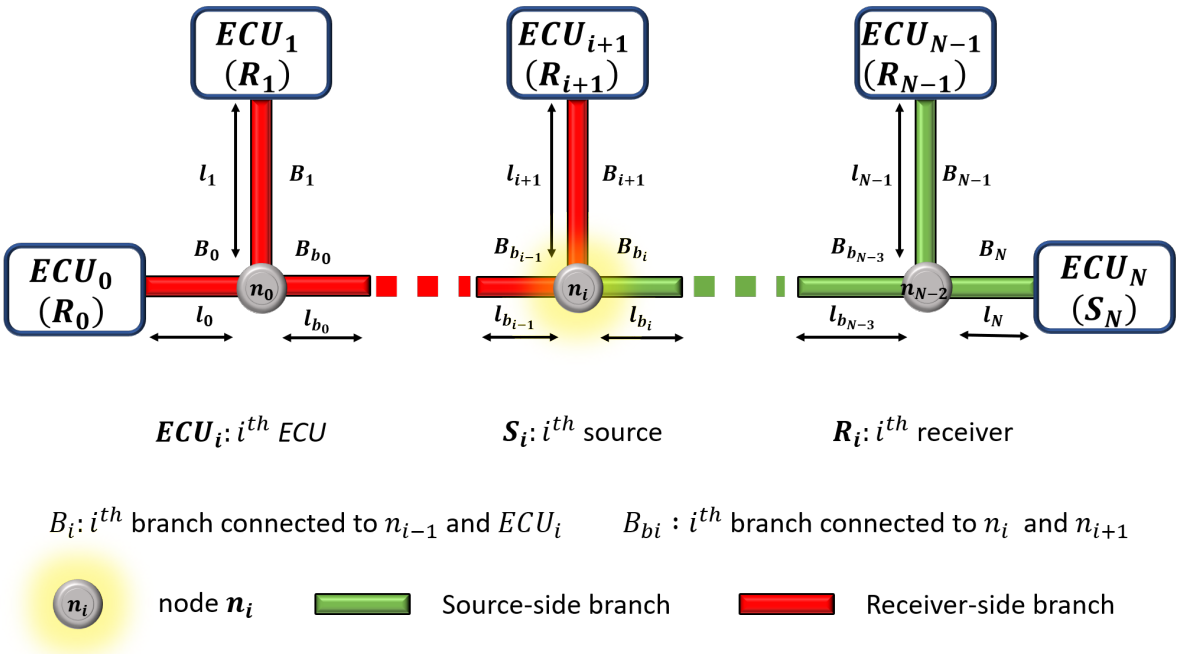

FIGURE 3.4: Source-side and receiver-side branches in bus network with source S_N.

transmission coefficients between the source S_N and the receivers R_i $\forall i \in \{1,2,\ldots,N-1\}$ are estimated. The health indicators $I_{R_{i,N}}$ are then computed and the residual $r_N^{i,0}$ is computed at the source S_N. This residuals is defined as follows:

$$r_N^{i,0} = \frac{1}{N_f}\sum_{f_1}^{f_{N_f}} |I_{R_{i,N}}(f) - I_{R_{0,N}}(f)|$$
$$with\ f \in BW = [f_1 : \Delta_f : f_{N_f}]\ and\ i \in \{1;2;\ldots;N-1\} \tag{3.2}$$

The residual $r_N^{i,0}$ is used to compare the health indicator $I_{R_{i,N}}(f)$ computed at the receiver R_i with $i = \{1,2,\ldots,N-1\}$ and the health indicator $I_{R_{0,N}}(f)$ computed at the receiver R_0 with the objective to construct a signature matrix (Table 3.1 and 3.2) with the fewest possible ambiguities. health indicators $I_{R_{i,N}}(f)$ are compared to $I_{R_{0,N}}(f)$ since the receiver R_0 is the farthest receiver from the source S_N. A signature matrix, shown in Table 3.2, is obtained based on the residuals $r_N^{i,0}$ with $i = \{1,2,\ldots,N-1\}$.

Combining the two signature matrices, thus considering $2\cdot(N-1)$ residuals, we obtain the signature matrix shown in Table 3.3. For each network situation

TABLE 3.2: Residual-based bus network signature matrix (residual $r_N^{i,0}$) .

r_k	No-fault	Faulty B_0	Faulty B_1	Faulty B_{b_0}	$\cdots$	Faulty B_i	Faulty $B_{b_{i-1}}$	$\cdots$	Faulty B_{N-1}	Faulty B_N
$r_N^{0,N-1}$	0	1	1	1		1	1		1	0
$r_N^{0,N-2}$	0	1	1	1	$\cdots$	1	1	$\cdots$	0	0
$\vdots$	$\vdots$	$\vdots$	$\vdots$	$\vdots$	$\cdots$	$\vdots$	$\vdots$	$\cdots$	$\vdots$	$\vdots$
$r_N^{0,i}$	0	1	1	1	$\cdots$	1	0	$\cdots$	0	0
$r_N^{0,i-1}$	0	1	1	1	$\cdots$	0	0	$\cdots$	0	0
					$\cdots$			$\cdots$		
$\vdots$	$\vdots$	$\vdots$	$\vdots$	$\vdots$	$\cdots$	$\vdots$	$\vdots$	$\cdots$	$\vdots$	$\vdots$
$r_N^{0,1}$	0	1	1	0		0	0		0	0

0 indicates that $r_k^{j,i}$ is equal to zero.
1 indicates that $r_k^{j,i}$ is different from zero.

(no-fault or one faulty branch), a unique signature is obtained. A fault can be detected and the faulty branch can be localized with no ambiguity. The fault detection and localization method for a bus network is summarized in Fig. 3.5. It consists of several steps :

- The receivers estimate the transmission coefficients through pilot signals sent by the source S_0.The health indicators are computed for all frequencies in the BW by the receivers. The indicators values are sent to the sources S_0. The residuals are computed.
- The receivers estimate the transmission coefficients through pilot signals sent by the source S_N. The health indicators are computed for all frequencies in the BW by the receivers. The indicators values are sent to the sources S_N.The residuals are computed.
- The residuals values computed by the two sources are sent to the supervisor. The supervisor may be one of the two sources.
- The residuals values are compared to the preconstructed signature matrix in Table 3.3.

The huge number of computed residuals is a drawback of this method. A reduction of the required number of residuals for fault detection and localization is proposed in the next subsection.

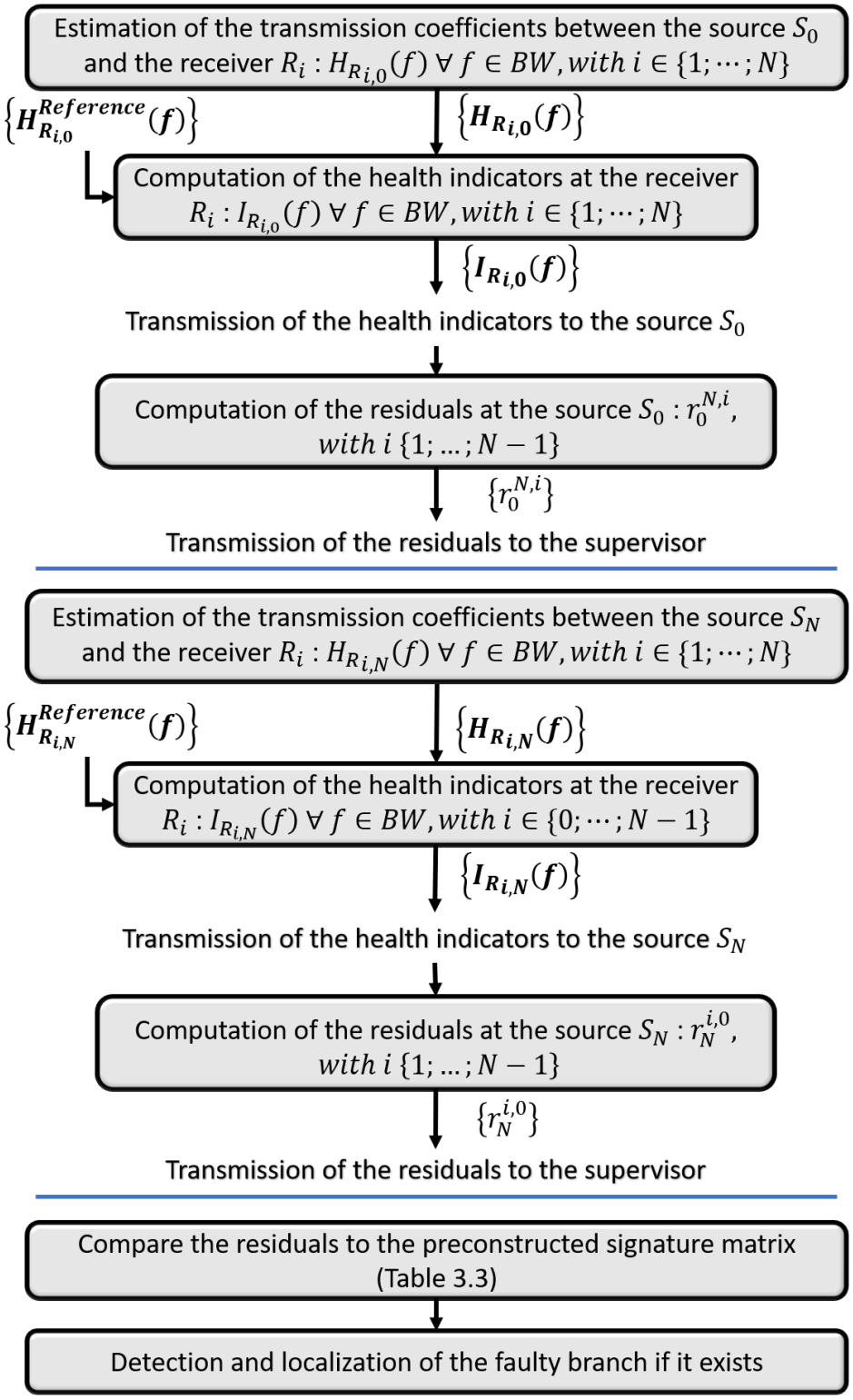

FIGURE 3.5: Fault detection and localization algorithm for a bus network - Method I.

TABLE 3.3: Residual-based bus network signature matrix (residuals $r_0^{N,i}$ and $r_N^{0,i}$).

r_k	No-fault	Faulty B_0	Faulty B_1	Faulty B_{b_0}	$\cdots$	Faulty B_i	Faulty $B_{b_{i-1}}$	$\cdots$	Faulty B_{N-1}	Faulty B_N
$r_0^{N,1}$	0	0	1	1		1	1		1	1
$r_0^{N,2}$	0	0	0	0	$\cdots$	1	1	$\cdots$	1	1
$\vdots$	$\vdots$	$\vdots$	$\vdots$	$\vdots$	$\cdots$	$\vdots$	$\vdots$	$\cdots$	$\vdots$	$\vdots$
$r_0^{N,i}$	0	0	0	0	$\cdots$	1	1	$\cdots$	1	1
$r_0^{N,i+1}$	0	0	0	0	$\cdots$	0	0	$\cdots$	1	1
$\vdots$	$\vdots$	$\vdots$	$\vdots$	$\vdots$	$\cdots$	$\vdots$	$\vdots$	$\cdots$	$\vdots$	$\vdots$
$r_0^{N,N-1}$	0	0	0	0	$\cdots$	0	0	$\cdots$	1	1
					$\cdots$			$\cdots$		
$r_N^{0,N-1}$	0	1	1	1		1	1		1	0
$r_N^{0,N-2}$	0	1	1	1	$\cdots$	1	1	$\cdots$	0	0
$\vdots$	$\vdots$	$\vdots$	$\vdots$	$\vdots$	$\cdots$	$\vdots$	$\vdots$	$\cdots$	$\vdots$	$\vdots$
$r_N^{0,i}$	0	1	1	1	$\cdots$	1	0	$\cdots$	0	0
$r_N^{0,i-1}$	0	1	1	1	$\cdots$	0	0	$\cdots$	0	0
$\vdots$	$\vdots$	$\vdots$	$\vdots$	$\vdots$	$\cdots$	$\vdots$	$\vdots$	$\cdots$	$\vdots$	$\vdots$
$r_N^{0,1}$	0	1	1	0		0	0		0	0

0 indicates that $r_k^{j,i}$ is equal to zero.
1 indicates that $r_k^{j,i}$ is different from zero.

3.1.2.2 A sequential fault detection and localization method applied on a bus network - Method II

To reduce the number of residuals required for soft fault detection and faulty branch localization, a sequential fault detection and localization method is proposed in this section.
The first step consists in considering the $N-1$ residuals $r_0^{N,i}$ with $i = \{1, 2, \ldots, N-1\}$ that lead to the fault signature matrix given in Table 3.1. As it was pointed out previously, this table has identical fault signatures for each pair of network situations. Each ambiguity can be removed in a second step with only one additional specific residual as follows:

- Ambiguity between the no-fault and the faulty B_0 situations. To differentiate the two situations, the extra residual $r_N^{0,1}$ may be computed. If $r_N^{0,1} \neq 0$, the network is considered to be in the faulty B_0 situation. Otherwise, it is considered in the no-fault situation.
- Ambiguity between the faulty B_i and the faulty $B_{b_{i-1}}$ situations. To differentiate the two situations, the extra residual $r_N^{0,i}$ may be computed. If $r_N^{0,i} \neq 0$, the network is considered to be in the faulty B_i situation. Otherwise, it is considered in the $B_{b_{i-1}}$ situation.
- Ambiguity between the faulty B_N and the faulty B_{N-1} situations. To differentiate the two situations, the extra residual $r_N^{0,N-1}$ may be computed. If $r_N^{0,N-1} \neq 0$, the network is considered to be in the faulty B_{N-1} situation. Otherwise, it is considered in the B_N situation.

Instead of computing at each time a huge number $(2 \cdot (N-1))$ of residuals, a sequential method may be used. The first step consists in computing the $N-1$ residuals $r_0^{N,i}$ with $i = \{1, 2, \ldots, N-1\}$. The second step consists in computing only one specific residual by using the source S_N, which is selected to remove the ambiguity.

This method is summarized in the Fig. 3.6. Only N residuals are computed to identify with no ambiguity the situation.

A hierarchical method is proposed in the next part which will allow to reduce even more the number of required residuals for fault detection and faulty branch localization.

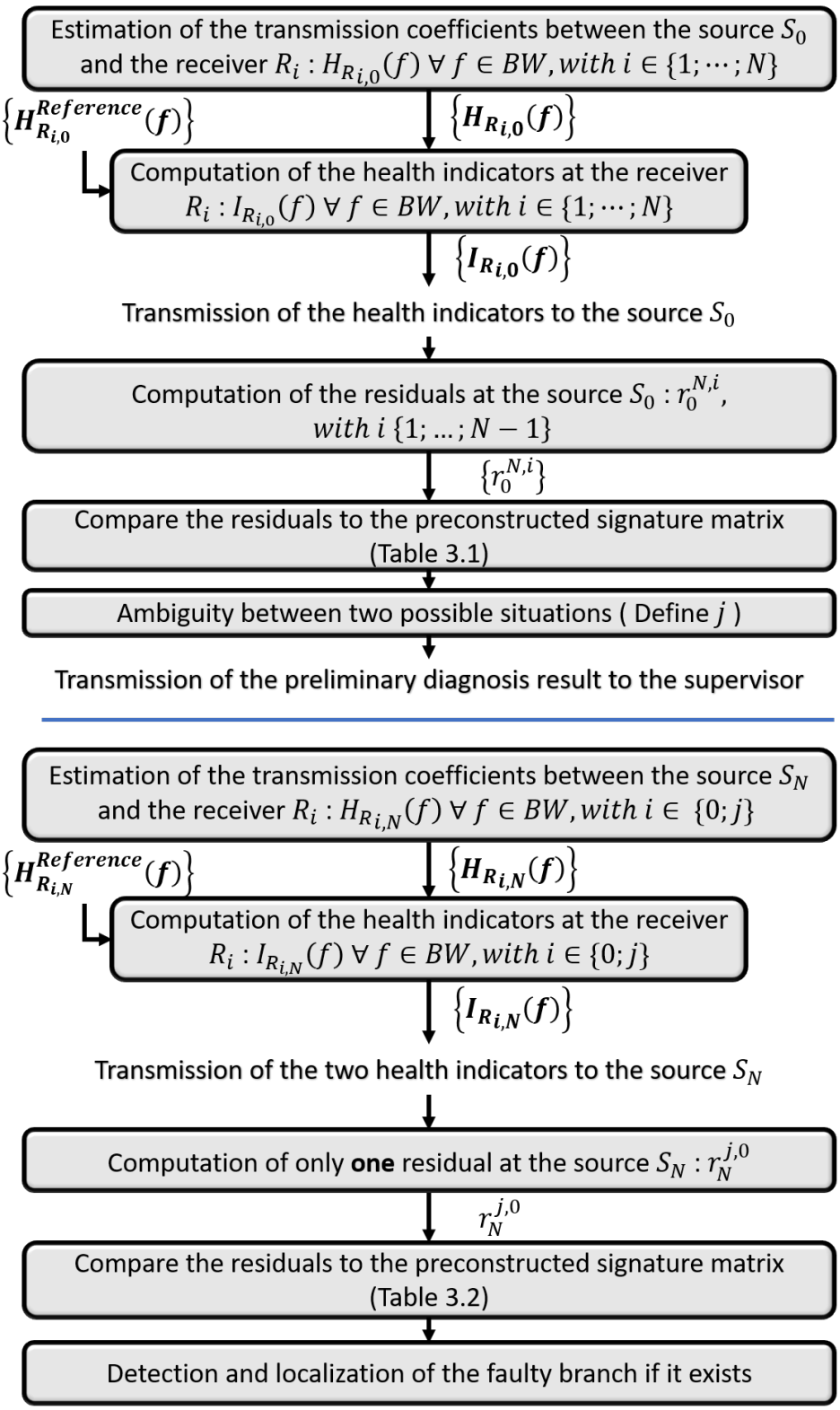

FIGURE 3.6: Fault detection and localization for a bus network - Sequential method.

3.1.2.3 Hierarchical fault detection and localization method applied on a bus network - Method III

The number of computed residuals is equal to $2 \cdot (N-1)$ using the first method and is equal to N using the second method. According to the signature matrix presented in Table 3.3, a lower number of residuals may be computed to detect and localize any fault with no ambiguity. A hierarchical method is detailed in the following.

As previously explained, in a bus network, the branches may be divided into two sets with respect to each node : a source-side branches set and a receiver side branches set, as shown in Fig. 3.7. In a bus network with $N-1$ nodes, it is thus possible to define $N-1$ different source-side branches sets and $N-1$ corresponding receiver-side branches sets.

According to the signature matrix presented in Table 3.3, for each pair of sets, $\{B_{S_i}\}$ and $\{B_{R_i}\}$ with $i = \{0, 1, \ldots, N-1\}$, only two residuals, $r_0^{N,i+1}$ and $r_N^{0,i+1}$, are required to determine which set the faulty branch belongs to.

As it was previously discussed for a Y-shaped network, the residual computed by the source is equal to zero if the fault is located at the source branch and non-zero if the fault is located at a receiver branch. The network is in the no-fault situation if two of the computed residuals are null. Following the same reasoning and from Fig. 3.7, the residuals $r_0^{N,i+1}$ and $r_N^{i+1,0}$ $\forall i \in \{0, 1, ..., N-2\}$ are characterized as follows:

- If the two residuals $r_0^{N,i+1}$ and $r_N^{i+1,0}$ are equal to zero, the network is in the no-fault situation.
- If the residual $r_0^{N,i+1}$ is zero and the residual $r_N^{i+1,0}$ is non-zero, the fault is located in one of the branches of the source-side branches set $\{B_{S_i}\}_{S_0}$.
- If the residual $r_N^{i+1,0}$ is zero and the residual $r_0^{N,i+1}$ is non-zero, the fault is located in one of the branches of the source-side branches set $\{B_{S_i}\}_{S_N}$.
- If the two residuals $r_0^{N,i+1}$ and $r_N^{i+1,0}$ are non-zero, the fault is located in the branch B_{i+1}.

As a consequence, only some specific residuals are needed to identify the situation of the network. The proposed method consists in bisecting the network by half and check each sub-network separately. If two residuals are different from zero, the faulty branch is directly located. If only one residual is different from zero, the

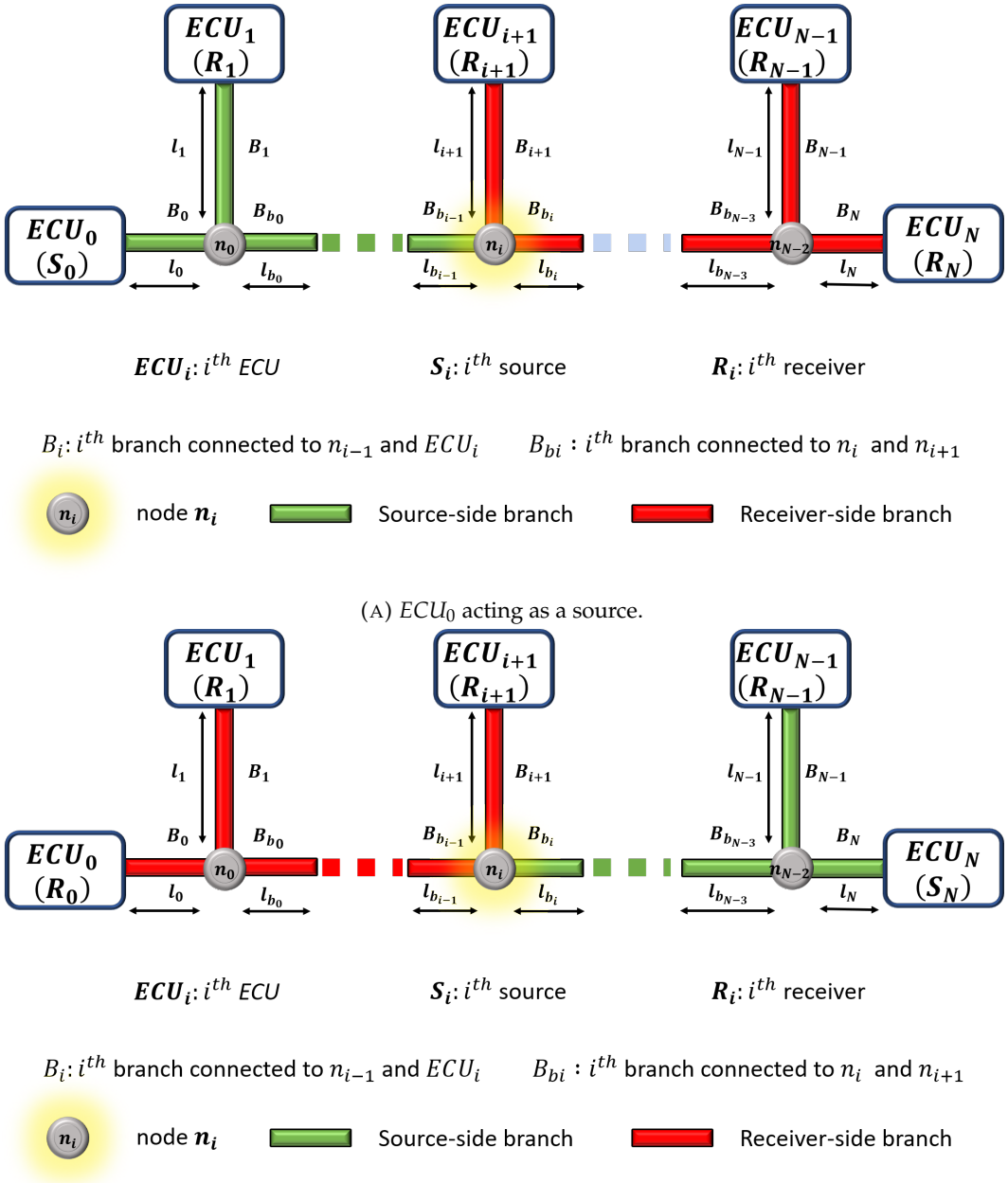

(A) ECU_0 acting as a source.

(B) ECU_N acting as a source.

FIGURE 3.7: Source-side and receiver-side branches representation.

corresponding source-side branches set containing the faulty branch is identified. This set may be bisected again, and the same procedure is repeated until the set contains only one branch, which is the identified faulty branch.

This step-by-step method is summarized as follows and in Fig. 3.8:

1. To start the algorithm, the node $n_{\lfloor (N-2)/2 \rceil}$ is chosen (where $\lfloor x \rceil$ is the nearest integer to x).
2. The two residuals, $r_0^{N,\lfloor (N-2)/2 \rceil+1}$ and $r_N^{\lfloor (N-2)/2 \rceil+1,0}$, are computed. Depending on the values of these two residuals, four cases may arise:
   - If the two residuals are null, the network is in the no-fault situation ($r_0^{N,\lfloor (N-2)/2 \rceil+1} = r_N^{\lfloor (N-2)/2 \rceil+1,0} = 0$).
   - If the residual $r_0^{N,\lfloor (N-2)/2 \rceil+1}$ is zero and the residual $r_N^{N,\lfloor (N-2)/2 \rceil+1}$ is non-zero, the fault is at one of the branches in the source-side branches $\{B_{S_{\lfloor (N-2)/2 \rceil}}\}_{S_0}$.
   - If the residual $r_0^{N,\lfloor (N-2)/2 \rceil+1}$ is non-zero and the residual $r_N^{N,\lfloor (N-2)/2 \rceil+1}$ is zero, the fault is at one of the branches in the source-side branches $\{B_{S_{\lfloor (N-2)/2 \rceil}}\}_{S_N}$.
   - If the two residuals are non-zero, the fault is at the branch $B_{\lfloor (N-2)/2 \rceil+1}$ ($r_0^{N,\lfloor (N-2)/2 \rceil+1} \neq 0$ and $r_N^{\lfloor (N-2)/2 \rceil+1,0} \neq 0$).
3. The faulty source-side branches set $\{B_{S_i}\}_{S_k}$, is bisected with $k \in \{0; N\}$ and $i = \lfloor (N-2)/2 \rceil$.
4. The same steps are repeated until the network can no longer be bisected. The faulty branch is identified.

Fig. 3.8 summarizes the hierarchical fault detection and localization method.

The number of residuals required for fault detection and faulty branch localization depends on the number of times the faulty source-side branches set is split in two, which is at most equal to $log_2(N)$. 2 residuals are computed at each bisection, thus a total of $2 \cdot \log_2(N)$ is at most computed to identify the situation of the network.

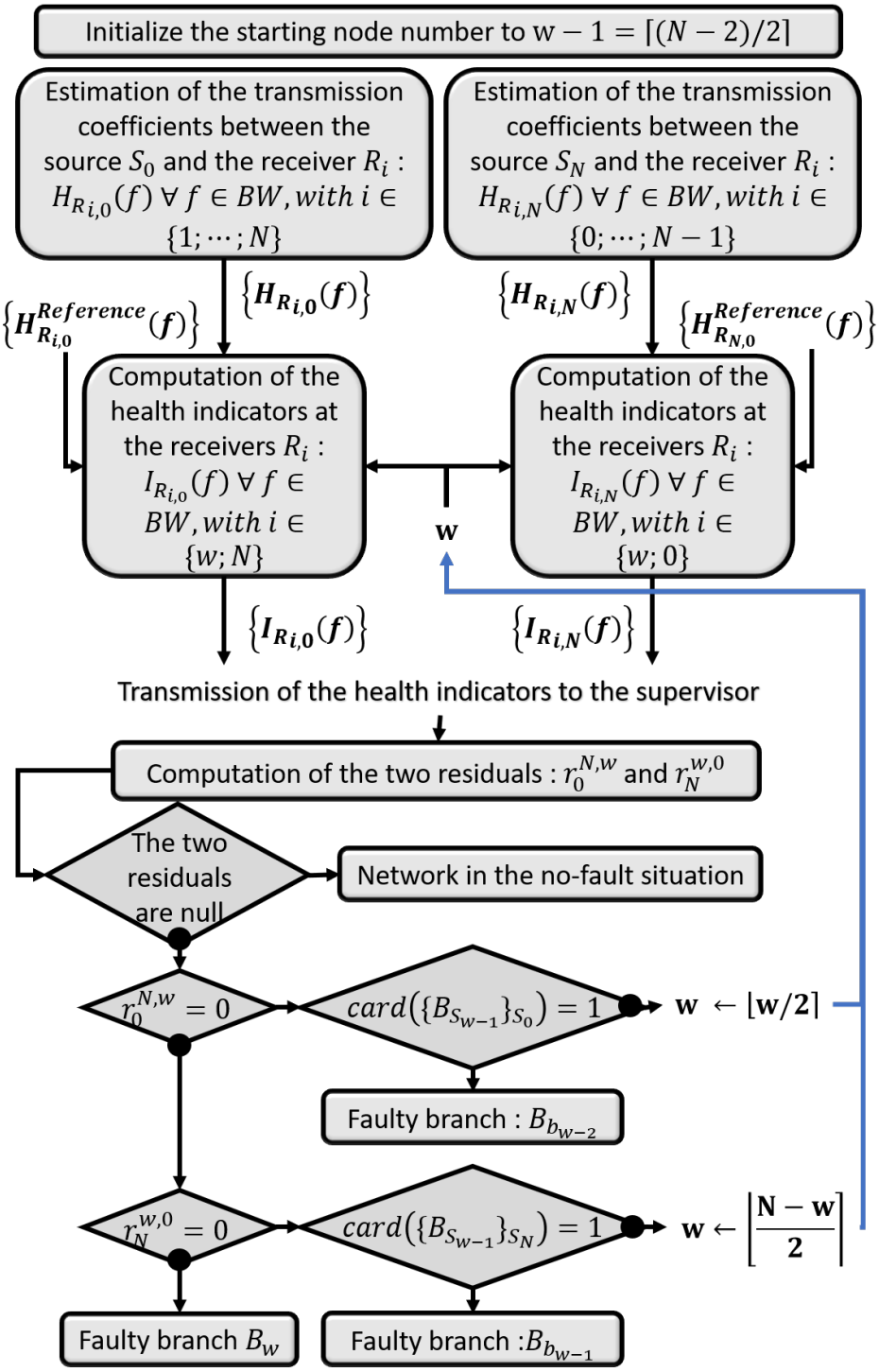

FIGURE 3.8: Fault detection and localization method for a bus network - Hierarchical method.

3.1.3 Comparison of the proposed fault detection and localization methods

Three different fault detection and localization methods have been proposed. They can be compared in terms of number of residuals that are computed and the number of transmitted messages (communication burden).

3.1.3.1 Comparison in terms of the number of required residuals

Table 3.4 summarizes the required number of residuals to be computed for the three fault detection and localization methods for a bus network with $N+1$ ECU.

TABLE 3.4: Number of required residuals for the 3 methods with $N+1$ *ECU* .

Method	Number of required residuals
Method I	$2 \cdot (N-1)$
Method II (Sequential)	N
Method III (Hierarchical)	$2 \cdot \lfloor log_2(N) \rceil$ at worst

The number of required residuals as a function of the number of *ECU* in a bus network is plotted in Fig. 3.9 for the three proposed fault detection and localization methods. It is shown that when the bus network connects more than $7ECU$, the hierarchical method (method III) computes the lowest number of residuals. If the bus network connects less than $7ECU$, the number of computed residuals is quite the same for the three proposed methods.

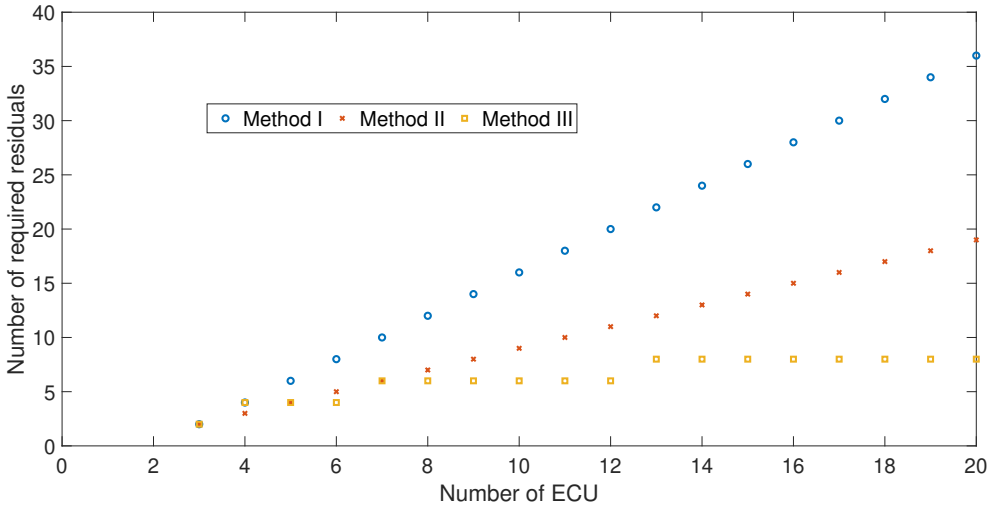

FIGURE 3.9: Comparison between the three fault detection and localization methods in terms of number of required residuals.

The three fault detection and localization methods are now compared in terms of communication burden in the following.

3.1.3.2 Comparison in terms of communication burden

The OFDM modulation scheme is used in PLC systems. Using this process, the estimation of the transmission coefficients is always required. The number of transmitted messages needed specifically for the three fault detection and localization methods will thus not consider the communication burden to perform these TC estimations.
A communication protocol needs to be used, so that the *ECU* communicate with each other for diagnosis purposes. Even though it is outside the scope of this work, some suggestions are made regarding the communication protocol between *ECU* in a bus network. In the three previously detailed fault detection and localization methods, the two *ECU* located at the extremities of the backbone branch of the network are chosen to act as sources and the remaining *ECU* act as receivers. Let's consider that ECU_0 is the supervisor of the network, it will first send a message to all receivers to start the monitoring cycle. Each *ECU* computes its health indicators on a local level. Then the communication and the number of transmitted messages differ with respect to the applied fault detection and localization method.

- Method I : All the *ECU* send their health indicators to the corresponding source ECU_0 or ECU_N. Each health indicator is composed of frequency-dependent variables. Therefore, N_f *messages* are required to transmit a health indicator, where N_f stands for the number of frequency components. This results in a total of $2 \cdot N \cdot N_f$ *messages*. The source ECU_N computes its residuals and sends the $N-1$ residuals' values to the source ECU_0. In order to compare the computed residuals and the received residuals to the preconstructed signature matrix, ECU_0 also computes its residuals. The diagnosis result is acquired by ECU_0 after comparing the residuals to the signature matrix. Thus, a total of $2 \cdot N \cdot N_f + N - 1$ *messages* are exchanged across the network for this monitoring method I.

- Method II : All the *ECU* send their health indicators, resulting in $N \cdot N_f$ *messages* in total. ECU_0 compute the $N-1$ residuals and compare their values to the preconstructed signature matrix. The ECU_0 send *a message* containing the preliminary diagnosis results to the ECU_N. Then, the ECU_N, which acts now as the source S_N, will send *a message* to the two specific *ECU* identified by

TABLE 3.5: Number of transmitted messages per method for $N+1$ ECU.

Method	Number of transmitted messages
Method I	$2 \cdot N \cdot N_f + N - 1$
Method II (Sequential)	$(N+2) \cdot N_f + 3$
Method III (Hierarchical)	$(1 + 2 \cdot N_f) \cdot \lfloor log_2(N) \rceil + 3 \cdot N_f$

the preliminary diagnosis result to ask them to send their new health indicators. The source ECU_N will receive $2N_f$ *distinct messages* from the two concerned ECU to collect the health indicators. The ECU_N will compute the additional residual and send it via *a message* to the supervisor ECU_0, who will take the final diagnosis result. Thus, a total of $(N+2) \cdot N_f + 3$ *messages* are exchanged across the network for this monitoring method II.

- Method III : The two ECU, ECU_N and ECU_w send their health indicators to the source ECU_0 with $w = \lfloor (N-2)/2 \rceil + 1$. The health indicator $I_{R_{N,0}}(f)$ is sent by ECU_N via N_f *messages* to ECU_0. The two health indicators $I_{R_{w,0}}(f)$ and $I_{R_{w,N}}(f)$ are sent by ECU_w via $2 \cdot N_f$ *messages* to ECU_0. At the first bisection of the network, $3 \cdot N_f$ *messages* are delivered across the network. Following the receipt of these indications, ECU_0 computes its first two residuals, from which it generates a preliminary diagnosis result. This result may be :
  - The final diagnosis result, if the network is in its no-fault or faulty B_w situations.
  - The first preliminary result, if the fault is at one of the faulty source-side branches sets $\{B_{S_{\lfloor (N-2)/2 \rceil}}\}_{S_N}$ or $\{B_{S_{\lfloor (N-2)/2 \rceil}}\}_{S_0}$.

  In the first case, the final diagnosis result is reached with only $3 \cdot N_f$ *messages*. In the second case, the network should be bisected to localize the faulty branch. Whatever the situation is, the health indicator computed by the ECU_N will be sent once to the ECU_0. Afterwards, if the network is bisected, at each bisection the ECU_0 sends *a message* across the network requesting for ECU_w, with $w \in \{\lfloor w2 \rceil; \lfloor \frac{N-w}{2} \rceil\}$, to send its two computed health indicators. Therefore, for each new bisection a total of $1 + 2 \cdot N_f$ *messages* must be delivered. In order to receive a final diagnosis result using this method, a total of $(1 + 2 \cdot N_f) \cdot \lfloor log_2(N) \rceil + 3 \cdot N_f$ *messages* must be delivered across the network.

Table 3.5 summarizes the number of the transmitted messages for each fault detection and localization method for a bus network with $N+1$ ECU.

The number of transmitted messages as a function of the number of ECU in a bus network is plotted in Fig. 3.10 for the three proposed fault detection and

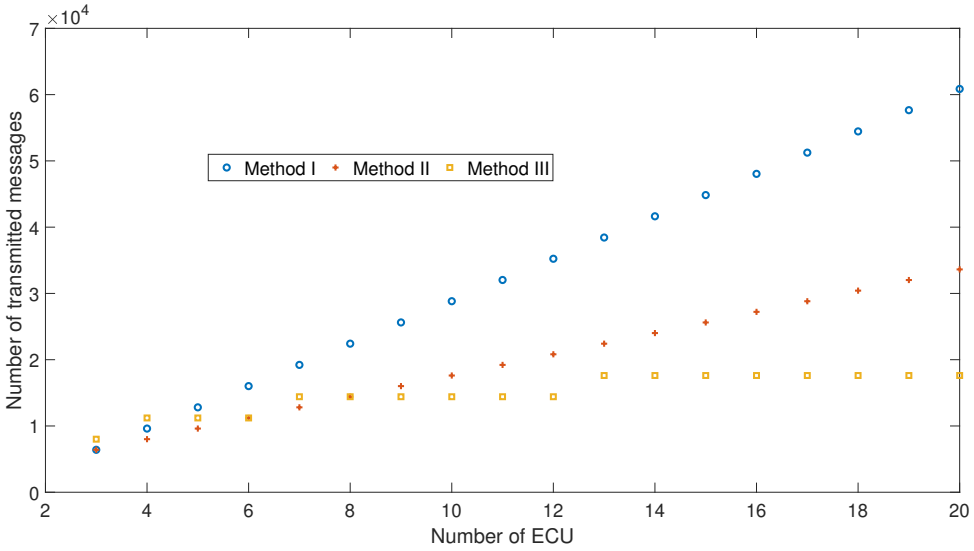

FIGURE 3.10: Comparison between the three fault detection and localization methods in terms of communication burden ($N_f = 1601$).

localization methods. Let us suppose that the number of frequency components N_f is equal to 1601. It is shown that when the bus network connects more than $9ECU$, the hierarchical method (method III) transmits always the lowest number of messages. If the bus connects less than $9ECU$, the numbers of messages are comparable for the three methods.

With respect to the two comparison criteria, the number of required residuals and the communication burden, the method III is the most effective method.

The fault detection and localization method III is illustrated for a simulated bus network in section 3.3. Typical topologies such as ring, point-to-point, Y-shaped, star-shaped and bus networks were studied in chapter 2 and in this section 3.1.1. The most complex network is the hybrid network that combines at least two of the previously mentioned topologies. The methodology for fault detection and localization in hybrid networks is presented and discussed in the following Section 3.2.

3.2 Transmission-based fault diagnosis in a hybrid network

In luxury and modern vehicles, communication networks are hybrid networks, combining ring sub-networks, point-to-point sub-networks and bus sub-networks as shown in Fig. 3.11 [44]. It is possible to monitor each sub-network

independently. One of the *ECU* is designated as the supervisor in each sub-network. The supervisor is in charge of managing the communication for fault detection and localisation purpose. When PLC technology is used, all ECU of the network can estimate the transmission coefficient between a given source and itself. Moreover, each ECU can play the role of a source or of a receiver. The role of an ECU, for a fault detection and localization procedure, depends on the topology of the sub-network :

- For a point-to-point sub-network, one ECU is chosen as a source, the other as a receiver. The choice of the source is indifferent because each one is able to estimate the transmission coefficient between the two ECU. However, it is recommended to choose the ECU that is connected to the largest number of ECU to reduce the number of ECU source and reduce the communication load.
- For a ring sub-network, the ECU are chosen as sources and receivers alternatively to treat point-to-point sub-networks.
- For a bus sub-network, the sources are the two extremities of the backbone branch.

To diagnose a hybrid network, we first highlight each point-to-point link between the ECU and highlight each node.
In networks with point-to-point connections (ring, tree, mesh, star communication network etc . . .) between components, once a fault is detected, the faulty branch is directly localized. This is not the case for bus networks, Y-shaped networks and star energy networks. For sub-networks with only one node, that is to say for Y-shaped network or star-shaped network, the fault detection and localization method is detailed in chapter 2. For sub-networks with successive nodes, that is to say for bus network, the diagnosis method is detailed in the subsection 3.1.2. A hybrid network decomposition is illustrated in the following.

Illustration of hybrid network decomposition The hybrid network illustrated in Fig. 3.12 can be decomposed into three sub-networks, i.e. two bus networks and one star network as seen in Fig. 3.13. Each network may be monitored separately. The fault detection and localization procedure for the bus sub-networks shown in Fig. 3.13a and Fig. 3.13c is detailed in the section 3.1.2.
For the star sub-network in Fig. 3.13b, all the *ECU* of this network are point-to point connected to the ECU_4. Therefore, the fault detection and localization mechanism is straight forward :

ECU interconnection in a modern mid-size vehicle

CAN Controller Area Network, **LIN** Local Interconnected Network,
MOST Media Oriented Systems Transport.

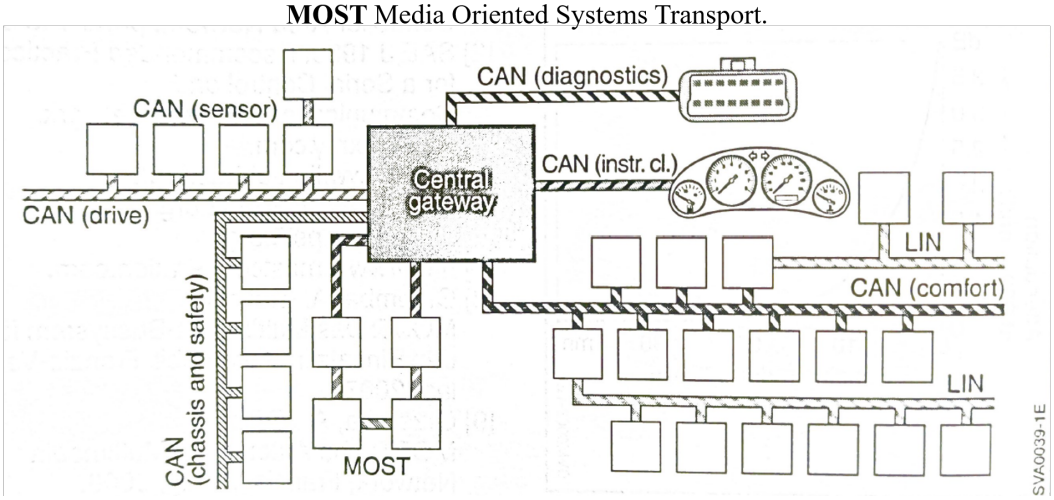

(A) Modern midsize vehicle.

Possible scenario for a future luxury-class vehicle

CAN Controller Area Network, **CGW** Central Gateway, **BCM** Body Computer Module,
IHU Integrated Head Unit, **VDU** Vehicle Dynamics Unit, **PSM** Passive Safety Manager,
EPM Engine & Powertrain Manager, **WLAN** Wireless Local Area Network,
LIN Local Interconnected Network, **MOST** Media Oriented Systems Transport,
PSI Peripheral Sensor Interface, **LVDS** Low Voltage Differential Signaling.

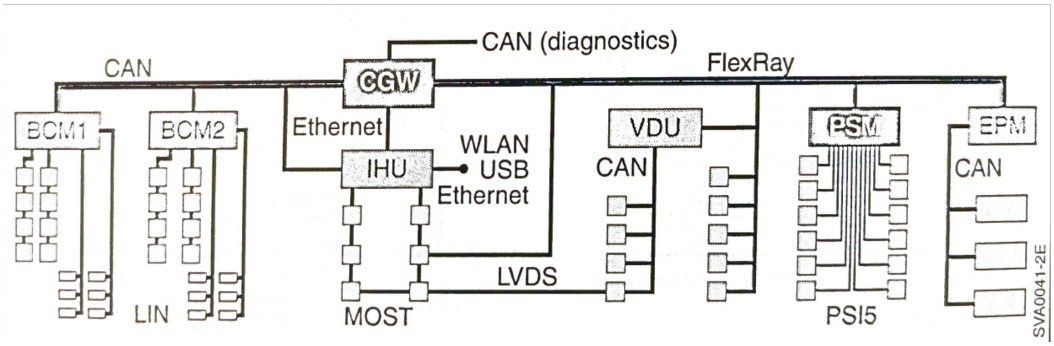

(B) Luxury vehicle.

FIGURE 3.11: ECU interconnection in mid-size and luxury vehicles [44].

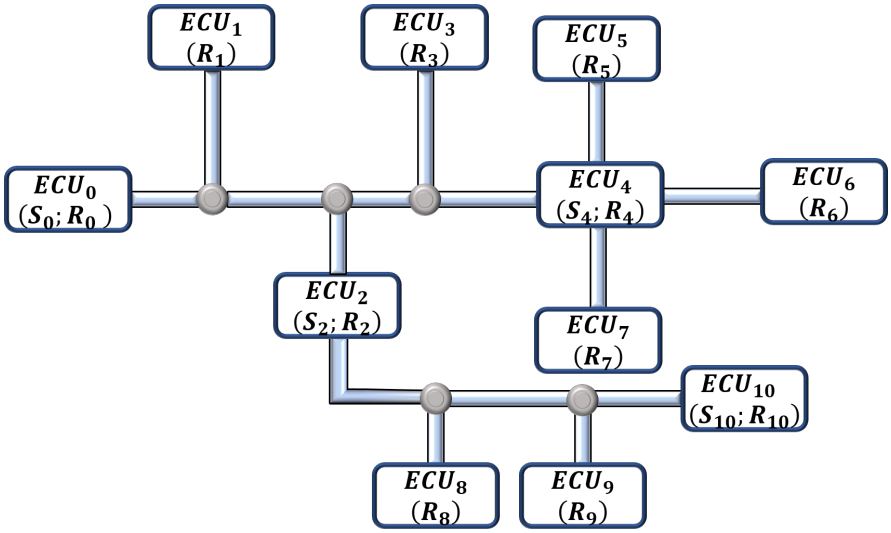

FIGURE 3.12: Hybrid network illustration.

- The ECU_4 plays the role of a source S_4 and a receiver R_4. The other ECU, namely ECU_5, ECU_6 and ECU_7 play the role of receivers denoted respectively R_5, R_6 and R_7.
- The transmission coefficients $H_{R_{5,4}}(f)$, $H_{R_{6,4}}(f)$ and $H_{R_{7,4}}(f)$ between the source S_4 and each one of the receivers are estimated.
- The health indicators $I_{R_{5,4}}(f)$, $I_{R_{6,4}}(f)$ and $I_{R_{7,4}}(f)$ are computed by each receiver and sent back to the source ECU_4.
- The branch between ECU_4 and one of the receivers R_i is considered as faulty if its corresponding health indicator $I_{R_{i,4}}$ is not null (with $i \in \{5;6;7\}$).

The fault detection and localization method on hybrid network is based on the decomposition into simple sub-networks, where our proposed method can be carried out. It should be noted that as each monitoring mechanism for each sub-network is independent of the others, multiple faults can be detected and localized if they are not localized in the same sub-network.

3.3 Illustration of the diagnosis method for a simulated bus network

We propose in this section to illustrate the fault detection and localization method on the simulated bus network shown in Fig. 3.14 (the same as the bus network in Fig 3.13a).

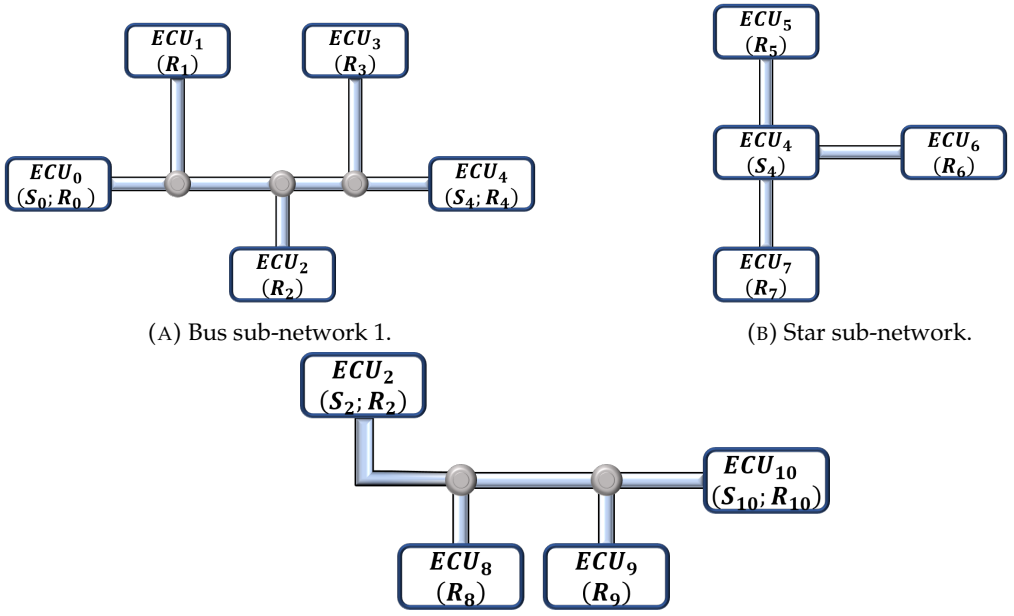

(A) Bus sub-network 1.

(B) Star sub-network.

(C) Bus sub-network 2.

FIGURE 3.13: Hybrid network decomposition.

3.3.1 Studied network

The studied network, shown in Fig. 3.14, is simulated using the chain matrix model (Chapter 1, subsection 1.4.1). The network consists of $N+1=5$ ECU, $2N-1=7$ branches and $N-1=3$ nodes. Two branches B_{b_1} and B_{b_2} are situated between two nodes. Five branches, B_i with $i \in \{0;1;2;3;4\}$, are situated between a node and an ECU. The nodes are denoted n_i, with $i \in \{0;1;2\}$.
In what follows, three different faulty network situations are detailed :

- Faulty B_2: The fault is inserted in the branch B_2.
- Faulty B_3: The fault is inserted in the branch B_3
- Faulty B_{b_1}: The fault is inserted in the branch B_{b_1}.

A soft fault is represented by an impedance of 5 Ω inserted in series in the faulty branch.

3.3.2 Hierarchical fault detection and localization method application

To illustrate the hierarchical fault detection and localization method detailed in 3.1.2.3 (method III), simulation-based data in the bandwidth

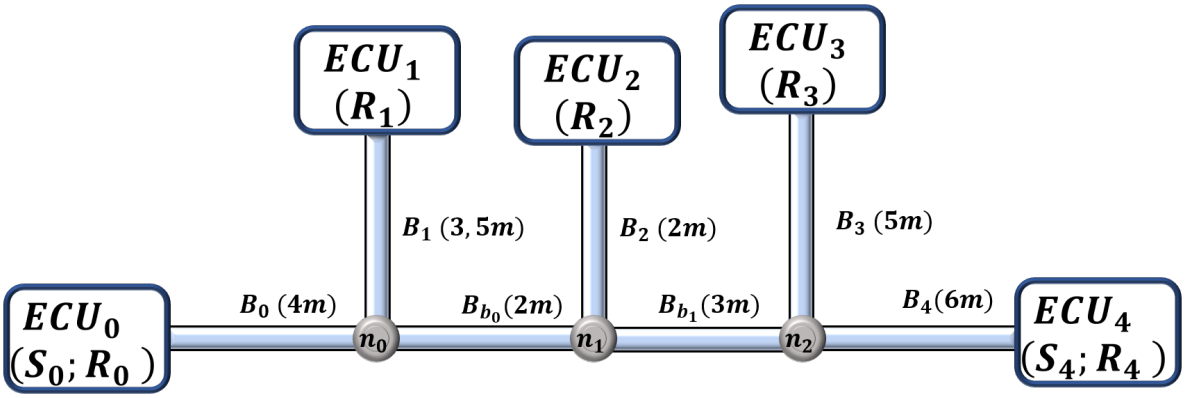

FIGURE 3.14: Bus network

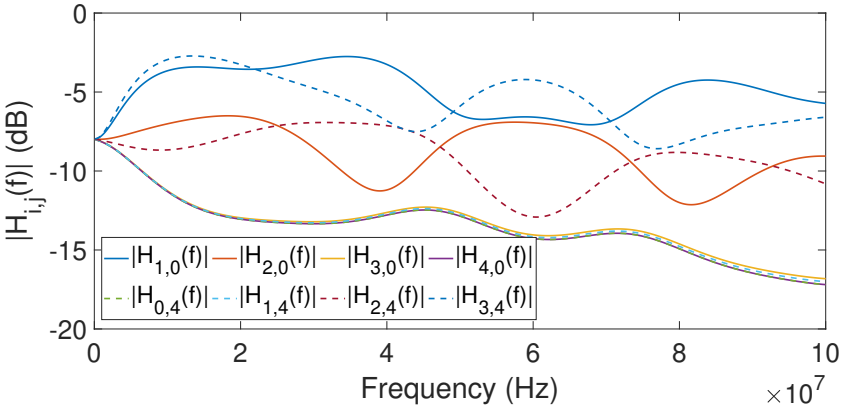

FIGURE 3.15: Computed transmission coefficients.

$BW = [1MHz : 1kHz : 100MHz]$ are used. ECU_0 and ECU_4 are acting as sources and as receivers.

In the no-fault situation, the transmission coefficients, denoted $H_{j,i}(f)$, are estimated at each receiver R_j when the source S_i is transmitting OFDM pilot symbols. Each ECU acting as source is connected to four receivers. In total, eight transmission coefficients are estimated. Their module is represented in Fig. 3.15. We can notice that the transmission coefficients $H_{3,0}(f)$ and $H_{4,0}(f)$ between the source S_0 and the receivers R_3 and R_4 respectively have close values. It is straightforward because the receivers R_3 and R_4 are connected to the same node n_2 and the branches B_3 and B_4 have almost the same length. For the same reasons, the transmission coefficients $H_{0,4}(f)$ and $H_{1,4}(f)$ have also close values. Note that since $H_{4,0}(f)$ and $H_{0,4}(f)$ are equal, they are superimposed.

The health indicators are computed from the transmission coefficients using (2.1) in Chapter 2. Four different situations, no-fault, faulty B_2, faulty B_3 and faulty B_{b_1} , are presented in the Fig. 3.16, Fig. 3.17, Fig. 3.18 and Fig. 3.19 respectively.

1. In the no-fault situation, all the health indicators are null as shown in Fig. 3.16.

2. In the faulty B_2 situation, we have two sets of health indicators that behave as follows :

   - ECU_0 is acting as a source : the health indicators computed at the receivers directly connected to any branch of the receiver-side branches set $\{B_{R_2}\}_{S_0} = \{B_3; B_4\}$ are equal, i.e. $I_{R_{3,0}}(f) = I_{R_{4,0}}(f) = I_{R_{\{3,4\},0}}(f)$.
   - ECU_4 is acting as a source : the health indicators computed at the receivers directly connected to any branch of the receiver-side branches set $\{B_{R_0}\}_{S_N} = \{B_0; B_1\}$ are equal, i.e. $I_{R_{0,4}}(f) = I_{R_{1,4}}(f) = I_{R_{\{0,1\},4}}(f)$.

   Moreover, we have $I_{R_{0,4}}(f) = I_{R_{4,0}}(f)$. As a consequence, the health indicators $I_{R_{\{3,4\},0}}(f)$ and $I_{R_{\{0,1\},4}}(f)$ are equal and thus superimposed. They are drawn in yellow color in Fig. 3.17.

3. In the faulty B_3 situation, we have two sets of health indicators that behave as follows:

   - ECU_0 is acting as a source : all the health indicators are different from each others, $I_{R_{i,0}}(f) \neq I_{R_{j,0}}(f), \forall\, i, j \in \{0; 1; 2; 3; 4\}$.
   - ECU_4 is acting as a source : the health indicators computed at the receivers directly connected to any branch of the receiver-side branches set $\{B_{R_2}\}_{S_4} = \{B_0; B_1; B_{b_1}; B_2; B_{b_2}\}$ are equal. Thus we have $I_{R_{0,4}}(f) = I_{R_{1,4}}(f) = I_{R_{2,4}}(f) = I_{R_{\{0,1,2\},4}}(f)$. The health indicator $I_{R_{3,4}}(f)$ is different.

   Moreover, we have $I_{R_{4,0}}(f) = I_{R_{0,4}}(f)$. Therefore, $I_{R_{\{0,1,2\},4}}(f)$ and $I_{R_{4,0}}(f)$ are equal and thus superimposed. They are drawn in purple color in Fig. 3.18.

4. In the faulty B_{b_1} situation, we have two sets of health indicators that behave as follows :

   - ECU_0 is acting as a source : the health indicators computed at the receivers directly connected to any branch of the receiver-side branches set $\{B_{R_1}\}_{S_0} = \{B_2; B_{b_2}; B_3; B_4\}$ are equal, thus we have $I_{R_{2,0}}(f) = I_{R_{3,0}}(f) = I_{R_{4,0}}(f) = I_{R_{\{2,3,4\},0}}(f)$ while $I_{R_{1,0}}(f)$ is different.
   - ECU_4 is acting as a source : the health indicators computed at the receivers directly connected to any branch of the receiver-side branches set $\{B_{R_1}\}_{S_4} = \{B_0; B_1; B_{b_1}\}$ are equal : $I_{R_{0,4}}(f) = I_{R_{1,4}}(f) = I_{R_{\{0,1\},4}}(f)$. The two health indicators $I_{R_{2,4}}(f)$ and $I_{R_{3,4}}(f)$ are different.

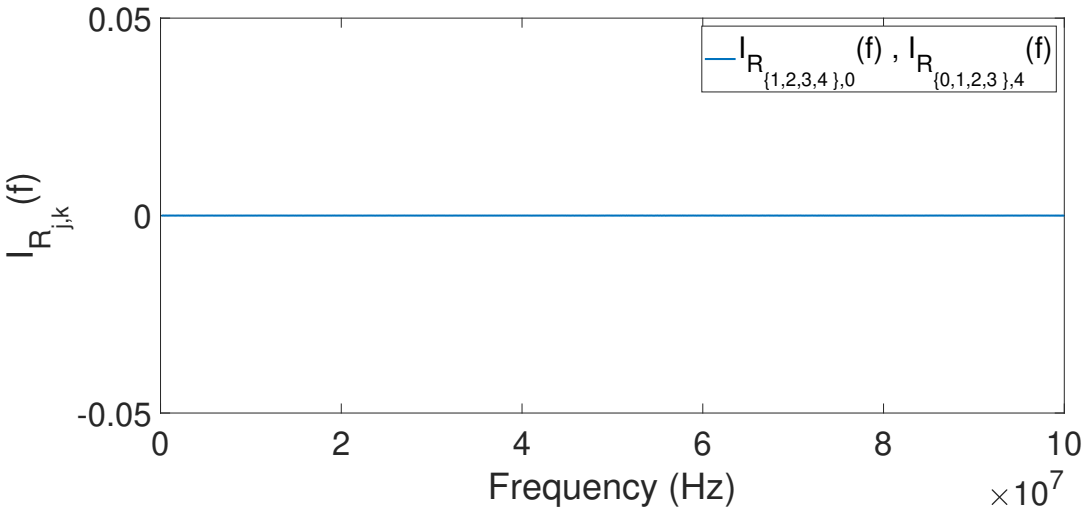

FIGURE 3.16: The health indicators in the no-fault situation of the network.

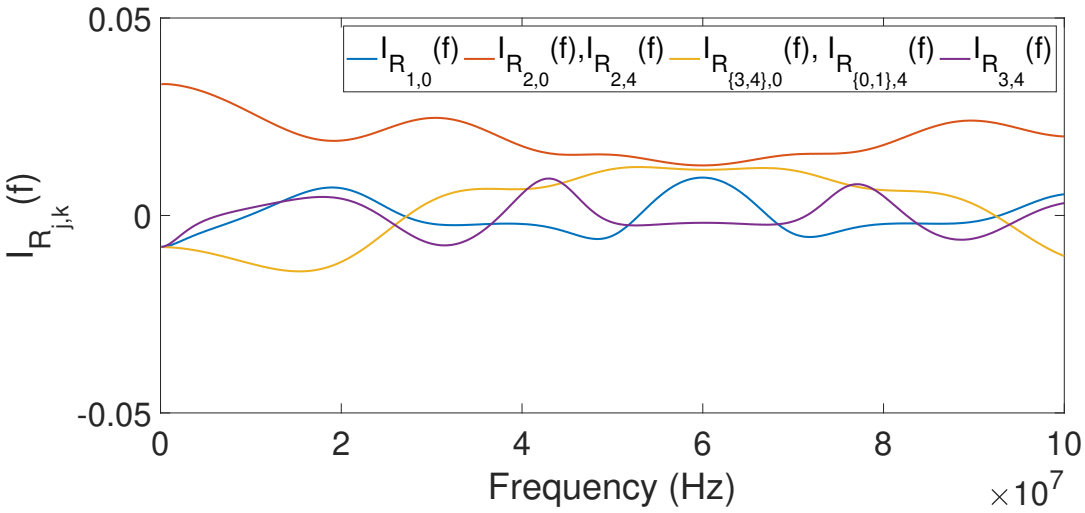

FIGURE 3.17: The health indicators in the faulty B_2 situation of the network.

Moreover, we have $I_{R_{0,4}}(f) = I_{R_{4,0}}(f)$. Therefore $I_{R_{\{2,3,4\},0}}(f)$ and $I_{R_{\{0,1\},4}}(f)$ are equal. They are drawn in purple color in Fig. 3.19.

The health indicators in the other four faulty situations can be deduced.

The chain matrix model of the network is simulated to get the transmission coefficients (TC). A Gaussian noise is added to the TC, with a $SNR = 100\ dB$. The health indicators and the residuals are computed. As in Chapter 2, in order to reduce the noise effect on the residuals, all residuals $r_i^{j,k}$ are weighted by the correlation function $(1 - MFRAC(I_{R_{i,j}}(f), I_{R_{i,k}}(f)))$, which leads to the practical residuals $\rho_i^{j,k}$. Only the practical residuals are considered in the following, which are called residuals to shorten. 100 simulations are performed for each situation (no

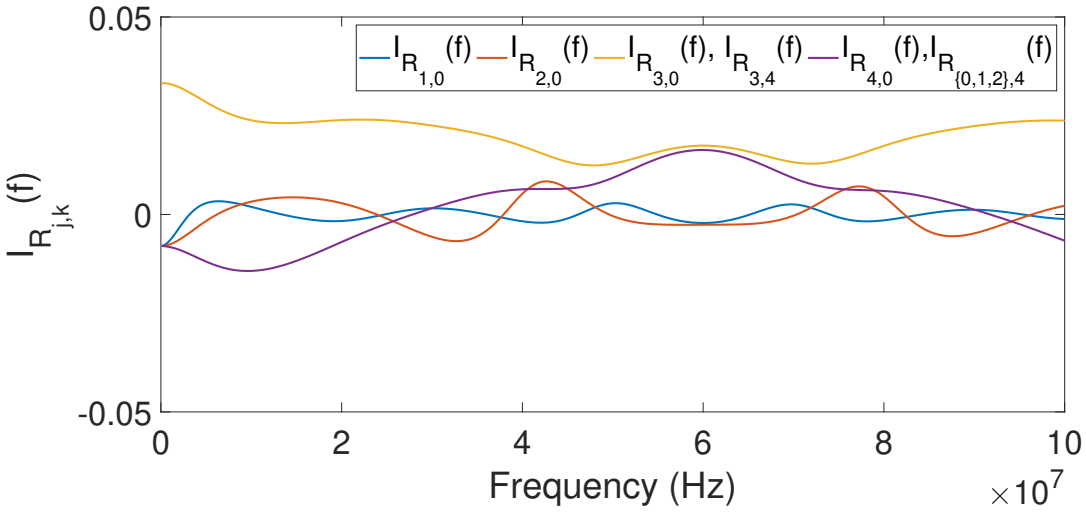

FIGURE 3.18: The health indicators in the faulty B_3 situation of the network.

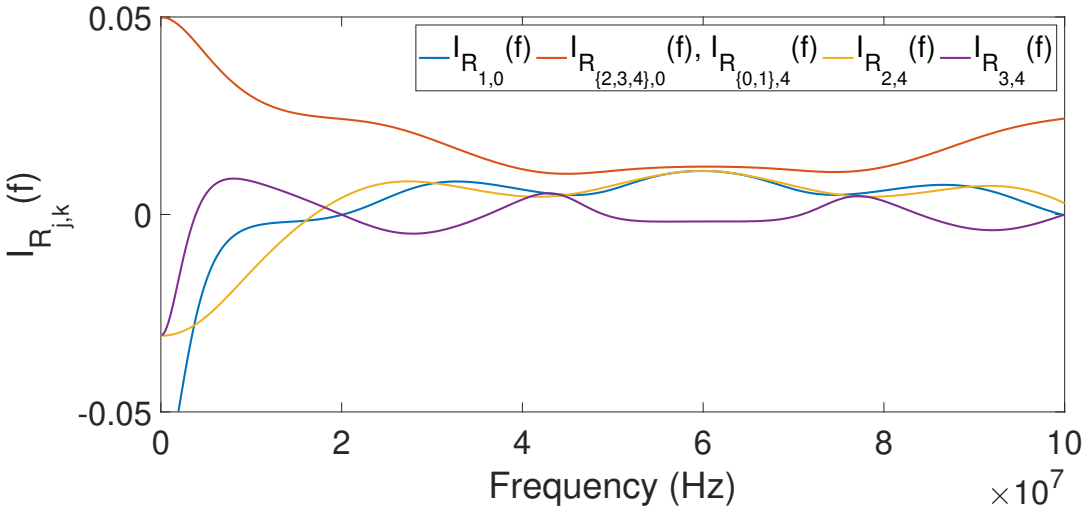

FIGURE 3.19: The health indicators in the faulty B_{b_1} situation of the network.

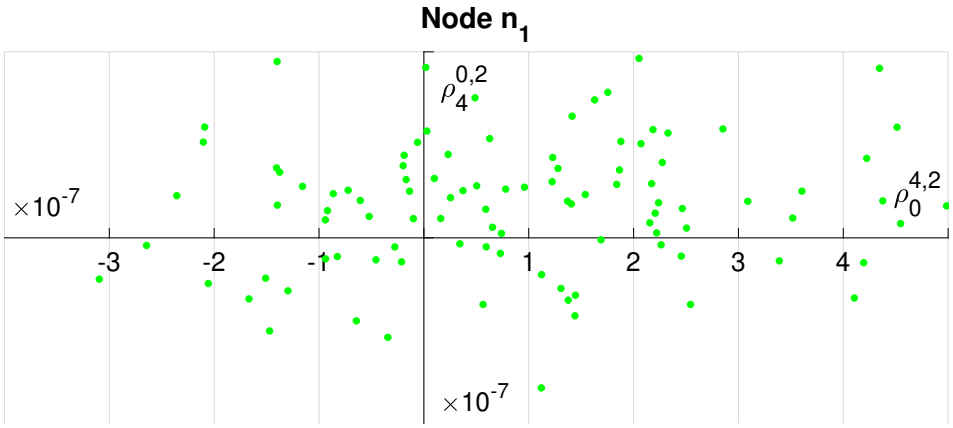

FIGURE 3.20: Residuals in the no-fault situation (Reference cluster).

fault and one faulty branch).

We will follow the hierarchical fault detection and localization procedure detailed in 3.1.2.3.

The source-side branches sets and the receiver-side branches sets are initially defined by selecting the node n_1. The source-side branches sets, when considering the 2 sources S_0 and S_4 are respectively $\{B_{S_1}\}_{S_0} = \{B_0; B_1; B_{b_1}\}$ and $\{B_{S_1}\}_{S_N} = \{B_{b_2}; B_3; B_4\}$. The receiver-side branches sets are $\{B_{R_1}\}_{S_0} = \{B_2; B_{b_2}; B_3; B_4\}$ and $\{B_{R_1}\}_{S_N} = \{B_0; B_1; B_{b_1}\}$. The residuals $\rho_0^{4,2}$ and $\rho_4^{0,2}$ are initially computed respectively by the sources S_0 and S_4 from the health indicators sent by the receivers R_0, R_4 and R_2 to their appropriate sources. Then, the second step is determined in accordance with the residual values.
In the no-fault situation, the residuals, $\rho_0^{4,2}$ and $\rho_4^{0,2}$, are first computed. They are represented by a green cluster of samples in the residual space in Fig. 3.20. Henceforth, this green cluster is addressed as the reference cluster. The three faulty situations of the network are considered in the following:

1. Faulty B_2: A fault, represented by 5 Ω in series is inserted in the branch B_2 at $1m$ from the position of the node n_1. The residuals $\rho_0^{4,2}$ and $\rho_4^{0,2}$ are computed and plotted in the residual space in Fig. 3.21. The reference cluster is shown in green and the cluster corresponding to the faulty situation is represented in red. The values of the two residuals, $\rho_0^{4,2}$ and $\rho_4^{0,2}$, are different from zero which indicates that the fault is located in the branch B_2.

2. Faulty B_3 : A fault, represented by a 5 Ω resistance in series is inserted in the branch B_3 at $1m$ from the position of the node n_2. The residuals, $\rho_0^{4,2}$ and $\rho_4^{0,2}$, are computed and plotted in the residual space in Fig. 3.22a. The reference cluster is shown in green and the cluster corresponding to the faulty situation

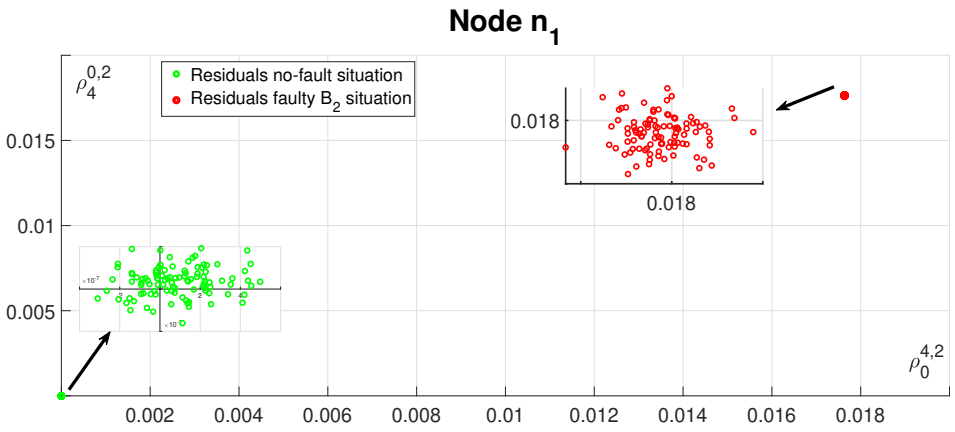

FIGURE 3.21: Residuals in the faulty B_2 situation.

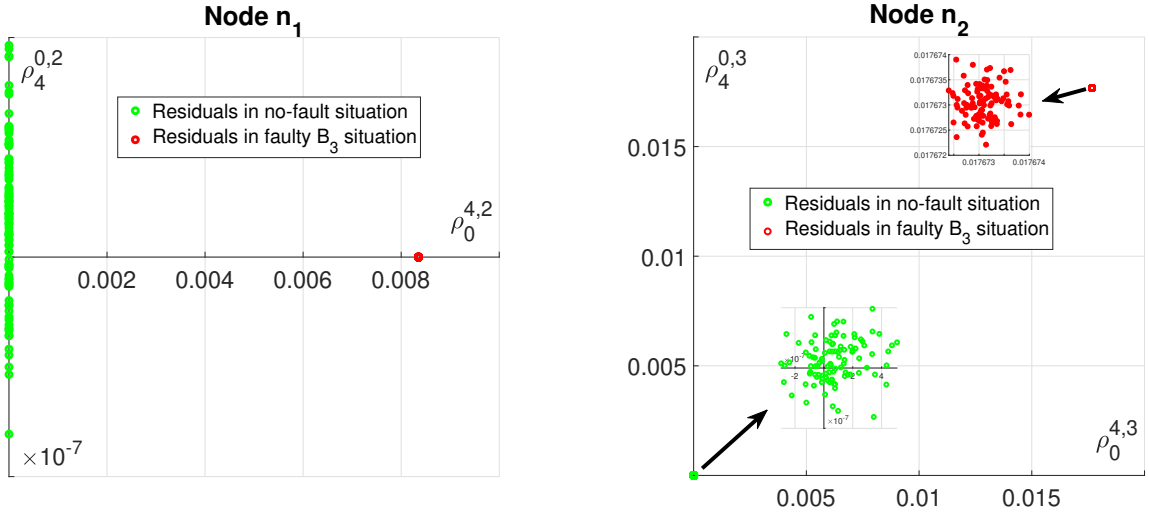

(A) (B)

FIGURE 3.22: Residuals in the faulty B_3 situation. (A) Clusters formed by the residuals $\rho_0^{4,2}$ and $\rho_4^{0,2}$, (B) Clusters formed by the residuals $\rho_0^{4,3}$ and $\rho_4^{0,3}$.

is represented in red. The values of $\rho_0^{4,2}$ are different from zero and the values of $\rho_4^{0,2}$ are near zero which indicates that the fault is located at one of the branches of the source-side branches set $\{B_{S_1}\}_{S_N} = \{B_{b_2}; B_3; B_4\}$.
According to the hierarchical algorithm in Fig. 3.8, the source-side branches set $\{B_{S_1}\}_{S_N}$ is considered to be faulty. The source-side branches set is divided in two by selecting the node n_2. The new source-side branches sets are $\{B_{S_2}\}_{S_0} = \{B_{b_2}\}$ and $\{B_{S_2}\}_{S_N} = \{B_4\}$, the other branches are left out of the sets since they are considered as non-faulty from the first step. The residuals, $\rho_0^{4,3}$ and $\rho_4^{0,3}$, are computed and represented in Fig. 3.22b. The two residuals are different from zero which indicates that the fault is located in the branch B_3.

3. Faulty B_{b_1}: A fault, represented by a 5 Ω resistance in series is inserted in the branch B_{b_1} at $1m$ from the position of the node n_1. The residuals $\rho_0^{4,2}$ and $\rho_4^{0,2}$

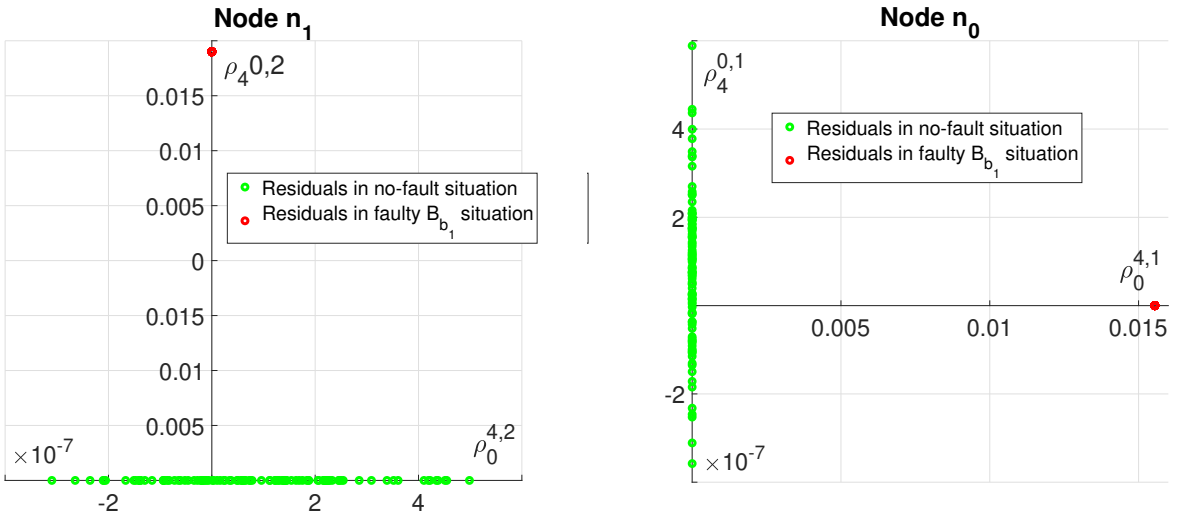

FIGURE 3.23: Residuals in the faulty B_{b_1} situation. (A) Clusters formed by the residuals $\rho_0^{4,2}$ and $\rho_4^{0,2}$, (B) Clusters formed by the residuals $\rho_0^{4,1}$ and $\rho_4^{0,1}$.

are computed and plotted in the residual space in Fig. 3.23a. The reference cluster is shown in green and the cluster corresponding to the faulty situation is represented in red. The residuals $\rho_4^{0,2}$ are different from zero and the residuals $\rho_0^{4,2}$ are equal to zero which indicates that the fault is located at one of the branches of the source-side branches set $\{B_{S_1}\}_{S_0} = \{B_0; B_1; B_{b_1}\}$. According to the hierarchical algorithm in Fig. 3.8, the node n_0 is selected. The new source-side branches sets are $\{B_{S_0}\}_{S_0} = \{B_0\}$ and $\{B_{S_0}\}_{S_N} = \{B_{b_1}\}$. The residuals $\rho_0^{4,1}$ and $\rho_4^{0,1}$ are computed and plotted in Fig. 3.23b. The values of the residual $\rho_4^{0,1}$ are around zero and the values of the residual $\rho_0^{4,1}$ are different from zero indicating that the fault is located in the branch B_{b_1}.

The minimum required residuals for fault detection and localization in the studied bus network is only two residuals and the maximum required residuals is $2 * \lfloor log2(N) \rceil = 4$.

3.4 Conclusion

In chapter 2, a residual-based soft fault diagnosis method for point-to-point network and a Y-shaped network has been proposed. This chapter has extended this method to more complex networks as bus networks and hybrid networks. Hybrid networks may be decomposed into typical classical networks such as point-to-point, Y-shaped network, star-shaped network and a bus network.

Three methodologies are proposed to deal with bus networks. These methodologies are compared in terms of computation and communication burden. This comparison reveals that the hierarchical method (method III) is superior to the two others. The hierarchical fault diagnosis method is illustrated using realistic intensive simulations of a bus network.

Chapter 4

General conclusion and future work

This research work proposes a method for detecting and locating cable faults based on data transmission. The method is based on the comparison of transmission coefficients between an ECU acting as a source and another ECU acting as a receiver. From these transmission coefficients, fault-sensitive health indicators and residuals, are computed. The residuals are then compared to a pre-constructed signature matrix based on the topology of the network. This comparison leads to the detection of a fault and to the location of the faulty branch. The methodology is initially detailed for a Y-shaped network and then it is further extended to a more complex network (a combination of different network topologies). In a complex network, a decomposition network approach is proposed, allowing to represent each complex network as a cascading Y-shaped networks, thus facilitating the detection and localisation process. The proposed approach is validated on data real and illustrated on simulated based data. The real data are obtained by means of measurements performed on a Y-shaped test bench built at the IEMN laboratory. The simulated data are obtained using the transmission line chain matrix model. The considered soft faults are represented by adding impedances in series, where the fault severity is represented by this impedance value. The results obtained show the potential of our transmission-based method to detect soft fault and locate the faulty branch, that is to say to follow the health state, of a complex network. This preliminary work opens many research perspectives.

We have considered additive white Gaussian noise on the estimated transmission coefficients. However, depending on the system and its environment, several other types of noise more relevant in industrial applications can be considered, such as: impulsive noise, and narrowband noise in vehicular networks. Impulsive noise mainly due to the switching of the insulated gate bipolar transistor (aperiodic) in power conversion systems and the power supply in the main

network (periodic), has a high power spectral density over a limited and short duration affecting high speed communication. In addition, narrowband noise, mainly from broadcast transmitters, has a variable level depending on the day [84, 141–146]. The impact of both types of noise on the performance of our proposed fault detection and localization method needs to be studied.

The analysis of the residuals with respect to the fault characteristics in Chapter 2 showed that both the position of the fault and its severity have an influence on the residuals. Experimental data has shown that the variation of the residuals is quite linear with the severity of the fault but this has not been proved theoretically. If this qualitative result is proved formally, it could be possible to estimate the severity of the fault. This estimation can be used to track the evolution of the fault and to potentially predict the remaining useful life of the cable (prognostic approach). Preliminary studies using the Mahalanobis distance between the clusters formed by the residuals have been conducted to determine the minimum detectable fault but are not yet finalized. The problem is that the residuals depend on two fault's characteristics, the severity and the position of the fault. For one characteristic (fault severity) to be estimated, the other must be known (fault position).

As explained in Chapter 1, two different approaches of wireline diagnostic methods may be applied : reflectometry-based and transferometry-based approaches. These two approaches can be compared and their complementarity can be studied. The two approaches may be combined in order to improve the fault detection and localization performance, and try to estimate the severity (Z_f) and the exact position of the fault in any branch.

When a fault is detected and the faulty branch located, the network and the communication protocol have to be reconfigured, leading to a fault-tolerant network. If possible, the data transmission route may be changed to avoid the faulty branch. If it is not possible, the communication burden on the faulty part of the network can be kept to a minimum until a maintenance operation is made.

Several assumptions are made to apply our method. We suppose that the terminal loads of the network are matched, that the topology of the network is perfectly known and we consider that only single resistive faults are present in the network. Relaxing these assumptions are very challenging.

The experimental validations must also be continued on the experimental communication network test-bench and carried out on the Zoé autonomous electric vehicle (CRIStAL-PRETIL platform: Robotics and Intelligent Transport Research

Platform of Lille - platform labelled by the University of Lille and the Equipex Robotex). It will be interesting to study real PLC systems and measure the robustness of the diagnosis methods with respect to the performance of the communication link.

List Of Publications

- **International Communication:**

  Abdel Karim, A., Degardin, V., Cocquempot, V. and Atoui, M., “Soft Fault Detection and Localization in an Unshielded Twisted Pair Network using Power Line Communication.” In: *Proceedings of the 7th International Conference on Vehicle Technology and Intelligent Transport Systems (VEHITS)*, 2021, pages 82-89, DOI: 10.5220/0010438000820089.

  Abdel Karim, A., Atoui, M., Degardin, V. and Cocquempot, V., "Fault Detection and Localization in Vehicular Embedded Network Using Power Line Communication." In : *9th International Conference on Systems and Control (ICSC)*, 2021, pp. 119-126, DOI: 10.1109/ICSC50472.2021.9666522.

  Abdel Karim, A., Atoui, M., Degardin, V. and Cocquempot, V., "Fault detection and localization in Y-shaped network through power line communication," In: *5th International Conference on Control and Fault-Tolerant Systems (SysTol)*, 2021, pp. 103-108, DOI: 10.1109/SysTol52990.2021.9595477.

  Abdel Karim, A., Atoui, M., Degardin, V. and Cocquempot, V., "Using Power Line Communication for Fault Detection and Localization in Star-shaped Network," In: *11th IFAC Symposium on Fault Detection, Supervision and Safety for Technical Processes SAFEPROCESS*, 2022, pp. 526-532, DOI: 10.1016/j.ifacol.2022.07.182.

  Abdel Karim, A., Degardin, V. and Cocquempot, V., "Sensitivity analysis of residuals for soft fault monitoring in Y-shaped networks," In: *2022 International Conference on Control, Automation and Diagnosis (ICCAD)*, 2021, p. 1-6, DOI: 10.1109/ICCAD55197.2022.9854008.

Bibliography

[1] DL Zhang, LY Xiao, Y Wang, and GZ Huang. "Study on vehicle fire safety: Statistic, investigation methods and experimental analysis". In: *Safety science* 117 (2019), pp. 194–204 (cit. on pp. xxi, 9).

[2] Layane Abboud, Andrea Cozza, and Lionel Pichon. "A matched-pulse approach for soft-fault detection in complex wire networks". In: *IEEE Transactions on Instrumentation and Measurement* 61.6 (2012), pp. 1719–1732 (cit. on pp. xxi, 9).

[3] Fabrice Auzanneau. "Transferometry: A new tool for complex wired networks diagnosis". In: *Progress In Electromagnetics Research B* 70 (2016), pp. 87–100 (cit. on pp. xxii, 40, 42).

[4] *Rapport d'activité du CEA-LIST 2021*, https://list.cea.fr/app/uploads/2022/06/RA-CEA-List-2021-FR.pdf (cit. on p. xxii).

[5] Lutz Lampe, Andrea M Tonello, and Theo G Swart. *Power Line Communications: Principles, Standards and Applications from multimedia to smart grid*. John Wiley & Sons, 2016 (cit. on pp. xxii, 2, 30).

[6] *Automotive Power Line Communication | Yamar Electronics*. URL: https://yamar.com/automotive/ (cit. on pp. xxii, 30).

[7] Gianluca Cena, Adriao Valenzano, and Stefano Vitturi. "Hybrid wired/wireless networks for real-time communications". In: *IEEE industrial electronics magazine* 2.1 (2008), pp. 8–20 (cit. on p. 1).

[8] M Vijayarani and Mrs N Srividya. "Wired vs Wireless Using Advanced Network". In: *International Journal of Engineering Research and General Science* 3.2 (2015), pp. 825–832 (cit. on p. 1).

[9] *Wires and Cables Market Size, Growth & Share | Report [2029]*. URL: https://www.fortunebusinessinsights.com/wires-and-cables-market-103322 (cit. on p. 2).

[10] Alberto Bemporad, Maurice Heemels, and Mikael Johansson. *Networked control systems*. Vol. 406. Springer, 2010 (cit. on p. 2).

[11] Adebayo Segun, AO Akinwunmi, and Erastus O Ogunti. "A survey of medium access control protocols in wireless sensor network". In: *International Journal of Computer Applications* 116.22 (2015) (cit. on p. 2).

[12] Saleh Faruque. "Time division multiple access (TDMA)". In: *Radio Frequency Multiple Access Techniques Made Easy*. Springer, 2019, pp. 35–43 (cit. on p. 2).

[13] Saleh Faruque. "Frequency division multiple access (FDMA)". In: *Radio Frequency Multiple Access Techniques Made Easy*. Springer, 2019, pp. 21–33 (cit. on p. 2).

[14] Kamil Sh Zigangirov. *Theory of code division multiple access communication*. John Wiley & Sons, 2004 (cit. on p. 2).

[15] Simon S Lam. "A carrier sense multiple access protocol for local networks". In: *Computer Networks (1976)* 4.1 (1980), pp. 21–32 (cit. on p. 2).

[16] Alan Colvin. "CSMA with collision avoidance". In: *Computer communications* 6.5 (1983), pp. 227–235 (cit. on p. 2).

[17] Andreas Willig. "Polling-based MAC protocols for improving real-time performance in a wireless PROFIBUS". In: *IEEE Transactions on Industrial Electronics* 50.4 (2003), pp. 806–817 (cit. on p. 2).

[18] Nicholas Malcolm and Wei Zhao. "The timed-token protocol for real-time communications". In: *Computer* 27.1 (1994), pp. 35–41 (cit. on p. 2).

[19] Eduardo Tovar and Francisco Vasques. "Real-time fieldbus communications using Profibus networks". In: *IEEE transactions on Industrial Electronics* 46.6 (1999), pp. 1241–1251 (cit. on p. 2).

[20] Steve Corrigan HPL. "Introduction to the controller area network (CAN)". In: *Application Report SLOA101* (2002), pp. 1–17 (cit. on p. 2).

[21] Matthew Ruff. "Evolution of local interconnect network (LIN) solutions". In: *2003 IEEE 58th Vehicular Technology Conference. VTC 2003-Fall (IEEE Cat. No. 03CH37484)*. Vol. 5. IEEE. 2003, pp. 3382–3389 (cit. on p. 2).

[22] Ing Andreas Grzemba. *MOST: the automotive multimedia network*. Franzis Verlag, 2012 (cit. on p. 2).

[23] Rainer Makowitz and Christopher Temple. "Flexray-a communication network for automotive control systems". In: *2006 IEEE International Workshop on Factory Communication Systems*. IEEE. 2006, pp. 207–212 (cit. on p. 2).

[24] Kirsten Matheus and Thomas Königseder. *Automotive ethernet*. Cambridge University Press, 2021 (cit. on p. 2).

[25] Donovan Porter. "100BASE-T1 Ethernet: the evolution of automotive networking". In: *Texas Instruments, Techn. Ber* (2018) (cit. on p. 2).

[26] GV Bezprozvannych, IA Kostiukov, and OA Pushkar. "Synthesis of Constructive-Technological Decisions of Regulation of Working Capacitance of Cables of Industrial Networks". In: *Electrical Engineering & Electromechanics* 1 (2021), pp. 44–49 (cit. on p. 2).

[27] Konark Sharma and Lalit Mohan Saini. "Power-line communications for smart grid: Progress, challenges, opportunities and status". In: *Renewable and Sustainable Energy Reviews* 67 (2017), pp. 704–751 (cit. on p. 2).

[28] Anim Adrian Amarsingh, Haniph A Latchman, and Duotong Yang. "Narrowband power line communications: Enabling the smart grid". In: *IEEE Potentials* 33.1 (2014), pp. 16–21 (cit. on p. 2).

[29] Samuel C Pereira, Alexandre S Caporali, and Ivan RS Casella. "Power line communication technology in industrial networks". In: *2015 IEEE International Symposium on Power Line Communications and Its Applications (ISPLC)*. IEEE. 2015, pp. 216–221 (cit. on p. 2).

[30] Kaveh Razazian, Maher Umari, Amir Kamalizad, Victor Loginov, and Michael Navid. "G3-PLC specification for powerline communication: Overview, system simulation and field trial results". In: *ISPLC2010*. IEEE. 2010, pp. 313–318 (cit. on pp. 2, 30).

[31] SA Schelkunoff. "Conversion of Maxwell's equations into generalized telegraphist's equations". In: *Bell System Technical Journal* 34.5 (1955), pp. 995–1043 (cit. on p. 3).

[32] Stephen D Gedney. "Introduction to the finite-difference time-domain (FDTD) method for electromagnetics". In: *Synthesis Lectures on Computational Electromagnetics* 6.1 (2011), pp. 1–250 (cit. on p. 4).

[33] Dale Liu, Brian Barber, and Luigi DiGrande. "Introduction to Networking". In: *Cisco CCNA/CCENT Exam 640-802, 640-822, 640-816 Preparation Kit* (2009), pp. 1–46 (cit. on p. 4).

[34] Lola El Sahmarany. "Méthodes d'amélioration pour le diagnostic de câble par réflectométrie". In: (2013) (cit. on pp. 5, 10, 11, 79).

[35] T Kien Truong. "Twisted-pair transmission-line distributed parameters". In: *The Boeing CO* (2000) (cit. on p. 5).

[36] Wafa Ben Hassen, Moussa Kafal, and Esteban Cabanillas. "A Stranded Unshielded Twisted Pair Modeling for Online Fault Location using OMTDR-based Diagnosis Sensor." In: *SENSORNETS*. 2019, pp. 40–46 (cit. on p. 5).

[37] Javier Espina, Thomas Falck, Athanasia Panousopoulou, Lars Schmitt, Oliver Mülhens, and Guang-Zhong Yang. "Network topologies, communication protocols, and standards". In: *Body sensor networks*. Springer, 2014, pp. 189–236 (cit. on pp. 6, 20).

[38] Debra Littlejohn Shinder. *Computer networking essentials*. Cisco Press, 2001 (cit. on p. 6).

[39] Santanu Santra and Pinaki Pratim Acharjya. "A Study And Analysis on Computer Network Topology For Data Communication". In: *International Journal of Emerging Technology and Advanced Engineering* 3.1 (2013), pp. 522–525 (cit. on p. 6).

[40] Bogdan Ciubotaru and Gabriel-Miro Muntean. *Advanced Network Programming–Principles and Techniques: Network Application Programming with Java*. Springer Science & Business Media, 2013 (cit. on p. 6).

[41] Franco Davoli, M Repetto, C Tornelli, G Proserpio, and F Cucchietti. "Boosting energy efficiency through smart grids". In: *International Telecommunication Union (ITU)* 7 (2012), pp. 14–16 (cit. on p. 7).

[42] Hein Marais. "RS-485/RS-422 circuit implementation guide". In: *AN-960 Analog Devices* (2008) (cit. on p. 7).

[43] Shane Tuohy, Martin Glavin, Ciarán Hughes, Edward Jones, Mohan Trivedi, and Liam Kilmartin. "Intra-vehicle networks: A review". In: *IEEE Transactions on Intelligent Transportation Systems* 16.2 (2014), pp. 534–545 (cit. on p. 7).

[44] Robert Bosch. *Automotive Handbook, 8th Edition*. Wiley, 2011 (cit. on pp. 7, 103, 105).

[45] AT Bulinski, SS Bamji, and RJ Densley. "The effects of frequency and temperature on water tree degradation of miniature XLPE cables". In: *IEEE transactions on electrical insulation* 4 (1986), pp. 645–650 (cit. on p. 8).

[46] Rolf Isermann and Peter Balle. "Trends in the application of model-based fault detection and diagnosis of technical processes". In: *Control engineering practice* 5.5 (1997), pp. 709–719 (cit. on pp. 9, 38).

[47] Cynthia M Furse, Moussa Kafal, Reza Razzaghi, and Yong-June Shin. "Fault diagnosis for electrical systems and power networks: A review". In: *IEEE Sensors Journal* 21.2 (2020), pp. 888–906 (cit. on pp. 9, 42).

[48] European Standard EN 13306. *Maintenance terminology*. 2001 (cit. on p. 9).

[49] *International Electrotechnical Commission, Area: 192: Dependability*. URL: https://www.electropedia.org/iev/iev.nsf/index?openform&part=192 (cit. on p. 9).

[50] Kenneth S Komisarek, KA Chamerberlin, and Kondagunta Sivaprasad. "A method of moment analysis of a twisted-pair transmission line". In: *Proceedings of IEEE Antennas and Propagation Society International Symposium*. IEEE. 1993, pp. 64–67 (cit. on p. 9).

[51] Kevin R. Wheeler, Nasa, Dogan A. Timucin, Arc I Xander Twombly, Riacs, Kai F Goebel-Riacs, Phil F Wysocki-Asrc, Aerospace, Keith Stevenson, and Michael Bequette. "Aging Aircraft Wiring Fault Detection Survey". In: *NASA Ames Research Center, CA 94035*. 2007 (cit. on p. 9).

[52] Eric J Lundquist, James R Nagel, Shang Wu, Brian Jones, and Cynthia Furse. "Advanced forward methods for complex wire fault modeling". In: *IEEE Sensors Journal* 13.4 (2012), pp. 1172–1179 (cit. on pp. 10, 11).

[53] Lena Förstel and Lutz Lampe. "Grid diagnostics: Monitoring cable aging using power line transmission". In: *2017 IEEE International Symposium on Power Line Communications and its Applications (ISPLC)*. IEEE. 2017, pp. 1–6 (cit. on pp. 10, 11).

[54] Gavita Mugala. "High frequency characteristics of medium voltage XLPE power cables". PhD thesis. KTH, 2005 (cit. on p. 10).

[55] J. Cohen. *CEA LIST activity on Cable Monitoring and Diagnosis*. URL: https://www.nae.fr/wp-content/uploads/2015/06/ComiteRTI_Juin2015_NAE_CEA-LIST_DF_-Pr%5C%C3%5C%A9sentation-1.1.pdf (cit. on pp. 10, 11).

[56] Anthony Manet, Abelin Kameni, Florent Loete, Jérôme Genoulaz, Lionel Pichon, and Odile Picon. "Equivalent circuit model of soft shield defects in coaxial cables using numerical modeling". In: *IEEE Transactions on Electromagnetic Compatibility* 59.2 (2016), pp. 533–536 (cit. on pp. 10, 11).

[57] Hossein Manesh, J Genoulaz, A Kameni, F Loete, Lionel Pichon, and Odile Picon. "Experimental analysis and modelling of coaxial transmission lines with soft shield defects". In: *2015 IEEE International Symposium on Electromagnetic Compatibility (EMC)*. IEEE. 2015, pp. 1553–1558 (cit. on p. 11).

[58] Gautham Prasad, Yinjia Huo, Lutz Lampe, Anil Mengi, and Victor CM Leung. "Fault diagnostics with legacy power line modems". In: *2019 IEEE International Symposium on Power Line Communications and its Applications (ISPLC)*. IEEE. 2019, pp. 1–6 (cit. on p. 11).

[59] Yinjia Huo, Gautham Prasad, Lazar Atanackovic, Lutz Lampe, and Victor CM Leung. "Cable diagnostics with power line modems for smart grid monitoring". In: *IEEE Access* 7 (2019), pp. 60206–60220 (cit. on p. 11).

[60] Laurent Sommervogel. "Various Models for Faults in Transmission Lines and Their Detection Using Time Domain Reflectometry". In: *Progress In Electromagnetics Research C* 103 (2020), pp. 123–135 (cit. on p. 11).

[61] Moussa Kafal and Wafa Ben Hassen. *Method for characterising a fault in a transmission line network with unknown topology*. US Patent App. 17/253,099. Sept. 2021 (cit. on pp. 11, 12).

[62] Wenfei Zhu, Xu Zhu, Enggee Lim, and Yi Huang. "State-of-art power line communications channel modelling". In: *Procedia Computer Science* 17 (2013), pp. 563–570 (cit. on p. 12).

[63] Manfred Zimmermann and Klaus Dostert. "A multipath model for the powerline channel". In: *IEEE Transactions on communications* 50.4 (2002), pp. 553–559 (cit. on p. 12).

[64] Holger Philipps. "Modeling of powerline communication channels". In: *Proc. of 3rd International Symposium on Power-Line Communications and its Applications (ISPLC'99)*. 1999, pp. 14–21 (cit. on p. 12).

[65] Justinian Anatory, MM Kissaka, and Nerey H Mvungi. "Channel model for broadband power-line communication". In: *IEEE transactions on power delivery* 22.1 (2006), pp. 135–141 (cit. on p. 12).

[66] Justinian Anatory, Nelson Theethayi, and Nerey H Mvungi. "Power line channel models: Comparisons between different modeling adopted in bplc systems". In: *Third workshop on power line communications*. 2009 (cit. on p. 12).

[67] Manfred Zimmermann and Klaus Dostert. "A multi-path signal propagation model for the power line channel in the high frequency range". In: *Proceedings of the 3rd International Symposium on Power-Line Communications, Lancaster, UK*. Vol. 30. 1.4. 1999 (cit. on p. 12).

[68] Tooraj Esmailian, Frank R Kschischang, and P Glenn Gulak. "In-building power lines as high-speed communication channels: channel characterization and a test channel ensemble". In: *International Journal of Communication Systems* 16.5 (2003), pp. 381–400 (cit. on p. 12).

[69] Fabrice Auzanneau. "Wire troubleshooting and diagnosis: Review and perspectives". In: *Progress In Electromagnetics Research B* 49 (2013), pp. 253–279 (cit. on pp. 12, 40–42).

[70] Stefano Galli and Thomas Banwell. "A novel approach to the modeling of the indoor power line channel-Part II: transfer function and its properties". In: *IEEE Transactions on Power Delivery* 20.3 (2005), pp. 1869–1878 (cit. on p. 13).

[71] Clayton R Paul. *Analysis of multiconductor transmission lines*. John Wiley & Sons, 2007 (cit. on pp. 13, 14).

[72] Pedro LD Peres, Carlos R De Souza, and Ivanil S Bonatti. "ABCD matrix: a unique tool for linear two-wire transmission line modelling". In: *International Journal of Electrical Engineering Education* 40.3 (2003), pp. 220–229 (cit. on p. 15).

[73] Hamid Bouassam. "Analyse et modélisation de l'effet des impédances de charge sur les performances d'une liaison CPL sur le réseau électrique domestique". PhD thesis. Lille 1, 2017 (cit. on p. 16).

[74] Dean A Frickey. "Conversions between S, Z, Y, H, ABCD, and T parameters which are valid for complex source and load impedances". In: *IEEE Transactions on microwave theory and techniques* 42.2 (1994), pp. 205–211 (cit. on p. 17).

[75] Dean A Frickey. "Calculation of S parameters from ABCD parameters with complex normalizing impedances". In: *Microwave and Optical Technology Letters* 5.12 (1992), pp. 613–615 (cit. on p. 17).

[76] Madhav Mishra and Maarten van Riet. "A channel model for power line communication using 4PSK technology for diagnosis: Some lessons learned". In: *International Journal of Electrical Power & Energy Systems* 95 (2018), pp. 617–634 (cit. on p. 30).

[77] Xavier Carcelle and Thomas Bourgeau. "Power Line Communication Technology Overview". In: *The Internet of things: connecting objects to the web* (2013), pp. 97–128 (cit. on p. 30).

[78] Inigo Berganza, Alberto Sendin, and Javier Arriola. "PRIME: Powerline intelligent metering evolution". In: *CIRED Seminar 2008: SmartGrids for Distribution*. IET. 2008, pp. 1–3 (cit. on p. 30).

[79] Christina Vlachou and Sébastien Henri. *A Practical Guide to Power-line Communication*. Cambridge University Press, 2022 (cit. on p. 31).

[80] Lars Torsten Berger, Andreas Schwager, and J Joaquín Escudero-Garzás. "Power line communications for smart grid applications". In: *Journal of Electrical and Computer Engineering* 2013 (2013) (cit. on pp. 31, 46).

[81] Larry Yonge, Jose Abad, Kaywan Afkhamie, Lorenzo Guerrieri, Srinivas Katar, Hidayat Lioe, Pascal Pagani, Raffaele Riva, Daniel M Schneider, and

Andreas Schwager. "An overview of the HomePlug AV2 technology". In: *Journal of Electrical and Computer Engineering* 2013 (2013) (cit. on pp. 31, 46).

[82] Yushi Shen and Ed Martinez. "Channel estimation in OFDM systems". In: *Freescale semiconductor application note* (2006), pp. 1–15 (cit. on pp. 31, 35).

[83] Lajos Hanzo, Soon Xin Ng, WT Webb, and T Keller. *Quadrature amplitude modulation: From basics to adaptive trellis-coded, turbo-equalised and space-time coded OFDM, CDMA and MC-CDMA systems*. IEEE Press-John Wiley, 2004 (cit. on p. 31).

[84] Martine Lienard, Marc Olivas Carrion, Virginie Degardin, and Pierre Degauque. "Modeling and analysis of in-vehicle power line communication channels". In: *IEEE Transactions on Vehicular Technology* 57.2 (2008), pp. 670–679 (cit. on pp. 34, 118).

[85] Hui Xie. "Sparse Channel Estimation in OFDM System To cite this version : Thèse de Doctorat". In: *PhD Thesis, Universite de Nantes; South China university of technology* Paris VI (2015). URL: https://hal.archives-ouvertes.fr/tel-01104830 (cit. on p. 34).

[86] Sinem Coleri, Mustafa Ergen, Anuj Puri, and Ahmad Bahai. "Channel estimation techniques based on pilot arrangement in OFDM systems". In: *IEEE Transactions on broadcasting* 48.3 (2002), pp. 223–229 (cit. on p. 35).

[87] Dongsheng Du, Bin Jiang, and Peng Shi. "Active fault tolerant control for switched systems with time delay". In: *Fault Tolerant Control for Switched Linear Systems*. Springer, 2015, pp. 119–134 (cit. on p. 38).

[88] Khoder Makkawi, Nourdine Ait-Tmazirte, Maan El Badaoui El Najjar, and Nazih Moubayed. "Adaptive diagnosis for fault tolerant data fusion based on α-rényi divergence strategy for vehicle localization". In: *Entropy* 23.4 (2021), p. 463 (cit. on p. 38).

[89] Rolf Isermann. "Process fault detection based on modeling and estimation methods—A survey". In: *automatica* 20.4 (1984), pp. 387–404 (cit. on p. 38).

[90] Venkat Venkatasubramanian, Raghunathan Rengaswamy, Kewen Yin, and Surya N Kavuri. "A review of process fault detection and diagnosis: Part I: Quantitative model-based methods". In: *Computers & chemical engineering* 27.3 (2003), pp. 293–311 (cit. on p. 38).

[91] Paul Martin Frank. "Analytical and qualitative model-based fault diagnosis–a survey and some new results". In: *European Journal of control* 2.1 (1996), pp. 6–28 (cit. on p. 38).

[92] Dubravko Miljković. "Fault detection methods: A literature survey". In: *2011 Proceedings of the 34th international convention MIPRO*. IEEE. 2011, pp. 750–755 (cit. on p. 38).

[93] Anam Abid, Muhammad Tahir Khan, and Javaid Iqbal. "A review on fault detection and diagnosis techniques: basics and beyond". In: *Artificial Intelligence Review* 54.5 (2021), pp. 3639–3664 (cit. on p. 38).

[94] Elena Dubrova. "Hardware redundancy". In: *Fault-Tolerant Design*. Springer, 2013, pp. 55–86 (cit. on p. 38).

[95] Janos Gertler. "Analytical redundancy methods in fault detection and isolation-survey and synthesis". In: *IFAC Proceedings Volumes* 24.6 (1991), pp. 9–21 (cit. on p. 38).

[96] Behrooz Parhami. "Voting algorithms". In: *IEEE transactions on reliability* 43.4 (1994), pp. 617–629 (cit. on p. 38).

[97] Michele Basseville. "Detecting changes in signals and systems—a survey". In: *Automatica* 24.3 (1988), pp. 309–326 (cit. on p. 38).

[98] Paul M Frank. "Fault diagnosis in dynamic systems using analytical and knowledge-based redundancy: A survey and some new results". In: *automatica* 26.3 (1990), pp. 459–474 (cit. on p. 38).

[99] M. Staroswiecki, J.P. Cassar, and V. Cocquempot. "Generation of Optimal Structured Residuals in the Parity Space". In: *IFAC Proceedings Volumes* 26.2, Part 5 (1993). 12th Triennal Wold Congress of the International Federation of Automatic control. Volume 5 Associated Technologies and Recent Developments, Sydney, Australia, 18-23 July, pp. 535–542. ISSN: 1474-6670. URL: https://www.sciencedirect.com/science/article/pii/S1474667017483248 (cit. on p. 38).

[100] Dongsheng Du, Shengyuan Xu, and Vincent Cocquempot. *Observer-Based Fault Diagnosis and Fault-Tolerant Control for Switched Systems*. Vol. 323. Springer (cit. on p. 38).

[101] Paul M Frank. "Fault diagnosis in dynamic systems via state estimation-a survey". In: *System fault diagnostics, reliability and related knowledge-based approaches*. Springer, 1987, pp. 35–98 (cit. on p. 38).

[102] Zhiwei Gao, Carlo Cecati, and Steven X Ding. "A survey of fault diagnosis and fault-tolerant techniques—Part I: Fault diagnosis with model-based and signal-based approaches". In: *IEEE transactions on industrial electronics* 62.6 (2015), pp. 3757–3767 (cit. on p. 38).

[103] Venkat Venkatasubramanian, Raghunathan Rengaswamy, Surya N Kavuri, and Kewen Yin. "A review of process fault detection and diagnosis: Part III: Process history based methods". In: *Computers & chemical engineering* 27.3 (2003), pp. 327–346 (cit. on p. 38).

[104] Christophe Aubrun, Jean-Philippe Georges, Dominique Sauter, and Eric Rondeau. "Network calculus based fault diagnosis decision-making for Networked Control Systems". In: *2008 IEEE International Conference on Emerging Technologies and Factory Automation*. IEEE. 2008, pp. 552–558 (cit. on p. 40).

[105] Hashem M Hashemian. "State-of-the-art predictive maintenance techniques". In: *IEEE Transactions on Instrumentation and measurement* 60.1 (2010), pp. 226–236 (cit. on p. 40).

[106] L Lamarre, D Fournier, and R Morin. "Early detection of faults in underground distribution cable joints by partial discharge measurements". In: *Proceedings of 1994 4th International Conference on Properties and Applications of Dielectric Materials (ICPADM)*. Vol. 2. IEEE. 1994, pp. 864–867 (cit. on p. 40).

[107] R Mijarez and A Baltazar. "Guided wave propagation study in an ACSR cable with artificial damage". In: *AIP Conference Proceedings*. Vol. 1511. 1. American Institute of Physics. 2013, pp. 1417–1424 (cit. on p. 40).

[108] Mira Mitra and S Gopalakrishnan. "Guided wave based structural health monitoring: A review". In: *Smart Materials and Structures* 25.5 (2016), p. 053001 (cit. on p. 40).

[109] Hyunuk Ha, Sunsin Han, and Jangmyung Lee. "Fault detection on transmission lines using a microphone array and an infrared thermal imaging camera". In: *IEEE*

Transactions on Instrumentation and Measurement 61.1 (2011), pp. 267–275 (cit. on p. 40).

[110] Philip A Nobile and Clifton A Laplatney. "Field testing of cables: Theory and practice". In: *IEEE transactions on industry applications* 5 (1987), pp. 786–795 (cit. on p. 40).

[111] Craig H Benson and Peter J Bosscher. *Time-domain reflectometry (TDR) in geotechnics: a review*. ASTM International, 1999 (cit. on p. 40).

[112] Nour Taki, Wafa Ben Hassen, Nicolas Ravot, Claude Delpha, and Demba Diallo. "Sensors Selection for Distributed Reflectometry-based Soft Fault Detection using Principal Component Analysis". In: *2019 IEEE AUTOTESTCON*. IEEE. 2019, pp. 1–5 (cit. on pp. 41, 42).

[113] Cynthia Furse and Nilesh Kamdar. "An inexpensive distance measuring system for navigation of robotic vehicles". In: *Microwave and Optical Technology Letters* 33.2 (2002), pp. 84–87 (cit. on p. 40).

[114] Mostafa Kamel Smail, Lionel Pichon, Marc Olivas, Fabrice Auzanneau, and Marc Lambert. "Detection of defects in wiring networks using time domain reflectometry". In: *IEEE Transactions on Magnetics* 46.8 (2010), pp. 2998–3001 (cit. on p. 40).

[115] Cynthia Furse, You Chung Chung, Rakesh Dangol, Marc Nielsen, Glen Mabey, and Raymond Woodward. "Frequency-domain reflectometry for on-board testing of aging aircraft wiring". In: *IEEE Transactions on Electromagnetic Compatibility* 45.2 (2003), pp. 306–315 (cit. on p. 42).

[116] Paul Smith, Cynthia Furse, and Jacob Gunther. "Analysis of spread spectrum time domain reflectometry for wire fault location". In: *IEEE sensors journal* 5.6 (2005), pp. 1469–1478 (cit. on p. 42).

[117] Adrien Lelong and Marc O Carrion. "On line wire diagnosis using multicarrier time domain reflectometry for fault location". In: *SENSORS, 2009 IEEE*. IEEE. 2009, pp. 751–754 (cit. on p. 42).

[118] Wafa Ben Hassen, Fabrice Auzanneau, Luca Incarbone, François Pérès, and Ayeley P Tchangani. "On-line diagnosis using Orthogonal Multi-Tone Time Domain Reflectometry in a lossy cable". In: *10th International Multi-Conferences on Systems, Signals & Devices 2013 (SSD13)*. IEEE. 2013, pp. 1–6 (cit. on p. 42).

[119] Kevin R Wheeler, Tolga Kurtoglu, and Scott D Poll. "A survey of health management user objectives related to diagnostic and prognostic metrics". In: *International Design Engineering Technical Conferences and Computers and Information in Engineering Conference*. Vol. 48999. 2009, pp. 1287–1298 (cit. on p. 42).

[120] Wafa Ben Hassen, Fabrice Auzanneau, Luca Incarbone, François Pérès, and Ayeley P Tchangani. "Distributed sensor fusion for wire fault location using sensor clustering strategy". In: *International Journal of Distributed Sensor Networks* 11.4 (2015), p. 538643 (cit. on p. 42).

[121] Wafa Ben Hassen, Fabrice Auzanneau, François Péres, and Ayeley P Tchangani. "Diagnosis sensor fusion for wire fault location in CAN bus systems". In: *SENSORS, 2013 IEEE*. IEEE. 2013, pp. 1–4 (cit. on p. 42).

[122] Ousama Osman, Soumaya Sallem, Laurent Sommervogel, Marc Olivas Carrion, Pierre Bonnet, and Françoise Paladian. "Distributed reflectometry for soft fault identification in wired networks using neural network and genetic algorithm". In: *IEEE Sensors Journal* 20.9 (2020), pp. 4850–4858 (cit. on p. 42).

[123] Fang Yang, Wenbo Ding, and Jian Song. "Non-intrusive power line quality monitoring based on power line communications". In: *2013 IEEE 17th International Symposium on Power Line Communications and Its Applications*. IEEE. 2013, pp. 191–196 (cit. on p. 43).

[124] Yinjia Huo, Gautham Prasad, Lazar Atanackovic, Lutz Lampe, and Victor CM Leung. "Grid surveillance and diagnostics using power line communications". In: *2018 IEEE International Symposium on Power Line Communications and its Applications (ISPLC)*. IEEE. 2018, pp. 1–6 (cit. on p. 43).

[125] Yinjia Huo, Gautham Prasad, Lutz Lampe, and Victor CM Leung. "Cable health monitoring in distribution networks using power line communications". In: *2018*

IEEE International Conference on Communications, Control, and Computing Technologies for Smart Grids (SmartGridComm). IEEE. 2018, pp. 1–6 (cit. on p. 43).

[126] Yinjia Huo, Gautham Prasad, Lutz Lampe, Victor CM Leung, Rathinamala Vijay, and TV Prabhakar. "Measurement Aided Training of Machine Learning Techniques for Fault Detection Using PLC Signals". In: *2021 IEEE International Symposium on Power Line Communications and its Applications (ISPLC)*. IEEE. 2021, pp. 78–83 (cit. on p. 43).

[127] Yinjia Huo, Gautham Prasad, Lutz Lampe, and Victor CM Leung. "Advanced smart grid monitoring: Intelligent cable diagnostics using neural networks". In: *2020 IEEE International Symposium on Power Line Communications and its Applications (ISPLC)*. IEEE. 2020, pp. 1–6 (cit. on p. 43).

[128] Andreas M Lehmann, Katrin Raab, Florian Gruber, Erik Fischer, Ralf Müller, and Johannes B Huber. "A diagnostic method for power line networks by channel estimation of PLC devices". In: *2016 IEEE International Conference on Smart Grid Communications (SmartGridComm)*. IEEE. 2016, pp. 320–325 (cit. on p. 43).

[129] Navish Lallbeeharry, Rose Mazari, Virginie Dégardin, and Christophe Trebosc. "PLC applied to fault detection on in-vehicle power line". In: *2018 IEEE International Symposium on Power Line Communications and its Applications (ISPLC)*. IEEE. 2018, pp. 1–5 (cit. on p. 43).

[130] Sinem Coleri, Mustafa Ergen, Anuj Puri, and Ahmad Bahai. "Channel estimation techniques based on pilot arrangement in OFDM systems". In: *IEEE Transactions on Broadcasting* 48.3 (2002), pp. 223–229. ISSN: 00189316 (cit. on p. 44).

[131] D Fotsch and DJ Ewins. "Application of MAC in the frequency domain". In: *Rolls Royce PLC-Report-PNR* (2000) (cit. on p. 53).

[132] Randall J Allemang. "The modal assurance criterion–twenty years of use and abuse". In: *Sound and vibration* 37.8 (2003), pp. 14–23 (cit. on pp. 53, 54).

[133] Jacob Benesty, Jingdong Chen, Yiteng Huang, and Israel Cohen. "Pearson correlation coefficient". In: *Noise reduction in speech processing*. Springer, 2009, pp. 1–4 (cit. on p. 53).

[134] DJ Nefske and SH Sung. "Correlation of a coarse-mesh finite element model using structural system identification and a frequency response assurance criterion". In: *Proceedings-SPIE the International Society for Optical Engineering*. SPIE International Society for Optical. 1996, pp. 597–602 (cit. on p. 53).

[135] Dennis Göge and Michael Link. "Assessment of computational model updating procedures with regard to model validation". In: *Aerospace Science and Technology* 7.1 (2003), pp. 47–61 (cit. on p. 53).

[136] Rodrigo Pascual, Jean-Claude Golinval, and Mario Razeto. "A frequency domain correlation technique for model correlation and updating". In: (1997) (cit. on p. 53).

[137] Dooho Lee, Tae-Soo Ahn, and Hyeon-Seok Kim. "A metric on the similarity between two frequency response functions". In: *Journal of Sound and Vibration* 436 (2018), pp. 32–45 (cit. on pp. 53, 54).

[138] Janos Gertler. "Structured residuals for fault isolation, disturbance decoupling and modelling error robustness". In: *IFAC Proceedings Volumes* 25.4 (1992), pp. 15–23 (cit. on p. 56).

[139] V Degardin, P Laly, M Lienard, and P Degauque. "Impulsive noise on in-vehicle power lines: Characterization and impact on communication performance". In: *2006 IEEE International Symposium on Power Line Communications and Its Applications*. IEEE. 2006, pp. 222–226 (cit. on p. 63).

[140] William G Cochran. "The $\chi 2$ test of goodness of fit". In: *The Annals of mathematical statistics* (1952), pp. 315–345 (cit. on p. 69).

[141] Manfred Zimmermann and Klaus Dostert. "Analysis and modeling of impulsive noise in broad-band powerline communications". In: *IEEE transactions on Electromagnetic compatibility* 44.1 (2002), pp. 249–258 (cit. on p. 118).

[142] Melike Yigit, V Cagri Gungor, Gurkan Tuna, Maria Rangoussi, and Etimad Fadel. "Power line communication technologies for smart grid applications: A review of advances and challenges". In: *Computer Networks* 70 (2014), pp. 366–383 (cit. on p. 118).

[143] Matthias Gotz, Manuel Rapp, and Klaus Dostert. "Power line channel characteristics and their effect on communication system design". In: *IEEE Communications Magazine* 42.4 (2004), pp. 78–86 (cit. on p. 118).

[144] Ezio Biglieri. "Coding and modulation for a horrible channel". In: *IEEE Communications magazine* 41.5 (2003), pp. 92–98 (cit. on p. 118).

[145] Alain Richard Ndjiongue and Hendrik C Ferreira. "Power line communications (PLC) technology: More than 20 years of intense research". In: *Transactions on Emerging Telecommunications Technologies* 30.7 (2019), e3575 (cit. on p. 118).

[146] H Meng, Y Ll Guan, and S Chen. "Modeling and analysis of noise effects on broadband power-line communications". In: *IEEE Transactions on Power delivery* 20.2 (2005), pp. 630–637 (cit. on p. 118).

Appendices

A0.1 Expressions of the transmission coefficients in a Y-shaped network

A0.1.1 No-fault situation

In the no-fault situation, the transmission coefficient between S_0 and R_i is :

$$H_{R_{i,0}}(f) = \frac{2}{A_Y^h + \frac{B_Y^h}{Z_c} + C_Y^h \cdot Z_c + D_Y^h} \tag{1}$$

According to (1.50) and (1.51):

$$\begin{aligned} & A_Y^h + \frac{B_Y^h}{Z_c} + C_Y^h \cdot Z_c + D_Y^h \\ =& \cosh\left[\gamma(l_0 + l_i)\right] + \sinh\left[\gamma l_0\right] \cdot \cosh\left[\gamma l_i\right] + \sinh\left[\gamma(l_0 + l_i)\right] + \sinh\left[\gamma l_0\right] \cdot \sinh\left[\gamma l_i\right] \\ & + \sinh\left[\gamma(l_0 + l_i)\right] + \cosh\left[\gamma l_0\right] \cdot \cosh\left[\gamma l_i\right] + \cosh([\gamma(l_0 + l_i)]) + \cosh\left[\gamma l_0\right] \cdot \sinh\left[\gamma l_i\right] \\ =& 2 \cdot e^{\gamma(l_0 + l_i)} + \cosh\left[\gamma(l_0 + l_i)\right] + \sinh\left[\gamma(l_0 + l_i)\right] \\ =& 3 \cdot e^{\gamma(l_0 + l_i)} \end{aligned} \tag{2}$$

Then,

$$H_{R_{i,0}}(f) = \frac{2}{3 \cdot e^{\gamma(l_0 + l_i)}} \tag{3}$$

A0.1.2 Faulty source branch

In the faulty source branch, B_0, situation, the transmission coefficient between S_0 and R_i is :

$$H_{R_{i,0}}(f) = \frac{2}{A_Y^{B_0} + \frac{B_Y^{B_0}}{Z_c} + C_Y^{B_0} \cdot Z_c + D_Y^{B_0}} \tag{4}$$

According to (1.52), (1.53), (1.54) and (1.55) ;

$$\begin{aligned}
&A_Y^{B_0} + \frac{B_Y^{B_0}}{Z_c} + C_Y^{B_0} \cdot Z_c + D_Y^{B_0} \\
=&A_Y^h + \frac{Z_f}{Z_c} \cdot (\cosh[\gamma(l_0 - x)] \sinh[\gamma(l_i + x)] + \cosh[\gamma(l_0 - x)] \cosh[\gamma x] \cosh[\gamma l_i]) \\
&+ \frac{B_Y^h}{Z_c} + \frac{Z_f}{Z_c} \cdot (\cosh[\gamma(l_0 - x)] \cosh[\gamma(l_i + x)] + \cosh[\gamma(l_0 - x)] \cosh[\gamma x] \sinh[\gamma l_i]) \\
&+ C_Y^h \cdot Z_c + \frac{Z_f}{Z_c} \cdot (\sinh[\gamma(l_0 - x)] \sinh[\gamma(l_i + x)] + \sinh[\gamma(l_0 - x)] \cosh[\gamma x] \cosh[\gamma l_i]) \\
&+ D_Y^h + \frac{Z_f}{Z_c} \cdot (\sinh[\gamma(l_0 - x)] \cosh[\gamma(l_i + x)] + \sinh[\gamma(l_0 - x)] \cosh[\gamma x] \sinh[\gamma l_i]) \\
=&A_Y^h + \frac{B_Y^h}{Z_c} + C_Y^h \cdot Z_c + D_Y^h + \frac{Z_f}{Z_c} e^{\gamma(l_0 + l_i)} + \frac{Z_f}{Z_c} \cdot (\cosh[\gamma x] \cdot e^{\gamma(l_0 + l_i - x)}) \\
=&3 \cdot e^{\gamma(l_0 + l_i)} + \frac{Z_f}{Z_c} e^{\gamma(l_0 + l_i)} + \frac{Z_f}{Z_c} \cdot (\frac{e^{\gamma x} + e^{-\gamma x}}{2} \cdot e^{\gamma(l_0 + l_i - x)}) \\
=&3 \cdot e^{\gamma(l_0 + l_i)} + \frac{Z_f}{2 \cdot Z_c} e^{\gamma(l_0 + l_i)} \cdot (3 + e^{-2\gamma x})
\end{aligned} \tag{5}$$

Then,

$$H_{R_{i,0}}(f) = \frac{2}{3 \cdot e^{\gamma(l_0 + l_i)} + \frac{Z_f}{2 \cdot Z_c} e^{\gamma(l_0 + l_i)} \cdot (3 + e^{-2\gamma x})} \tag{6}$$

A0.1.3 Faulty receiver branch

In the faulty receiver branch, B_i, situation, the transmission coefficient between S_0 and R_i is:

$$H_{R_{i,0}}(f) = \frac{2}{A_Y^{B_i} + \frac{B_Y^{B_i}}{Z_c} + C_Y^{B_i} \cdot Z_c + D_Y^{B_i}} \tag{7}$$

According to (1.56), (1.57), (1.58) and (1.59):

$$\begin{aligned}
&A_Y^{B_i} + \frac{B_Y^{B_i}}{Z_c} + C_Y^{B_i} \cdot Z_c + D_Y^{B_i} \\
=&A_Y^h + \frac{Z_f}{Z_c} \cdot (\sinh[\gamma(l_i - x_i)] \cosh[\gamma(l_0 + x_i)] + \sinh[\gamma l_0] \cosh[\gamma x_i] \sinh[\gamma(l_i - x_i)]) \\
&+ \frac{B_Y^h}{Z_c} + \frac{Z_f}{Z_c} \cdot (\cosh[\gamma(l_0 + x_i)] \cosh[\gamma(l_i - x_i)] + \cosh[\gamma(l_i - x_i)] \cosh[\gamma x_i] \sinh[\gamma l_0]) \\
&+ C_Y^h \cdot Z_c + \frac{Z_f}{Z_c} \cdot (\sinh[\gamma(l_0 + x_i)] \sinh[\gamma(l_i - x_i)] + \sinh[\gamma(l_i - x_i)] \cosh[\gamma x] \cosh[\gamma l_0]) \\
&+ D_Y^h + \frac{Z_f}{Z_c} \cdot (\sinh[\gamma(l_0 + x_i)] \cosh[\gamma(l_i - x_i)] + \cosh[\gamma(l_i - x_i)] \cosh[\gamma x_i] \cosh[\gamma l_0]) \\
=&A_Y^h + \frac{B_Y^h}{Z_c} + C_Y^h \cdot Z_c + D_Y^h + \frac{Z_f}{Z_c} \cdot e^{\gamma(l_0+l_i)} + \frac{Z_f}{Z_c} \cdot \cosh[\gamma x] \cdot e^{\gamma(l_0+l_i-x)} \\
=&3 \cdot e^{\gamma(l_0+l_i)} + \frac{Z_f}{Z_c} \cdot e^{\gamma(l_0+l_i)} + \frac{Z_f}{2 \cdot Z_c} \cdot e^{\gamma(l_0+l_i)} \cdot (1 + e^{-2\gamma x}) \\
=&3 \cdot e^{\gamma(l_0+l_i)} + \frac{Z_f}{2 \cdot Z_c} \cdot e^{\gamma(l_0+l_i)} \cdot (3 + e^{-2\gamma x})
\end{aligned} \tag{8}$$

Then,

$$H_{R_{i,0}}(f) = \frac{2}{3 \cdot e^{\gamma(l_0+l_i)} + \frac{Z_f}{2 \cdot Z_c} \cdot e^{\gamma(l_0+l_i)} \cdot (3 + e^{-2\gamma x})} \tag{9}$$

In the faulty receiver branch, B_j, situation, the transmission coefficient between S_0 and R_i is :

$$H_{R_{i,0}}(f) = \frac{2}{A_Y^{B_j} + \frac{B_Y^{B_j}}{Z_c} + C_Y^{B_j} \cdot Z_c + D_Y^{B_j}} \tag{10}$$

According to (1.60):

$$\begin{aligned}
=&A_Y^{B_j} + \frac{B_Y^{B_j}}{Z_c} + C_Y^{B_j} \cdot Z_c + D_Y^{B_j} \\
=&A_Y^h + (\frac{Z_c}{Z} - 1) \cdot (\sinh[\gamma l_0] \cosh[\gamma l_j]) + \frac{B_Y^h}{Z_c} + \frac{Z_f}{Z_c} \cdot (\frac{Z_c}{Z} - 1) \cdot (\sinh[\gamma l_0] \sinh[\gamma l_j]) \\
&+ C_Y^h \cdot Z_c + \frac{Z_f}{Z_c} \cdot (\frac{Z_c}{Z} - 1) \cdot (\cosh[\gamma l_0] \cosh[\gamma l_j]) + D_Y^h + (\frac{Z_c}{Z} - 1) \cdot (\cosh[\gamma l_0] \sinh[\gamma l_j]) \\
=&A_Y^h + \frac{B_Y^h}{Z_c} + C_Y^h \cdot Z_c + D_Y^h + (\frac{Z_c}{Z} - 1) \cdot e^{\gamma(l_0+l_j)} \\
=&3 \cdot e^{\gamma(l_0+l_i)} + (\frac{Z_c}{Z} - 1) \cdot e^{\gamma(l_0+l_j)} \\
=&3 \cdot e^{\gamma(l_0+l_i)} + (\frac{2Z_c + Z_f(1 - e^{-2\gamma x})}{2Z_c + Z_f(1 + e^{-2\gamma x})} - 1) \cdot e^{\gamma(l_0+l_j)} \\
=&3 \cdot e^{\gamma(l_0+l_i)} + \frac{-2 \cdot Z_f e^{-2\gamma x}}{2Z_c + Z_f(1 + e^{-2\gamma x})} \cdot e^{\gamma(l_0+l_j)}
\end{aligned} \tag{11}$$

Then,

$$H_{R_{i,0}}(f) = \frac{2}{3 \cdot e^{\gamma(l_0+l_i)} + \frac{-2 \cdot Z_f e^{-2\gamma x}}{2Z_c + Z_f(1+e^{-2\gamma x})} \cdot e^{\gamma(l_0+l_j)}} \tag{12}$$

A0.2 Expressions of the transmission coefficients in a star-shaped network

A0.2.1 No-fault situation

In the no-fault situation, the transmission coefficient between S_0 and R_i is:

$$H_{R_{i,0}}(f) = \frac{2}{A^h_{star} + \frac{B^h_{star}}{Z_c} + C^h_{star} \cdot Z_c + D^h_{star}} \tag{13}$$

According to (1.31) and (1.32):

$$\begin{aligned}
&A^h_{star} + \frac{B^h_{star}}{Z_c} + C^h_{star} \cdot Z_c + D^h_{star} \\
=&\cosh\left[\gamma(l_0+l_i)\right] + (m-1) \cdot \sinh\left[\gamma l_0\right] \cdot cosh[\gamma l_i] + \sinh\left[\gamma(l_0+l_i)\right] + (m-1) \cdot \sinh\left[\gamma l_0\right] \cdot \sinh\left[\gamma l_i\right] \\
&\sinh\left[\gamma(l_0+l_i)\right] + (m-1) \cdot \cosh\left[\gamma l_0\right] \cdot \cosh\left[\gamma l_i\right] + \cosh([\gamma(l_0+l_i)]) + (m-1) \cdot \cosh\left[\gamma l_0\right] \cdot \sinh\left[\gamma l_i\right] \\
=&2 \cdot e^{\gamma(l_0+l_i)} + (m-1) \cdot e^{\gamma(l_0+l_i)} \\
=&(m+1) \cdot e^{\gamma(l_0+l_i)}
\end{aligned} \tag{14}$$

Then,

$$H_{R_{i,0}}(f) = \frac{2}{(m+1) \cdot e^{\gamma(l_0+l_i)}} \tag{15}$$

A0.2.2 Faulty source branch

In the faulty source branch, B_0, situation, the transmission coefficient between S_0 and R_i is :

$$H_{R_{i,0}}(f) = \frac{2}{A^{B_0}_{star} + \frac{B^{B_0}_{star}}{Z_c} + C^{B_0}_{star} \cdot Z_c + D^{B_0}_{star}} \tag{16}$$

According to (1.35), (1.36), (1.37) and (1.38):

$$
\begin{aligned}
&A_{star}^{B_0} + \frac{B_{star}^{B_0}}{Z_c} + C_{star}^{B_0} \cdot Z_c + D_{star}^{B_0} \\
=&A_{star}^{h} + \frac{Z_f}{Z_c} \cdot (\cosh[\gamma(l_0 - x_0)] \sinh[\gamma(l_i + x_0)] + (m-1) \cdot \cosh[\gamma(l_0 - x_0)] \cosh[\gamma x_0] \cosh[\gamma l_i]) + \\
&\frac{B_{star}^{h}}{Z_c} + \frac{Z_f}{Z_c} \cdot (\cosh[\gamma(l_0 - x_0)] \cosh[\gamma(l_i + x_0)] + (m-1) \cdot \cosh[\gamma(l_0 - x_0)] \cosh[\gamma x_0] \sinh[\gamma l_i]) + \\
&C_{star}^{h} \cdot Z_c + \frac{Z_f}{Z_c} \cdot (\sinh[\gamma(l_0 - x_0)] \sinh[\gamma(l_i + x_0)] + (m-1) \cdot \sinh[\gamma(l_0 - x_0)] \cosh[\gamma x_0] \cosh[\gamma l_i]) + \\
&D_{star}^{h} + \frac{Z_f}{Z_c} \cdot (\sinh[\gamma(l_0 - x_0)] \cosh[\gamma(l_i + x_0)] + (m-1) \cdot \sinh[\gamma(l_0 - x_0)] \cosh[\gamma x_0 \sinh[\gamma l_i]) \\
=&(m+1) \cdot e^{\gamma(l_0+l_i)} + \frac{Z_f}{Z_c} \cdot (e^{\gamma(l_0+l_i)} + (m-1) \cdot \cosh[\gamma x_0] \cdot e^{\gamma(l_0+l_i-x_0)}) \\
=&(m+1) \cdot e^{\gamma(l_0+l_i)} + \frac{Z_f}{Z_c} \cdot (e^{\gamma(l_0+l_i)} + (m-1) \cdot \frac{e^{\gamma x_0} + e^{-\gamma x_0}}{2} \cdot e^{\gamma(l_0+l_i-x_0)}) \\
=&(m+1) \cdot e^{\gamma(l_0+l_i)} + \frac{Z_f}{2Z_c} \cdot (2e^{\gamma(l_0+l_i)} + (m-1) \cdot (e^{\gamma x_0} + e^{-\gamma x_0}) \cdot e^{\gamma(l_0+l_i-x_0)}) \\
=&(m+1) \cdot e^{\gamma(l_0+l_i)} + \frac{Z_f}{2Z_c} \cdot ((m+1) \cdot e^{\gamma(l_0+l_i)} + (m-1) \cdot \cdot e^{\gamma(l_0+l_i-2x_0)}) \\
=&(m+1) \cdot e^{\gamma(l_0+l_i)} + \frac{Z_f}{2Z_c} \cdot e^{\gamma(l_0+l_i)} \cdot ((m+1) + (m-1) \cdot e^{-2\gamma x_0}) \\
=&(m+1) \cdot e^{\gamma(l_0+l_i)} + \frac{Z_f}{2Z_c} \cdot e^{\gamma(l_0+l_i)} \cdot (2 + (m-1) \cdot (1 + e^{-2\gamma x_0}))
\end{aligned}
\tag{17}
$$

Then,

$$
H_{R_{i,0}}(f) = \frac{2}{(m+1) \cdot e^{\gamma(l_0+l_i)} + \frac{Z_f}{2Z_c} \cdot e^{\gamma(l_0+l_i)} \cdot (2 + (m-1) \cdot (1 + e^{-2\gamma x_0}))} \tag{18}
$$

A0.2.3 Faulty receiver branch

In the faulty receiver branch, B_i, situation, the transmission coefficient between S_0 and R_i is:

$$
H_{R_{i,0}}(f) = \frac{2}{A_{star}^{B_i} + \frac{B_{star}^{B_i}}{Z_c} + C_{star}^{B_i} \cdot Z_c + D_{star}^{B_i}} \tag{19}
$$

$m-1$ branches are connected to the node, one of which is faulty, in addition to the source branch B_0 and the one directly connected to the receiver R_i. A parallel impedance Z can replace the $m-1$ branches. It is computed as follows : The

ABCD-matrix of the faulty branch B_j is :

$$ABCD^f_{B_j}(l_j, x_j) = \begin{bmatrix} \cosh[\gamma l_j] + \frac{Z_f}{Z_c} \cdot \cosh[\gamma(l_j - x_j)] \cdot \sinh[\gamma x_j] & Z_c \cdot \sinh[\gamma l_j] + Z_f \cdot \cosh[\gamma(l_j - x_j)] \cdot \cosh[\gamma x_j] \\ \frac{1}{Z_c} \cdot \sinh[\gamma l_j] + \frac{Z_f}{Z_c^2} \cdot \sinh[\gamma(l_j - x_j)] \cdot \sinh[\gamma x_j] & \cosh[\gamma l_j] + \frac{Z_f}{Z_c} \cdot \sinh[\gamma(l_j - x_j)] \cdot \cosh[\gamma x_j] \end{bmatrix} \tag{20}$$

It can be replaced by an equivalent impedance Z_{eq_j} using the ABCD-parameters of (20) and using (1.30) :

$$\begin{aligned} Z_{eq_j} &= Z_c \frac{e^{\gamma \cdot l_j} + \frac{Z_f}{Z_c} \cdot e^{\gamma \cdot x_j} \cdot \cosh[\gamma \cdot (l_j - x_j)]}{e^{\gamma \cdot l_j} + \frac{Z_f}{Z_c} \cdot e^{\gamma \cdot x_j} \sinh[\gamma \cdot (l_j - x_j)]} \\ &= Z_c \cdot \frac{2 \cdot Z_c + Z_f \cdot (1 + e^{-2 \cdot \gamma \cdot x_j})}{2 \cdot Z_c + Zf \cdot (1 - e^{-2 \cdot \gamma \cdot x_j})} \end{aligned} \tag{21}$$

The equivalent impedance $Z_{p_{m-2}}$ of the $m-2$ branches is :

$$Z_{p_{m-2}} = \frac{m-2}{Z_c} \tag{22}$$

The impedance Z representing all the branches connected to the node except B_0 and B_i is :

$$\begin{aligned} \frac{1}{Z} &= \frac{m-2}{Z_c} + \frac{2 \cdot Z_c + Zf \cdot (1 - e^{-2 \cdot \gamma \cdot x_j})}{Z_c \cdot (2 \cdot Z_c + Z_f \cdot (1 + e^{-2 \cdot \gamma \cdot x_j}))} \\ &= \frac{1}{Z_c} \cdot \frac{2(m-1)Z_c + Z_f((m-1) + (m-3)e^{-2\gamma x})}{2Z_c + Z_f(1 + e^{-2\gamma x})} \end{aligned} \tag{23}$$

According to (1.40), (1.41), (1.42) and (1.43):

$$
\begin{aligned}
&A_{star}^{B_i} + \frac{B_{star}^{B_i}}{Z_c} + C_{star}^{B_i} \cdot Z_c + D_{star}^{B_i} \\
=&A_{star}^{h} + \frac{Z_f}{Z_c} \cdot (\sinh[\gamma(l_i - x_i)] \cosh[\gamma(l_0 + x_i)] + (m-1) \cdot \sinh[\gamma l_0] \cosh[\gamma x_i] \sinh[\gamma(l_i - x_i)]) + \\
&\frac{B_{star}^{h}}{Z_c} + \frac{Z_f}{Z_c} \cdot (\cosh[\gamma(l_0 + x_i)] \cosh[\gamma(l_i - x_i)] + (m-1) \cdot \cosh[\gamma(l_i - x_i)] \cosh[\gamma x_i] \sinh[\gamma l_0]) + \\
&C_{star}^{h} \cdot Z_c + \frac{Z_f}{Z_c} \cdot (\sinh[\gamma(l_0 + x_i)] \sinh[\gamma(l_i - x_i)] + (m-1) \cdot \sinh[\gamma(l_i - x_i)] \cosh[\gamma x] \cosh[\gamma l_0]) + \\
&D_{star}^{h} + \frac{Z_f}{Z_c} \cdot (\sinh[\gamma(l_0 + x_i)] \cosh[\gamma(l_i - x_i)] + (m-1) \cdot \cosh[\gamma(l_i - x_i)] \cosh[\gamma x_i] \cosh[\gamma l_0]) \\
=&A_{star}^{h} + \frac{B_{star}^{h}}{Z_c} + C_{star}^{h} \cdot Z_c + D_{star}^{h} + \frac{Z_f}{Z_c} \cdot (e^{\gamma(l_0+l_i)} + (m-1) \cdot (\cosh[\gamma x_i] \cdot e^{\gamma(l_0+l_i-x_i)})) \\
=&(m+1) \cdot e^{\gamma(l_0+l_i)} + \frac{Z_f}{2Z_c} \cdot e^{\gamma(l_0+l_i)} \cdot (2 + (m-1) \cdot (1 + e^{-2\gamma x_i}))
\end{aligned}
\tag{24}
$$

Then,

$$
H_{R_{i,0}}(f) = \frac{2}{(m+1) \cdot e^{\gamma(l_0+l_i)} + \frac{Z_f}{2Z_c} \cdot e^{\gamma(l_0+l_i)} \cdot (2 + (m-1) \cdot (1 + e^{-2\gamma x_i}))} \tag{25}
$$

In the faulty receiver branch, B_j, situation, the transmission coefficient between S_0 and R_i is :

$$
H_{R_{i,0}}(f) = \frac{2}{A_{star}^{B_j} + \frac{B_{star}^{B_j}}{Z_c} + C_{star}^{B_j} \cdot Z_c + D_{star}^{B_j}} \tag{26}
$$

According to (1.45):

$$
\begin{aligned}
&A_{star}^{B_j}+\frac{B_{star}^{B_j}}{Z_c}+C_{star}^{B_j}\cdot Z_c+D_{star}^{B_j}\\
=&A_{star}^{h}+(\frac{Z_c}{Z}-(m-1))\cdot(\sinh[\gamma l_0]\cosh[\gamma l_i])+\frac{B_{star}^{h}}{Z_c}+(\frac{Z_c}{Z}-(m-1))\cdot(\sinh[\gamma l_0]\sinh[\gamma l_i])+\\
&C_{star}^{h}\cdot Z_c+(\frac{Z_c}{Z}-(m-1))\cdot(\cosh[\gamma l_0]\cosh[\gamma l_i])+D_{star}^{h}+(\frac{Z_c}{Z}-(m-1))\cdot(\cosh[\gamma l_0]\sinh[\gamma l_i])\\
=&A_{star}^{h}+\frac{B_{star}^{h}}{Z_c}+C_{star}^{h}\cdot Z_c+D_{star}^{h}+(\frac{Z_c}{Z}-(m-1))\cdot e^{\gamma(l_0+l_i)}\\
=&(m+1)\cdot e^{\gamma(l_0+l_i)}+(\frac{Z_c}{Z}-(m-1))\cdot e^{\gamma(l_0+l_i)}\\
=&(m+1)\cdot e^{\gamma(l_0+l_i)}+(\frac{2(m-1)Z_c+Z_f((m-1)+(m-3)e^{-2\gamma x})}{2Z_c+Z_f(1+e^{-2\gamma x})}-(m-1))\cdot e^{\gamma(l_0+l_i)}\\
=&(m+1)\cdot e^{\gamma(l_0+l_i)}-\frac{2Z_f\cdot e^{-2\gamma x_i}}{2Z_c+Z_f(1+e^{-2\gamma x})}\cdot e^{\gamma(l_0+l_i)}
\end{aligned}
\tag{27}
$$

Then,

$$
H_{R_{i,0}}(f)=\frac{2}{(m+1)\cdot e^{\gamma(l_0+l_i)}-\frac{2Z_f\cdot e^{-2\gamma x_i}}{2Z_c+Z_f(1+e^{-2\gamma x})}\cdot e^{\gamma(l_0+l_i)}} \tag{28}
$$